Chapter 1
Commercial and Experimental Glass Fibers

Frederick T. Wallenberger

Abstract Continuous glass fibers can be formed from melts with a wide range of compositions and viscosities. This chapter reviews pure silica fibers which are formed from highly viscous melts, silicate glass fibers with 50–70% SiO_2 which are formed from moderately viscous melts, aluminate glass fibers with 50–80% Al_2O_3, as well as yttria-alumina-garnet (YAG) glass fibers which are formed from inviscid (literally non-viscous) melts. Commercial glass fibers are made for a variety of applications from pure silica rods and from silicate melts containing 50–70% SiO_2 and 10–25% Al_2O_3. Boron-free, essentially boron-free, and borosilicate E-glass are general-purpose fibers. ERC-glass offers high corrosion resistance, HS-glass offers high-strength composites, D-glass offers a low dielectric constant, and A-glass offers the possibility of using waste container glass for less demanding applications.

Keywords Continuous glass fibers · Viscous and inviscid fiberglass melts · Glass melting and fiber formation · Experimental and commercial glass fibers · Commercial E-glass · ECR-glass · D-glass · HS-glass and A-glass fibers · Structures and properties

1.1 Overview: Glass Melt and Fiber Formation

The viscosity of glass melts depends on the SiO_2 content, the crystallization resistance at the liquidus temperature of these melts depends, at the same Al_2O_3 level, on the SiO_2:RO ratio (RO = CaO + MgO), and the modulus of the resulting glass fibers depends on the Al_2O_3 content at the same SiO_2 content.

1.1.1 Principles of Glass Melt Formation

Viscous melts can be strong melts typically containing 50–100% SiO_2 and 25–0% Al_2O_3 [1, 2] or fragile melts typically containing 4–10% SiO_2 and 50–25% Al_2O_3

F.T. Wallenberger (✉)
Consultant, 708 Duncan Avenue, Apartment 1108, Pittsburgh, PA 15237, USA
e-mail: wallenbergerf@aol.com

F.T. Wallenberger, P.A. Bingham (eds.), *Fiberglass and Glass Technology*,
DOI 10.1007/978-1-4419-0736-3_1,

[3, 5]. Inviscid (literally non-viscous) melts contain 0–4% SiO_2 and 50–80% Al_2O_3 [4, 5]. All melts except those based on 100% SiO_2 may also contain CaO, MgO, B_2O_3, and/or other oxides (Table 1.1).

1.1.1.1 Important Glass Melt Properties

The most important melt properties of fiberglass melts are the fiber-forming viscosity (FV), the temperature at which fibers are formed (FT or T_F), the liquidus temperature at which crystals can form within hours (LT or T_L) and remain in equilibrium with the melt, and the delta temperature (ΔT) [1, 2], or the difference between the fiber-forming and liquidus temperatures.

In the technical and patent literature, the relationship between melt viscosity and melt temperature is expressed by a Fulcher curve that relates the melt viscosity (in log poise) to the linear melt temperature (in °C). At the point of fiber formation, glass melts have viscosities ranging from log 2.5 to log 3.0 poise and the temperature of a melt at a viscosity of log 3.0 poise is generally accepted as the "fiber-forming temperature" (or log 3 FT).

Other melt parameters, which are frequently used to characterize fiberglass melts, include the glass transition temperature (T_g), the liquidus temperature (LT), and the difference between the log 3 forming and liquidus temperatures that is also known as delta temperature (ΔT). The glass transition and log 3 forming temperatures are related to the viscosity. The liquidus temperature is related to the phase diagram and the delta temperature relates the phase diagram (the crystallization behavior of a melt) to the melt viscosity.

The melt viscosity (in log poise) has been correlated with the glass transition temperature (T_g, K) divided by the melt temperature (T_m, K) [3]. This theory distinguishes "strong" melts from "fragile" melts. Strong melts include the silica melt that is seen as the ideal melt because it exhibits a perfect straight-line behavior while fragile melts include all silicate melts, which deviate to various degrees from the ideal straight-line behavior.

According to this theory [3], fragile melts include glass fiber-forming aluminum silicate melts, which are viscous at the fiber-forming temperatures but only in a supercooled state. These melts show notable deviations from the straight-line behavior of an ideal strong melt. However, it would also include glass fiber-forming aluminate melts with <80% alumina as well as yttrium aluminum garnet melts. Both melts deviate dramatically from the ideal straight-line behavior. They have melt viscosities, which are comparable to that of honey at room temperature, and sharp melting points.

Another point of view [5], therefore, considers fiberglass melts with ultralow melt viscosities as "inviscid" (literally non-viscous) and as representing a third class of glass melts with regard to glass fiber formation. The most important reason for this classification is the fact that these melts require dramatically different fiber-forming processes. As a result, this point of view has been accepted throughout this book as the basis for classifying the fiberglass melts as strong, fragile, or inviscid.

The relationship between viscosity and melt temperature is generally represented by a Fulcher curve, wherein the viscosity is expressed in log poise and the

Table 1.1 Fiber formation from viscous and inviscid melts [1] (with kind permission of Springer Science and Business Media)

	Viscosity				Glass fiber formation		
Melt	< LT[a]	> LT[a]	> MP[a]	Composition	By	From	Environment
Strong viscous	Very high	Very high		Pure silica	Downdrawing > LT	Preform	Ambient air
Strong viscous	Very high	Very high		Silicate melts	Downdrawing > LT	Bushing	Ambient air
Fragile viscous	Very high	Very low		Yttria silicate	Downdrawing < LT	Precision bushings	Ambient air
Fragile viscous	Very high	Very low		Fluoride and aluminate	Up- or down- drawing < LT	Supercooled melts	Ambient air
Inviscid melt			Very low	Yttria-aluminate	Downdrawing < MP	Levitated, laser-heated melt	Containerless
Inviscid melt			Very low	Binary aluminate	Melt spinning > MP	Stabilized jet surface	Reactive gas

[a]Liquidus temperature (LT), melting point (MP), rapid solidification (RS) process

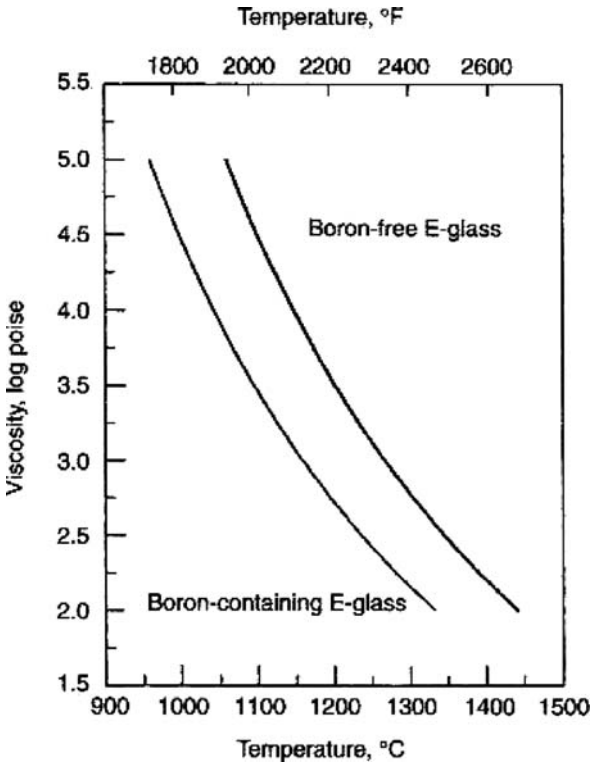

Fig. 1.1 Fulcher curves of boron-containing and boron-free E-glass melts [1, 53] (reprinted with permission of ASM International. All rights reserved. www.asminternational.org)

temperature in degree Celsius. Figure 1.1 shows the typical Fulcher curves of a standard borosilicate E-glass containing 6.6% B_2O_3 and 0.7% fluorine and of a boron-free E-glass with <0.2% fluorine.

By replacing the log viscosity with a linear viscosity [1] it becomes evident that the relationship between the viscosity of strong, fragile, and inviscid melts in the fiber-forming range between 317 (log 2.5) poise and 1000 (log 3.0) poise is essentially linear (Fig. 1.2). Minor changes of the melt viscosity in a commercial furnace will therefore not disproportionately affect the fiber formation at the bushing tips.

Figure 1.2 compares six fiberglass melts in the range of their fiber-forming viscosity (FV) between log 2.5 and log 3.0 poise, by comparing their log 3 fiber-forming temperature (FT) and their liquidus temperature (LT). In Fig. 1.2, the strong viscous E-glass melt with ~6% B_2O_3 has the lowest log 3 forming temperature (log 3 FT) and the inviscid yttrium aluminum garnet (or YAG) melt has the highest log 3 forming temperature.

The liquidus temperature (LT), i.e., the highest temperature at which crystals can form within hours and remain in an equilibrium state with the melt is an important factor in commercial use. Commercial experience suggests that the log 3 forming temperature of a strong melt must be at least 50°C higher in a continuous furnace than the liquidus temperature.

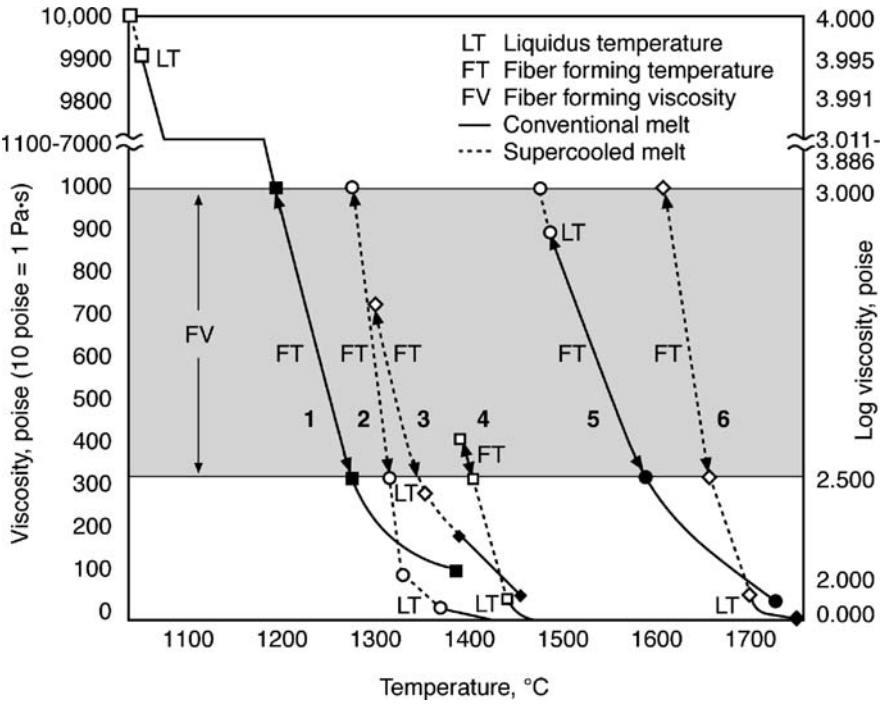

Fig. 1.2 Relationship between linear viscosity (poise) and melt temperature [1] (with kind permission of Springer Science and Business Media)

Commercial E-glass (Fig. 1.2, #1) and S-glass fibers (Fig. 1.2, #5) were formed from strong viscous melts in a continuous process. The yttria silicate (Fig. 1.2, #2) and the quaternary aluminate fiber (Fig. 1.2, #3) were formed from supercooled fragile viscous melts. The binary aluminate (Fig. 1.2, #4) and amorphous yttria-alumina-garnet fiber (Fig. 1.2, #6) were formed from inviscid melts. A viscosity-building fiber-forming process must be used to raise the viscosity of YAG glass fibers from <2 to >log 3 poise.

Two other important factors are the morphology of the crystalline phase and the crystal growth rate, both at and below the liquidus temperature (LT). The crystallization or devitrification at, and below, the liquidus temperature is related to the phase diagram. The crystallization rates of four fiber-forming glass melts [6] are shown in Fig. 1.3. They increase from left to right, i.e., from that of a commercial E-glass melt to that of an experimental yttrium-silicate glass melt.

In summary, in a continuous commercial process, strong viscous melts are operated above their liquidus temperature (LT) and a low crystallization rate at and below the liquidus temperature is preferred. In a stationary process of very short duration, pristine glass fibers can be formed from strong melts at and below the liquidus temperature before crystallization occurs. Fragile viscous melts must be supercooled to a temperature below the liquidus temperature before fibers can be

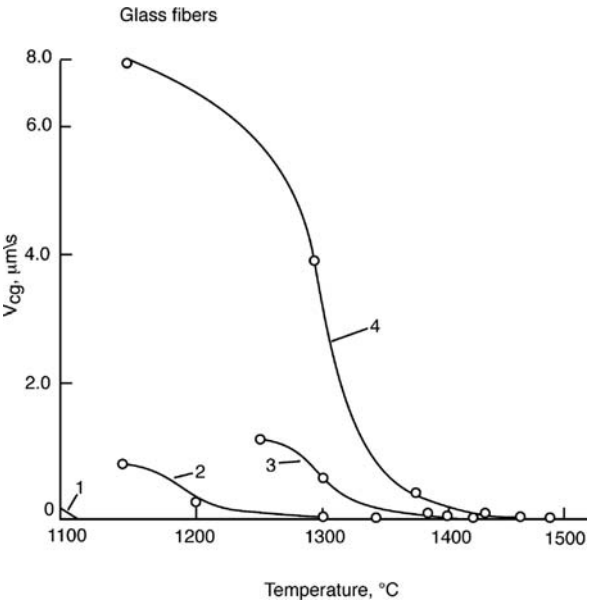

Fig. 1.3 Selected crystallization rates of fiber-forming melts: (1) commercial E-glass, (2) commercial S-glass, (3) experimental silicate glass, (4) yttria-modified silicate glass. Redrawn from Khazanov et al. [1, 6] (with kind permission of Springer Science and Business Media)

formed. Inviscid melts require special fiber-forming processes whereby a liquid jet is rapidly solidified and a solid glass fiber is formed before liquid droplets and shot are formed.

1.1.1.2 Behavior of Strong Viscous Melts

Commercial fiberglass compositions with 50–100% SiO_2, 0–25% Al_2O_3, 0–20% RO (= CaO + MgO), and 0–10% B_2O_3 [1] yield strong viscous melts. Three examples will suffice. Ultrapure SiO_2 fibers have melt temperature of >1800°C at a viscosity of log 3 poise. High-strength S-glass with 65% SiO_2 (Fig. 1.2, #5) has a log 3.0 forming temperature of 1560°C, a liquidus temperature of 1500°C, and therefore a delta temperature of 60°C. E-glass with 54% SiO_2 and ~6% B_2O_3 (Fig. 1.2, #1) is also based on strong viscous silicate melts. It has a low log 3.0 poise fiber-forming temperature of 1185°C and a delta temperature of 135°C. Although both silica and the above silicate glass fibers are based on strong viscous melts, they require different fiber-forming processes (Sections 1.2 and 1.3).

1.1.1.3 Behavior of Fragile Viscous Melts

Fragile viscous melt can be made from compositions with 4–10% SiO_2 and 50–25% Al_2O_3, 55–25% CaO, and 5% MgO [1]. Some also contain small amounts of Y_2O_3, ZnO, and/or Li_2O. Two examples may suffice. The melt of the fragile yttria-modified glass fiber (Fig. 1.2, #2) has melt temperature of 1280°C at a log 3 poise viscosity (or log 3 FT), a liquidus temperature (LT) of 1390°C, and therefore a delta temperature (ΔT) that is 110°C *higher* than the log 3 melt temperature. A related

melt (Fig. 1.2 #3), which does not contain yttria, has a log 3 fiber-forming temperature (or log 3 FT) of 1300°C, a liquidus temperature (LT) of 1350°C, and therefore a delta temperature (ΔT) that is 50°C *higher* than the log 3 forming temperature.

Both melts not only have relatively high log 3 forming temperatures (1280–1390°C) but also 50–110°C *higher* liquidus temperatures than log 3 forming temperatures [1]. If these melts were held in a continuous commercial furnace at or above their log 3 melt temperature, they would crystallize within hours and could not be fiberized. Nonetheless, glass fibers can be formed from supercooled fragile melts (Section 1.4.1).

1.1.1.4 Behavior of Inviscid Glass Melts

Many common inorganic oxides are crystalline in nature, and therefore have high as well as sharp melting points. These melts are inviscid and may contain 4–0% SiO_2 and 50–80% Al_2O_3 [1], as well as perhaps minor amounts of CaO and/or MgO. Above their melting point, their viscosities are comparable to that of heavy motor oil or honey at room temperature and when they crystallize, they instantly revert to polycrystalline ceramic solids.

Crystallization of inviscid melts can be prevented and glass fibers can be formed by increasing the quench rate of a liquid aluminate jet without increasing the viscosity (Fig. 1.2 #4) or by levitating a laser-heated YAG melt, i.e., by increasing the viscosity without increasing the quench rate (Fig. 1.2, #6) [1]. For details, see Section 1.4.2.

1.1.2 Principles of Glass Fiber Formation

Formation of continuous glass fibers requires the melt to have a viscosity of log 2.5–3.0 poise at the point of fiber formation. Five generic fiber-forming processes [1] are known to yield glass fibers either from viscous or inviscid melts. One process yields glassy metal ribbons and one process yields glass fibers from viscous solutions or sol–gels of organic or inorganic precursors.

1.1.2.1 Generic Fiber-Forming Processes

As illustrated in Fig. 1.4, glass fibers can be made from strong viscous melts by melt spinning, i.e., by downdrawing them from bushing tips (Example A) or by downdrawing them from solid preforms (Example B). Glass fibers can also be made by dry spinning from solutions or sol–gels. Conceptually, dry spinning is a variant of melt spinning (Example A). This process relies on removing the solvent in a spinning tower while the fiber consolidates.

In addition, glass fibers can be made by updrawing from fragile viscous, but supercooled, melts (Example C) and from inviscid melts by rapidly quenching of ribbon-like jets (Example D), by extruding inviscid jets into a chemically reactive environment (Example E), and by downdrawing fibers from acoustically levitated melts in a containerless process (Example F).

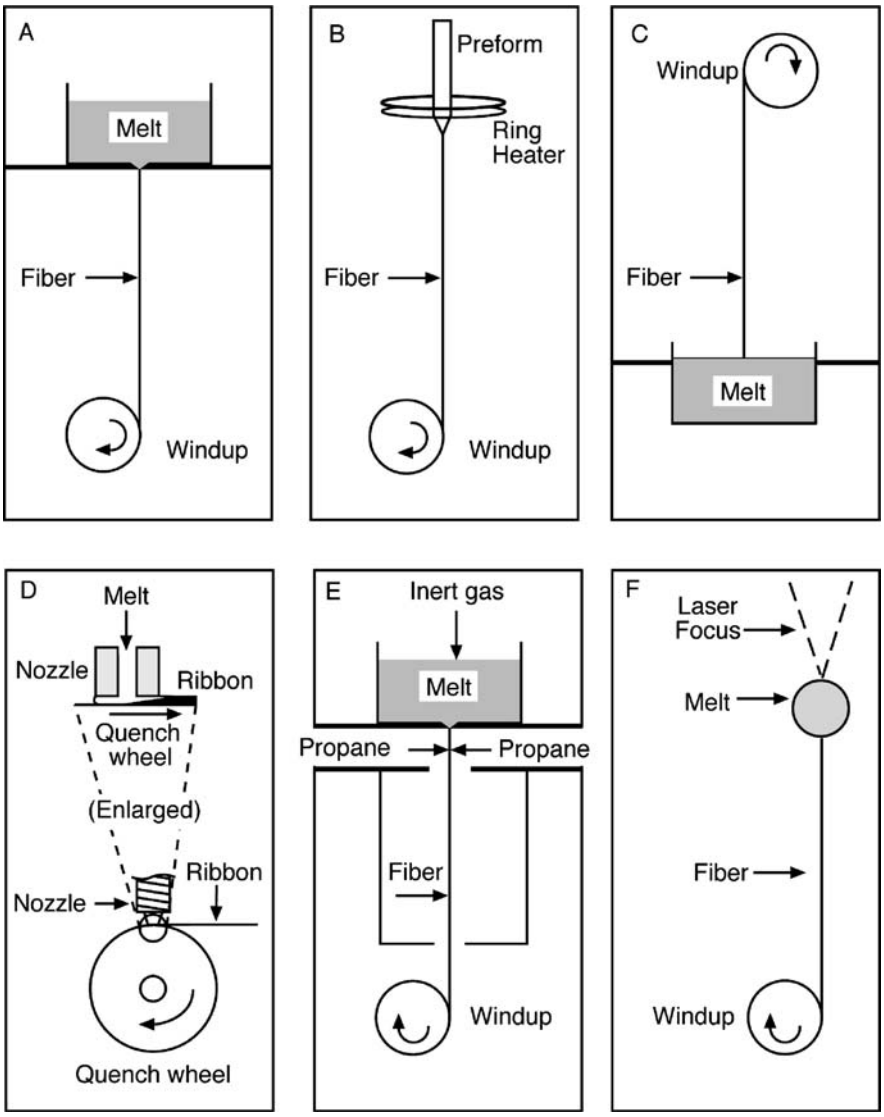

Fig. 1.4 Generic fiber-forming processes. Redrawn from Wallenberger and Brown [35, 36] (reprinted with permission of Elsevier Science Publishers)

1.1.2.2 Fibers from Strong Melts and Solutions

Structural silica fibers with 95–100% SiO_2 have extremely high melt viscosities. The temperature, at which they have a viscosity of log 3 poise (>1800°C), exceeds the capability of even the most costly precious metal bushing alloys. They cannot be melt spun but must be downdrawn from the surface of a solid silica preform rod (Fig. 1.4b). This process exposes only the surface of solid silica rods to such high

temperatures, and therefore does not require precious metal bushings (for details, see Section 1.2.1.1).

Silica glass fibers with 99.5–100% SiO_2 can also be made by "dry spinning" [7], i.e., by a variant of the melt spinning process (Fig. 1.4a) whereby the solvent that contains the silica precursor is removed from the as-spun fibers in a hot spinning tower before they are collected (Sections 1.2.1.2 and 1.2.2).

Structural silicate glass fibers with 50–65% SiO_2 and 10–25% Al_2O_3 can be formed from their strong viscous melts in a conventional melt spinning process. They have log 3.0 forming temperatures ranging from 1150 to 1500°C. And they are downdrawn from bushing tips (Fig. 1.4a) in an ambient, rapidly cooling atmosphere and collected on a winder (see Section 1.3).

1.1.2.3 Fibers from Fragile and Inviscid Melts

Continuous fibers can be updrawn (Fig. 1.4c) from fragile calcium aluminate glass melts with 4–10% SiO_2 and 25–50% Al_2O_3, which must be maintained in a supercooled state at a carefully controlled temperature [8, 5]. For details about fiber formation from fragile melts, see Section 1.4.1.

Continuous aluminate glass fibers with 55–80% Al_2O_3 [9, 10] and metal wires [11] can be melt spun from inviscid melts (Fig. 1.4e) by increasing the lifetime of the liquid jet without increasing the quench rate, i.e., by chemically stabilizing the surface of the inviscid jet; see Section 1.4.2.3. Continuous YAG glass fibers [12, 13] and mullite glass fibers [14] can be formed in a containerless process (Fig. 1.4f) from levitated, laser-heated, inviscid melts (Section 1.4.2.2). Continuous amorphous metal ribbons were made by increasing the quench rates of inviscid melts [15–17] from 10^4 to 10^6 K/s. In this process (Fig. 1.4d), a ribbon is extruded and cast onto the surface of a quench wheel. No ribbons were so far made from inviscid oxide glass melts by this process. For details, see Section 1.4.2.4.

These processes are fast and yield amorphous aluminate and YAG fibers from inviscid melts. Continuous single-crystal sapphire and YAG fibers can likewise be grown from inviscid melts [1] but the respective processes such as laser-assisted [18] or flux-assisted [19] crystal growth are very slow.

1.1.3 Structure of Melts and Fibers

The liquidus temperature and the delta between log 3 forming and liquidus temperatures of a glass melt can not only be determined but must actually be designed by the compositional trend line design model [2]. The modulus of a glass fiber increases with its internal structural order and the strength of a fiber depends on the uniformity of its internal structure.

1.1.3.1 From Glass Melts to Fibers

Pure silica melts have a uniform anisotropic network structure. As a result, they have an extremely high viscosity, a log 3 forming temperature of >1800°C, and a

lower fiber modulus. The two following examples conceptually highlight the effect of disrupting the anisotropic silica network structure.

Example (1): The anisotropic structure of a conceptually pure SiO_2 melt can be disrupted adding Al_2O_3 and MgO to yield the SiO_2–Al_2O_3–MgO eutectic or S-glass melt. As a result, the viscosity and log 3 forming temperature will drop and the liquidus temperature, crystallization potential, and fiber modulus will increase. Example (2): The ternary SiO_2–Al_2O_3–MgO structure of the eutectic melt can be disrupted by adding CaO and B_2O_3 to yield a borosilicate E-glass melt that is based on the quaternary SiO_2–Al_2O_3–CaO–MgO eutectic. As a result the melt viscosity, the log 3 forming temperature, the liquidus temperature, the crystallization potential, and the fiber modulus drop.

1.1.3.2 Melt Structure vs. Liquidus

The liquidus temperature and the delta between log 3 forming and liquidus temperatures are key properties [2, 20, 21, 22] with regard to both a continuous commercial melt and fiber-forming process and a brief experimental fiber-forming process with a single-tip bushing. In either case, crystallization (devitrification) will occur within a few hours when the log 3 forming temperature is the same as, or lower than, the liquidus temperature.

In a continuous commercial process the resulting crystals would plug the bushing tips and impair fiber formation. An adequate delta between the log 3 forming and liquidus temperatures is therefore required as a safety factor. In a brief experimental single-tip process with small melt volumes, fiber formation is complete before crystallization would otherwise start.

The delta temperature of commercial borosilicate melts is greater than 100°C [1] and that of other commercial fiberglass melts ranges from 55 to 85°C [1]. The magnitude of the delta temperature depends on the individual furnace configuration, but on average a delta temperature of at least 50°C is thought to be required by the fiberglass industry. An excessively high-forming and delta temperatures would translate into a higher energy demand, and therefore also into a higher energy use and cost than really required.

The design of new fiberglass compositions, which are more energy- and environmentally friendly than incumbent compositions [2, 20, 21–25], is based on the discovery [26, 27] that the delta temperature is a function of the SiO_2:RO ratio (RO = CaO + MgO). It is possible to obtain that compositional variant that has the lowest log 3 forming temperature (energy demand) at a pre-selected delta temperature (crystallization potential).

The design of new energy-friendly fiberglass compositions for commercial consideration will be reviewed in Chapter 2. Attempts to model soda-lime-silica glass compositions [28–30] and to reformulate them for environmental benefit [31] will be reported in Chapter 7.

1.1.3.3 Fiber Structure vs. Modulus

The modulus of a fiber reflects its structural or internal order [4]. The fibers in Table 1.2 have compositions that range from 100% silica to 100% alumina.

Table 1.2 Effect of alumina on melt behavior, fiber morphology, and modulus

Fibers from SiO_2 to Al_2O_3	Al_2O_3 (wt%)	Fiber precursor	Fiber morphology	Modulus (GPa)	References
Ultrapure SiO_2	0.0	Strong melt	Amorphous	69	[6]
E-glass (6.6% B_2O_3)	13.0	Strong melt	Amorphous	72	[67]
E-glass (<1.5% B_2O_3)	13.0	Strong melt	Amorphous	81	[21]
HS-glass (S-glass)	25.0	Strong melt	Amorphous	89	[50]
HM-glass (6% Y_2O_3)	35.8	Strong melt	Amorphous	100	[6]
HM-glass (4% SiO_2)	44.5	Fragile melt	Amorphous	109	[80]
IMS glass (4% SiO_2)	54.0	Inviscid melt	Amorphous	50	[9]
RIMS (redrawn IMS)	54.0	Glass fiber	Polycrystalline	135	[9]
Nextel 440	70.4	Sol–gel	Polycrystalline	190	[32]
Mullite glass	71.8	Inviscid melt	Amorphous	45	[9]
Nextel 480	71.8	Sol–gel	Polycrystalline	230	[32]
IMS glass (0% SiO_2)	80.2	Inviscid melt	Amorphous	40	[9]
Safimax	98.8	Sol–gel	Polycrystalline	300	[32]
Fiber FP	100.0	Sol–gel	Polycrystalline	380	[32]
Saphikon	100.0	Inviscid melt	Single crystal	430	[33]

Ultrapure amorphous SiO_2 (Quartzel or Astroquartz) fibers, borosilicate E-glass fibers, boron-free E-glass fibers, high-strength (HS) glass fibers including S-glass, and high-modulus (HM) glass fibers, including that which contains 6% Y_2O_3, are derived from strong viscous melts. These glass fibers have moduli ranging from 69 to 100 GPa. The HM-glass fiber with 4% SiO_2 is derived from a fragile melt. It has 44.4% Al_2O_3 and a modulus of 109 GPa but it cannot be made in a conventional glass melt furnace. The processes, which yield strong and fragile melts, are discussed in Sections 1.3.1 and 1.4.1.

The designation IMS refers to inviscid melt spun aluminate glass fibers which contain 54–80% Al_2O_3. Unlike strong and fragile viscous melts, inviscid (literally non-viscous) melts have a melt viscosity of <2 poise. The IMS glass with 72% Al_2O_3 has a mullite composition. The fiberizing processes, which yield glass fibers from inviscid melts, will be discussed in Sections 1.1.2 and 1.4.2. The extremely low melt viscosities and fiber moduli suggest that the melt as well as the resulting glass fibers lack internal order. The designation RIMS refers to a redrawn IMS glass fiber with 54% Al_2O_3 that became polycrystalline on redrawing.

Nextel 440, Nextel 480, Safimax, and Fiber FP are polycrystalline fibers which are of commercial value. They contain 70–99% Al_2O_3 and have moduli ranging from 190 to 380 GPa [32]. They are made by variants of either the generic sol–gel or the generic slurry spinning process. The amorphous IMS mullite glass fiber in Table 1.2 and the polycrystalline Nextel 480 fiber have nominally the same composition but, due to their different morphology, a vastly different modulus (i.e., 45 GPa vs. 230 GPa). Saphikon is a commercial single-crystal sapphire (100% Al_2O_3)

fiber that is made by variants of the very slow crystal growing process, e.g., by the edge-defined film-fed growth (EDG) process [33].

Except for the inviscid melt spun fibers, the modulus in Table 1.2 increases with increasing Al_2O_3 content and therefore with increasing directional structural order. Specifically, the modulus increases from 69 to 109 GPa for glass fibers from strong and fragile viscous melts, to 135 to 380 GPa for polycrystalline (including redrawn IMS) fibers, and to 410 GPa for single-crystal sapphire fibers. Although the observed modulus trend parallels the percent increase in Al_2O_3, truly amorphous and therefore very low modulus fibers are formed if the formation of any internal structure is prevented.

1.1.3.4 Fiber Structure vs. Strength

Strength is a measure of the internal structure as well as surface uniformity. Table 1.3 shows the average tensile strength of 16 glass fibers. Their strength ranges from 5.57 GPa for a military optical glass fiber (FOG-M) to 0.37 GPa for a highly porous, high silica fiber obtained by leaching E-glass with hydrochloric acid. These fibers have diameters ranging from 4 to 20 μm [6], except FOG-M [34] and the binary calcium aluminate fibers [35], which have a fiber diameter of >100 μm.

Table 1.3 Effect of composition on tensile strength [1] (with kind permission of Springer Science and Business Media)

Generic glass fiber	Strength (GPa)	References
Military fiber optics glass fiber, FOG-M	5.57	[34]
Magnesium aluminosilicate glass fiber, 10% MgO	4.80	[6]
Magnesium aluminosilicate glass fiber, 15% MgO	4.00	[6]
Ultrapure silica fiber, Astroquartz	3.50	[6]
Zn/Ti magnesium aluminosilicate glass fiber	3.20	[6]
Sodium calcium aluminosilicate glass fiber	2.75	[6]
E-type aluminum borosilicate glass fiber	2.70	[6]
Copper aluminum borosilicate glass fiber	2.70	[6]
Borate glass fiber	1.90	[6]
Lead silicate glass fiber	1.55	[6]
Phosphate glass fiber	1.50	[6]
Sodium silicate glass fiber	1.10	[6]
Calcium aluminate glass fiber, 54% CaO	0.95	[9]
Pure silica fiber from water glass	0.85	[45]
Calcium aluminate glass fiber, 80% CaO	0.50	[9]
Porous silica fiber from E-glass	0.37	[6]

Surface flaws or non-uniformities have a tendency to reduce the strength of individual glass fibers. Directionality or spin orientation, as inferred from birefringence measurements, tends to increase the strength of individual fibers. Surface uniformity and spin orientation are important factors but, even if their relative relationships were fully documented, the up to 15-fold differences in strength among the 16 generic fibers shown in Table 1.3 cannot be attributed to these factors alone.

A major reason for the observed differences in fiber-to-fiber strength must therefore be sought in differences in the uniformity of the internal structures. The extremely uniform network structure of FOG-M silica fibers [1, 34] translates into high tensile strength. The highly non-directional (random) arrangement of calcium oxide and aluminum oxide in a rapidly solidified binary calcium aluminate fiber translates into very low tensile strength. The ultralow strength of porous high silica glass is obviously due to its porosity.

1.1.4 Summary and Conclusions

The structure of a melt and fiber [4] determines the properties of the melt and fiber properties. The crystallization potential of a fiberglass melt depends on the liquidus temperature [2]. The modulus of a glass fiber depends on its structural or internal order [4]. The viscosity drops and the modulus increases with increasing Al_2O_3 content. In contrast, the tensile strength of a glass fiber does not only depend on the surface uniformity but also on the uniformity of the fiber structure itself. The principles governing the design of new energy-friendly fiberglass compositions will be discussed in Chapter 2.

1.2 Silica Fibers, Sliver, and Fabrics (95–100% SiO_2)

Temperatures well above 1800°C would be required to achieve silica melts with a viscosity of log 2.5–3.0 poise. Such temperatures would by far exceed the capability of the refractories of most furnace wall ceramics and of most precious metal bushing alloys. Silica glass fibers are therefore downdrawn from solid silica preform rods, dry spun from precursor solutions, or made from borosilicate or soda-lime-silica glass fibers by acid leaching.

1.2.1 Ultrapure Silica Fibers (99.99–99.999% SiO_2)

A commercial process has been developed to downdraw ultrapure silica glass fibers with 99.999% SiO_2 from the surface melt of solid silica preform rods. An experimental process can be used to make ultrapure silica fibers by dry spinning of tetraethylorthosilicate sol–gels [1, 36, 37].

1.2.1.1 Downdrawing from Strong Viscous Melts at the Preform Surface

In principle, the process of downdrawing fibers from preform rods is actually variant of the melt spinning process. A gas flame or an electrical furnace softens the ends of a solid quartz rod and facilitates the formation of continuous silica melt on its surface. The melt is not extruded though a bushing tip, but a fiber is pulled from the melt at the tip of the preform.

(a) Process concept. The process is schematically shown in Fig. 1.5. Thus, a large diameter silica preform rod is heated in a circumferential heater, i.e., a gas burner, an

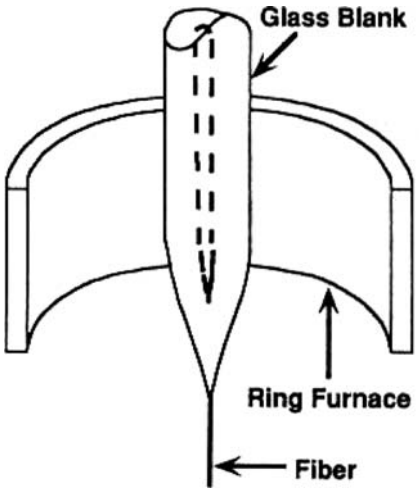

Fig. 1.5. Pure silica fibers from preforms. From Wallenberger et al. [151] (reproduced with permission from Materials Research Society)

electrical furnace, or a laser source. The molten jet solidifies and the resulting quartz filament is passed over a sizing. The coated filament is collected on a winding drum. A large number of single filaments are then combined to form a multifilament yarn bundle or roving.

(b) Products and properties. Preforms made from natural silica contain 99.99% SiO_2, 20–50 ppm Al, <5 ppm OH^-, and <4 ppm Na [38]. Preforms (blanks) made by oxidation of $SiCl_4$ in a plasma flame [38] afford even purer silica fibers with <1 ppm Al, <0.1 ppm OH^-, <1 ppm Na, and <50 ppm Cl. For details, see [1]. Commercial quartz fibers made by downdrawing can have diameters ranging from 7 to 14 μm (Fig. 1.5). Rovings can be made with up to 4800 filaments.

Two commercial ultrapure silica glass fibers are known, Astroquartz and Quartzel. Despite their name both are amorphous not crystalline. The mechanical and physical properties of a typical commercial silica glass fiber are shown in Table 1.4.

Silica glass fibers have higher glass transition temperatures than general-purpose borosilicate and boron-free E-glass fibers (1150–1200°C vs. 550–600°C) and lower coefficients of thermal expansion ($0.5 \times 10^{-6\circ}C^{-1}$ vs. $5 \times 10^{-6^\circ}C^{-1}$). In addition, they also have lower dielectric constants (3.4 vs. 6.1) and lower loss tangents (2×10^{-4} vs. 30×10^{-4}). These properties translate into significant product advantages but they demand a premium price.

(c) Value-in-use and applications. Structural ultrapure silica glass fibers are known as ultrahigh-temperature fibers. They can be continuously used at temperatures of ≤1090°C. In contrast, S-glass can be continuously used only at ≤815°C [1, 7, 36]. A complete comparison of strength and strength retention of ultrapure silica glass fibers, pure silica glass fibers, and silicate glass fibers (including E-glass and S-glass) is summarized in Section 1.3.3.

Another interesting property of silica glass fibers is their low coefficient of thermal expansion, $\alpha \approx 0.5 \times 10^{-6^\circ}C^{-1}$.This value can be lowered and even rendered

Table 1.4 Properties of ultrapure silica glass fibers [36] (with kind permission of Springer Science and Business Media)

Astroquartz and quartzel	
Mechanical properties	
Filament diameter, yarn, and fabric, μm	9.0
Specific gravity (density), g/cc	2.2
Hardness (Mohs scale)	5–6
Pristine filament strength, GPa, RT	6.0
Yarn strand tensile strength, GPa, RT	3.4
Yarn tensile modulus, GPa, RT	69
Physical properties	
Liquidus temperature, °C	1670
Temperature at max. crystallization, °C	1630
Coeff. of thermal exp., 0–1000°C, °C	5.4×10^{-7}
Thermal stability (short term), to °C	2000
Thermal stability (long term), to °C	1200
Thermal conductivity at 20°C, CGS	0.0033
Dielectric constant at 20°C, 1 MHz	3.78
Refractive index at 15°C, n_D	1.4585

negative by adding TiO_2 to silica [36]. Silica glass fibers also display excellent dielectric properties. Finally, they are known for their high resistance to corrosion in neutral or acid chemical environments.

These fibers offer superior heat resistance since they retain useful strength at very high temperatures. They also possess the high ablation resistance and the dielectric, acoustic, optical, and chemical properties of quartz from which they were made. Their pristine modulus is low (69 GPa), their pristine strength is as high as 4.8–6.0 GPa [6], and because of their low density (2.2 g/cc), their specific pristine strength (2.2–2.7 Mm) is the highest of any pristine glass fiber on record.

Quartz fibers offer superior IR and UV transmittance, but contain water, and therefore exhibit a strong hydroxyl group in their IR transmission spectra. The presence of water blocks IR transmission in a critical region of the spectra, but it can be avoided by selecting a synthetic route that yields water-free quartz for the preform fabrication. Mined quartz may contain traces of uranium or thorium, which emit alpha particles and can disturb delicate electronic circuits or signals. Uranium- and thorium-free quartz fibers afford quiet high-temperature circuit boards and/or electronic packaging.

Ultrapure silica or quartz fabrics are used to reinforce radomes, antenna windows for missiles, high-temperature circuit boards, and rocket nose cones. Braided yarns provide high-temperature electrical insulation, e.g., for coaxial cables, thermocouple wires, and space separators. Rovings are used to reinforce polymer matrix composites for ablative and electrical uses, as well as high-performance sporting goods, e.g., tennis racquets and skis, especially when hybridized with carbon fibers. Threads are used to stitch cable tray insulation for nuclear power plants.

1.2.1.2 Ultrapure Silica Fibers from Sol–Gels

An experimental dry spinning process can be used to make ultrapure silica glass fibers from tetraethylorthosilicate (TEOS) solutions in alcohol.

(a) Process concept. In a typical dry spinning process, a viscous solution is spun from, or extruded through, multiple spinneret orifices into a hot column that removes the solvent. The process resembles the typical commercial wet spinning process. In the wet spinning process, nascent filaments are extruded into an ambient environment. In the dry spinning process, they are extruded into a hot column that removes the residual solvent.

(b) Products and properties. Experimental fibers, which have been made from tetraethylorthosilicate (TEOS) sol–gel polymer, have an even higher purity level [39] than ultrapure silica fibers derived from quartz preforms [38]. Since the process relies on reagent grade $Si(OC_2H_5)_4$, the fibers contain 99.999% SiO_2 and absolutely minimal impurities (<1 ppm Al, OH^-, Na, and Cl). The process has been described in detail [1, 7, 36] and will only be reviewed here.

The first step is a polycondensation reaction [40]. TEOS is dissolved in pure ethanol (C_2H_5OH), and a dilute solution of the catalyst, hydrochloric acid (HCl), is added at <25°C. The reaction mixture is heated to 70–80°C, until the polymerization has reached a fiber-forming viscosity (Equations 1.1, 1.2, 1.3, 1.4 and 1.5):

$$(RO)_3Si-OR+HOH \rightarrow (RO)_3Si-OH+ROH(R=C_2H_5) \tag{1.1}$$

$$(RO)_3Si-OH+OH-Si(OR)_3 \rightarrow (RO)_3Si-O-Si(OR)_3+H_2O \tag{1.2}$$

$$(RO)_3Si-OR+OH-Si(OR)_3 \rightarrow (RO)_3Si-O-Si(OR)_3+ROH \tag{1.3}$$

for a chain-like polysiloxane polymer:

$$n\mathrm{Si(OR)_4}+\mathrm{H_2O} \rightarrow \mathrm{RO}-\underset{\mathrm{OR}}{\overset{\mathrm{OR}}{\mathrm{Si}}}-\left[-\mathrm{O}-\underset{\mathrm{OR}}{\overset{\mathrm{OR}}{\mathrm{Si}}}-\right]_{n-2}-\mathrm{O}-\underset{\mathrm{OR}}{\overset{\mathrm{OR}}{\mathrm{Si}}}-\mathrm{OH}+(2n-1)\mathrm{ROH} \tag{1.4}$$

for complete hydrolysis:

$$n\mathrm{Si(OR)_4}+4n\mathrm{H_2O} \rightarrow n\mathrm{Si(OH)_4}+4n\mathrm{ROH} \tag{1.5}$$

$$n\mathrm{Si(OH)_4} \rightarrow n\mathrm{SiO_2}+2n\mathrm{H_2O} \tag{1.6}$$

$$n\mathrm{Si(OR)_4}+2n\mathrm{H_2O} \rightarrow n\mathrm{SiO_2}+4n\mathrm{ROH} \tag{1.7}$$

In the second step [40] fibers are dry spun and drawn near a viscosity of log 2.5–3.0 poise. In the third step (Equations 1.6 and 1.7) the gel fiber is converted into a silica fiber by heating it with a low drawing tension in air to 800–900°C [40]. The gel fiber contains solvent and pendant C_2H_5O groups (Equation 1.5). Most of the

solvent is removed at <200°C and a porous fiber with a high surface area is obtained [37]. The pendant C_2H_5O groups are removed between 200 and 400°C. Weight loss and fiber shrinkage continue above 400°C. The silica fiber is sintered to full density (2.2 g/cm^3) at 900°C [37, 41].

Sol–gel-derived [42] and preform-derived silica fibers [1, 7, 36] are amorphous. Due to the disordered character of the SiO_4 tetrahedra skeleton, the density of glassy silica and silica glass fibers is lower than that of crystalline silicas (i.e., 2.2 g/cm^3 vs. 2.33 g/cm^3 for cristobalite and 2.65 g/cm^3 for quartz).

(c) Value-in-use and applications. Sol–gel-derived silica glass fibers with a 20 μm diameter have the highest purity of any type of silica fiber that is known. The purity can be selectively changed by adding components which cannot be added to silica preforms. Thus, they are therefore a superior compositional research and design tool.

Sol–gel-derived silica glass fibers have no commercial significance since they have low room temperature strength (800 MPa) [41] relative to that of E-glass (>3000 MPa) and other silica glass fibers (>5900 MPa). A further strength loss occurs when amorphous silica fibers are crystallized [43].

1.2.2 Pure Silica Sliver and Fabrics (95.5–99.5% SiO_2)

Pure silica sliver and fabrics (99.5–99.9% SiO_2) can be made from aqueous sodium silicate solutions [7, 44–46]. High silica fabrics (95.9–99.0% SiO_2) can be made by acid leaching of A- or E-glass fabrics [1, 36].

1.2.2.1 Pure Silica Sliver from Aqueous Solution

The preparation of pure silica sliver from aqueous silicate solutions is an adaptation of the dry spinning process that has been described in Section 1.2.1 for making ultrapure silica fibers from sol–gels. Both processes have their origin in the generic dry spinning process that has been practiced for over 50 years to fabricate acrylic fibers (Table 1.5). A commercial product that is currently being

Table 1.5 Dry spinning and sol-gel processing [7] (with kind permission of Springer Science and Business Media)

Process	Dry spinning	Dry spinning	Sol-gel
Solute	Acrylic polymer	Water glass	Tetraethoxylsilane
Solvent	Dimethylformamide	Water	
Solidification	Remove DMF	Remove water	Remove alcohol
Wet treatment	Remove DMF	Remove Na^+	
Drying step	Remove water	Remove water	Remove alcohol
Precursor fiber		Is not isolated	Is wound up
Consolidation		In-line step	Separate step
Process steps	One or two	One	One or two
Final product	Commercial fiber	Commercial fiber	Commercial fiber

made by dry spinning silica sliver from aqueous water glass solutions is known as Silfa yarn [47].

(a) Process concept. The inorganic dry spinning process can be used to make experimental continuous silica fibers but, so far, not commercial continuous multifilament yarns. It is also used to make commercial sliver yarns starting with an aqueous water glass solution. A sliver yarn is a continuous assembly of cohesive, slightly bonded staple fibers in an essentially parallel arrangement.

The commercial process (Fig. 1.6) utilizes a viscous solution of water glass in water and proceeds in 13 stages. A viscous water glass solution is extruded (1) through tiny spinneret holes (orifices) into a drying chimney (2). A spin finish is applied to the resulting sodium silicate filament yarn by a kiss roll (3). The yarn is taken up by a drawing drum and scraped off prior to complete rotation on the drum, intermingled in a conical chamber and drawn laterally (4). The resulting sodium silicate sliver (a cohesive staple yarn) is transported over a godet (5), placed on a conveyer belt and passed through an acid bath (6), a washing station, (7) and a drying zone (8). Silica sliver is formed in the calcining zone (9), and a textile sizing is applied (10) before it is dried (11), further intermingled in air (12) and wound onto a bobbin (13).

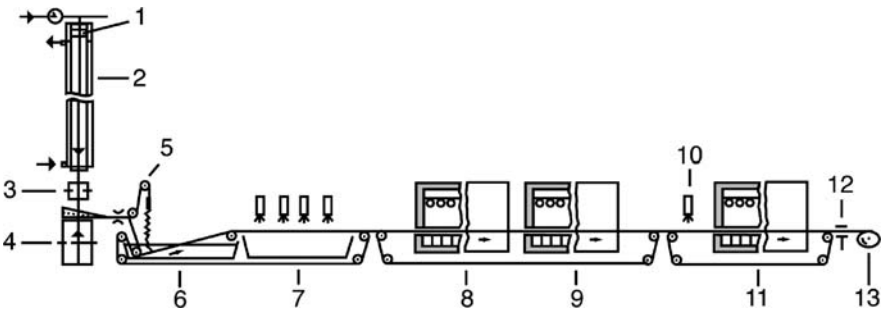

Fig. 1.6 Process for the fabrication of silica sliver from water glass. Redrawn from Achtsnit [152]

The drying step in the continuous process sequence is carried out at ∼150°C. It removes free water and produces sliver yarn containing weak nanoporous silica fibers with a highly hydroxylated surface. Consolidation of the nanoporous fibers within the continuous process sequence at 800°C causes the fibers to dehydroxylate and shrink, and also to increase in strength.

(b) Products and properties. This process facilitates the formation of pure silica Silfa sliver having linear densities of 135–330 g/1000 m of yarn [47]. The individual staple fibers have a length ranging from 50 to 1000 mm and an average diameter of 10 μm. Individual silica fibers have a lower density (1.8–2.0 g/cm^3) than E-glass (2.5 g/cm^3) and crystalline ceramic fibers (3.5 g/cm^3). Unconsolidated fibers are nanoporous and weak and have a density of 1.8 g/cm^3, but consolidated fibers are solid, moderately strong, and have a density of 2.0 g/cm^3. They retain their strength up to 1000°C.

Commercial Silfa silica sliver [46, 47] derived from water glass have a higher impurity level than downdrawn silica fibers. The impurities include 450 ppm Al, 206 ppm Fe, 120 ppm Na, and <0.5% water. And the process resembles the sol–gel process for dry spinning ultrapure silica fibers [1, 7]. At room temperature, their pristine strength is one-half that of ultrapure silica fibers derived from preforms (1.7 GPa vs. 3.4 GPa). At 600°C, the pristine strength of both fibers is the same (1.4 GPa). Between 600 and 1000°C, it is also identical but drops to 0.9 GPa.

In summary, the purity and cost of silica fibers made from water glass is much lower than that of downdrawn silica fibers from pure silica preforms and that of sol–gel-based silica fibers made from pure tetraorthosilicate. Furthermore silica fibers derived from water glass are not available as continuous filaments, only as sliver. Yet in high-temperature applications, the performance of dry spun and downdrawn silica fibers is nearly the same.

(c) Value-in-use and applications. Dry spun silica fibers made from water glass are less costly than downdrawn silica fibers, and may find increasing use in high-temperature markets except those requiring high specific strength at high temperatures, e.g., in aircraft or aerospace applications, or in high-temperature applications requiring high radiation resistance or electromagnetic shielding. Selected products include plied yarns for weaving narrow and broad fabrics, braided and twisted ropes, and sealings and sleevings for high-temperature uses, including turbine insulation, removable flexible insulation, and compensators [46, 47].

1.2.2.2 Acid-Leached E- and A-Glass Fabrics (95.0–95.5% SiO_2)

High silica glass fibers (95–99.5% SiO_2) represent the lowest cost variant of silica fibers. They also represent the weakest form of silica fibers. They are therefore not commercially available in fiber or sliver form. They must be obtained by leaching of E-glass fabrics and are available only in fabric form.

(a) Process concept. In the United States, borosilicate E-glass fabrics are leached with aqueous HCl solutions. A typical commercial product is called Refrasil. In Russia and Japan, sodium silicate A-glass fabrics with SiO_2/Na_2O ratios of 3:1–4:1 are leached with aqueous H_2SO_4 or HNO_3 solutions [1, 6, 7, 36]. Leaching removes nearly all oxides except SiO_2.

Leaching must be carried by leaching woven, braided, or other pre-designed E-glass or A-glass fabrics because the individual yarn strands are too weak after leaching to survive weaving. Almost all alumina, magnesia, calcia, iron oxide, and boron oxide [48] can be extracted from E-glass fibers in 8 h at 95°C in dilute H_2SO_4. Leaching proceeds by ion diffusion. The chemical nature of the acids does not affect leaching kinetics [6].

(b) Products and properties. High silica glass fibers containing 95–98% SiO_2 become porous on leaching [1]. The leached fabrics are sintered to turn the porous fiber structure into a solid silica structure. The resulting high silica fabrics can be used from room temperature to 1000°C. But because of their ultralow strength,

even the resulting high silica fabrics can be used only in non-load-bearing end uses. Pristine fiber strength decreases from room temperature (0.4 GPa) to 1000°C (0.1 GPa). Application of a chromium oxide coating increases the upper in-use temperature to 1200°C for long-term and multiple-cycle heat loads [6]. With increasing temperature, the decrease in fabric strength is accompanied by removal of water from the hydroxylated fiber surfaces and by increasing nanocrystallinity that may cause slight fabric shrinkage.

(c) Value-in-use and applications. High silica fabrics obtained by acid leaching of E-glass were introduced in the 1960s for aircraft and aerospace applications. Their use has declined in these applications by the advent of ultrapure and pure silica fibers which are stronger and can be woven and braided, but they are also more expensive. They are very desirable and cost-effective heat-insulating materials for less demanding uses than those which require pure or ultrapure silica fibers. Among others, they are used as high-temperature filtration media for ferrous, non-ferrous, and corrosive metals, as reinforcement for polymer composites, and as heat-resistant electrical insulation in nuclear reactors [1, 6, 7, 36].

1.2.3 Summary and Conclusions

Silica fibers, irrespective of process, are amorphous, including those called quartz fibers. Ultrapure silica fibers (99.99–99.999% SiO_2) can be formed by downdrawing from preforms or by dry spinning from a viscous tetraethylorthosilicate solutions. Pure silica sliver (95.5–98.9% SiO_2) can be formed by dry spinning from aqueous water glass solutions. High silica fabrics (95.0–95.5% SiO_2) are obtained by acid leaching A- or E-glass fabrics.

At room temperature (Table 1.6), the strongest fiber is S-glass (4.6 GPa), followed by E-glass (3.5 GPa); Nextel, a glass ceramic fiber (2.6 GPa); Astroquartz, an ultrapure silica fiber (2.4 GPa); Silfa, a pure silica sliver (1.7 GPa); a sol–gel-derived experimental ultrapure silica fiber (0.9 GPa); and Refrasil, a high silica fabric (0.4 GPa). Only S-glass, E-glass, Nextel, Astroquartz, and Silfa fabrics can be used in load-bearing applications.

Table 1.6 Tensile strength of high- and ultrahigh-temperature glass [36] (with kind permission of Springer Science and Business Media)

	Silicate		Silica		Ultrapure silica		
Strength (GPa)	E-glass	S-glass	High	Pure	Preform	Sol–gel	Nextel aluminate
RT,°C	3.5	4.6	0.4	1.7	2.4	0.9	2.6
400, °C	1.8	3.8	0.2	1.6	1.8	0.9	2.4
600,°C	0.9	2.4	0.1	1.4	1.4	0.9	2.4
800, °C	–	0.7	0.1	1.2	1.0	0.1	2.1
1000, °C	–	–	0.1	0.9	0.9	0.1	1.9
Cont. use	600°C	815°C	1040°C	1090°C	1090°C	1090°C	1200°C
Rel. cost	1	6	10	30	68	80	150

Borosilicate E-glass fibers support continuous use to 600°C, S-glass to 815°C, high silica glass fibers to 1040°C, pure and ultrapure silica glass fibers to 1090°C, and Nextel to 1200°C. The estimated cost per kilogram of fiber increases by a factor of 150, while the estimated continuous in-use temperature doubles.

1.3 Silicate Glass Fibers (50–70% SiO_2, 1–25% Al_2O_3)

The commercial process for forming continuous fibers from strong viscous silicate melts in a conventional furnace has been authoritatively reviewed in 1986 [49], 1988 [50], 1989 [51], 1993 [52], 1999 [1], and 2001 [53].

1.3.1 Forming Glass Fibers from Strong Viscous Melts

This section offers an overview of the generic process. Two specific advances have, however, been made in the last 10 years and will be discussed. One is the development of a novel plasma glass melting process [54] and the other is modeling of fiber drawing technology [55].

1.3.1.1 Critical Properties of Strong Viscous Melts

A generic strong viscous silicate melt is formed at a viscosity of log 1.7–log 2.0 poise, flows through the melt furnace at a viscosity of log 2.0–log 2.5 poise, and fibers are formed at a viscosity of log 2.5–log 3.0 poise. The fiber-forming temperature at a viscosity of log 3.0 poise must exceed the liquidus temperature by at least 50°C to avoid devitrification in the furnace, forehearth, and/or bushings.

The softening point represents the temperature at which the viscosity is log 7.65. At this temperature a glass fiber deforms under its own weight. The annealing point represents a temperature at which the viscosity is log 13.0. The strain point represents a temperature at which the viscosity is log 14.0. The strain point is near the glass transition temperature and approximately projects the highest tolerable in-use temperature.

1.3.1.2 Commercial Manufacturing Process

E-glass with 5–7% B_2O_3 [49] has been selected as the reference melt for the following overview of the highly automated process shown in Fig. 1.7. The furnace consists of three process sections. The ingredients are selected, weighed and mixed, and then entered into a furnace. In the first section of the furnace, the commercial batch ingredients are melted, gaseous inclusions are removed, and the melt is homogenized at ~1370°C. The melt flows into the refiner section where the temperature of the melt is reduced to ~1260°C [53]. The refined glass melt then enters the forehearth section that is located directly over fiber-forming stations and bushings.

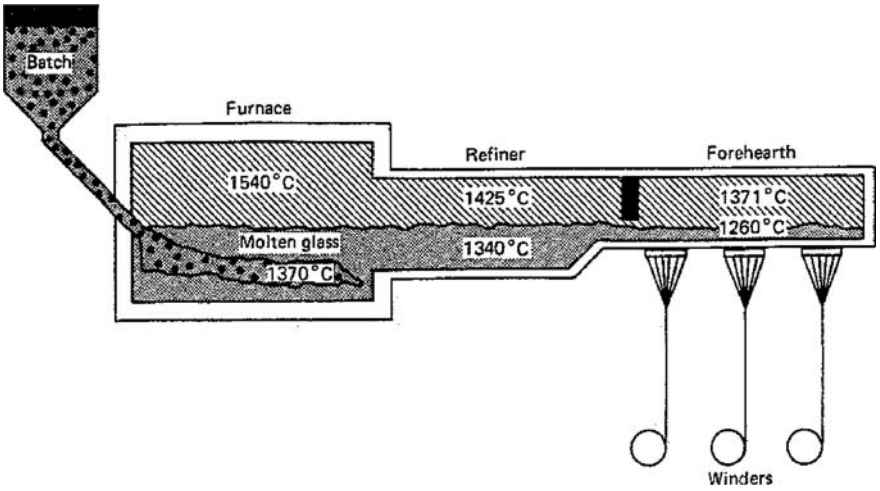

Fig. 1.7 Commercial furnace for melting fiberglass compositions [1, 53] (reprinted with permission of ASM International. All rights reserved www.asminternational.org)

Depending on the fiber diameter, optimum fiber formation is obtained with a melt viscosity ranging from log 2.5 to 3.0 poise as the molten glass passes through the bushing tips. The fibers are drawn down and cool rapidly. After the sizing is applied [53] the filaments are combined in a yarn bundle or strand and delivered to a forming winder, a direct draw winder, or a chopper (Fig. 1.8). A typical multifilament bushing can have 400–8000 tips and the resulting yarn will therefore have a corresponding number of filaments.

The commercial melting and forming process can be used for boron-free Chinese C- (or CC-)glass with >10% Na_2O, E-glass with ~6% B_2O_3, boron-free E-glass, essentially boron-free E-glass with <1.5% B_2O_3, boron-free ECR-glass with >2% ZnO, and boron-free S-glass (Table 1.7), as well as for other strong silicate melts with up to 75% SiO_2, i.e., as long as the bushing alloys and refractory materials can withstand the process temperature. The boron-free CC-glass is compositionally related to the boron-free A-glass that is no longer made in the United States, and it should not be confused with the former C-glass that contained boron and is likewise no longer available in the United States (see Section 1.3.3.5).

As shown in Table 1.7, the log 3 forming temperature (log 3 FT) of E-glass melts with ~6% B_2O_3 [1, 49] is 8°C higher than that of soda-lime-silica CC-glass melts [1, 2, 52]. The log 3 FT of essentially boron-free E-glass melts (<1.5% B_2O_3) is 23°C higher [2, 49, 56]. The log 3 FT of boron-free E-glass melts is 67°C higher [1, 25, 56]. The log 3 FT of boron-free ECR-glass melts (>2.0% ZnO) is 38°C higher [2, 57], and the log 3 FT of boron-free S-glass melts is 368°C higher than that of soda-lime-silica CC-glass melts. All melts have a delta temperature of >50°C, that is required to achieve a crystallization-resistant melt in a continuous commercial furnace.

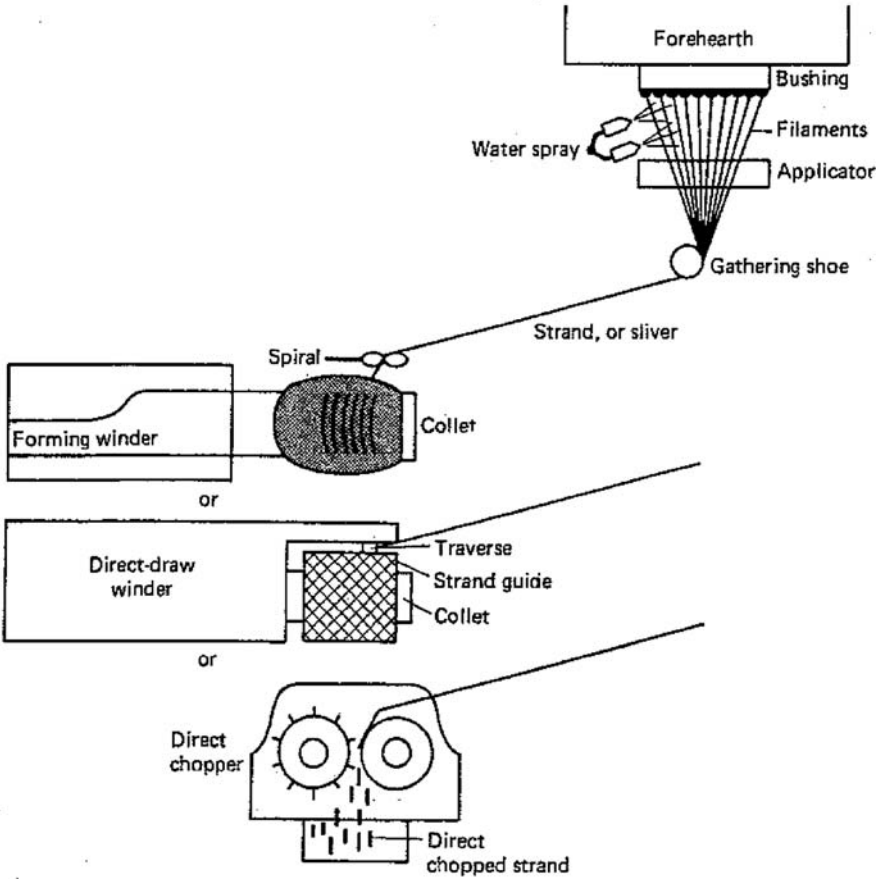

Fig. 1.8 Forming winders, direct-drawing winders, and choppers [1, 53] (reprinted with permission of ASM International. All rights reserved www.asminternational.org)

Energy cost, platinum losses at the bushings, and refractory wear rise with a rising viscosity or log 3 forming temperature. Reinforced bushings, bushings with high Rh content, and more frequent refractory replacement may therefore be needed. All compositions listed in Table 1.7, except S-glass, can be and are made in large conventional furnaces and with large bushings. The viscosity (or log 3 forming temperature) of S-glass melts is so high that a smaller furnace and smaller bushings from special alloys may be required.

In summary, the original E-glass contains $\leq$1% fluorine and $\sim$6% B_2O_3 and has a log 3 forming temperature of <1200°C [58]. Borosilicate melts with $\sim$6% B_2O_3 in Table 1.7 may emit boron and fluorine into the environment and may therefore require the installation of additional and costly emission control equipment. The fluorine- and boron-free E-glass [59, 56] has a log 3 forming temperature of 1260°C. The fluorine-free and essentially boron-free E-glass has a log 3 forming temperature of 1215°C [21, 27].

Table 1.7 Glass fibers by the commercial melt process [1]

Composition	CC-glass	E-glass variants			ECR-glass	HS-glass
Boron content	0.0%	>6%	<1.5%	0.0%	0.0%	0.0%
Weight %						
SiO_2	65.15	54.5	56.50	60.10	58.2	65.0
Al_2O_3	7.70	14.0	13.45	12.99	11.6	25.0
B_2O_3	–	6.6	1.30	–	–	–
CaO	9.23	22.1	24.50	22.13	21.7	–
MgO	4.33	0.6	2.55	3.11	2.0	10.0
ZnO	0.20	–	–	–	2.9	–
TiO_2	–	–	0.55	–	2.5	–
K_2O	–	0.2	–	0.63	–	–
Na_2O	12.92	0.8	0.90	0.14	1.0	–
Fe_2O_3	0.27	0.2	0.25	0.25	0.1	–
F_2	0.96	0.5		–	tr.	–
Log 3 FT, °C	1192	1200	1215	1259	1230	1560
LT, °C	1068	1064	1157	1174	1163	1500
Delta T, °C	123	136	58	85	67	60
Density, g/ccm		2.54	2.62	2.67	2.68	2.49
Strength, GPa	–	3.40	3.5	3.5	3.5	4.6
Modulus, GPa	–	72	81	81	80	88
References	[91]	[58]	[21, 27]	[59, 56]	[52, 57]	[50]

Fluorine-free and either boron-free or essentially boron-free E-glass variants are clearly more environmentally friendly than borosilicate E-glass. And the fluorine-free and essentially boron-free E-glass may be considered to be both energy- and environmentally friendly on the basis of its low log 3 forming temperature. The design of energy- and environmentally friendly E-glass compositions since 2000 will be reviewed in detail in Chapter 2.

1.3.1.3 Experimental Plasma Melt Process

In the typical fiberglass process, that is the backbone of the fiberglass industry, the energy sources are oil, natural gas, or electrical heat, and the throughput is measured in hours [1]. In recent years, extensive research has been conducted into glass melting with high-intensity DC arc plasmas. The still experimental technology differs in several ways from conventional glass furnace technology [54]: It will be described here by way of a brief review. Chapter 11 describes the technology in detail:

- It uses DC electrical arc plasmas
- It has energy densities that are 2.5 times greater than conventional electrical melting, resulting in more rapid melting [60]
- It has a small melter footprint, typically 1–2 m in diameter resulting in significantly lower capital costs
- It is highly flexible in converting from one glass composition to another
- It is capable of melting high-temperature glasses and other materials

Early work into the application of plasma melting was conducted by both Johns-Manville in the mid- to late 1980s [60, 61] and the British glass industry in the mid-1990s [62]. This body of work showed promising results of efficient specialty glass melting systems approaching 4 million BTU/ton, but both projects suffered from the lack of a reliable DC electrical torch design. Most recently, Plasmelt Glass Technologies has completed a DOE-sponsored project in which the torch design and operational systems were specifically addressed and significantly improved [63].

The technology involved in plasma melting uses the skull-melting concept in which the glass-batch forms its own refractory liner, using a high thermal gradient from the hot spot to the outer container. If properly designed and operated, the melter does not require water-jacketing or refractory liners, which greatly improve its energy efficiency. The small glass volume gives the melter a short response time, which has positive and negative aspects.

The benefits include immediate feedback on process adjustments, reduced process development times for new glasses, and rapid turnover for converting from one glass formulation to another. These attributes make the melter an ideal design for small, low-cost, research melting applications in which several melts of various compositions are desired.

Perhaps the main application of the new process is as a pilot melter for the continuous melting of smaller tonnages of newly developed R&D glasses beyond the laboratory scale, prior to the need for high production volumes. For applications requiring low seeds, insufficient refining time must be addressed by add-on refiners.

The experimental plasma melting process can melt a broad range of fiberglass compositions at throughputs at several hundred pounds per hour [54]. Most of the work on plasma melting has focused on making direct melt E-glass patties that were shown to be suitable for fiberizing in marble re-melt bushings. Zero stones, minimal cord, and high seeds were a common feature of these patties. The high seed levels do slightly increase the fine fiber break rates during fiberization, unless mitigated through add-on refining.

Other glasses have also been melted by Plasmelt (but not fiberized) using this technology [54] and they include boron-free E-glass, S-glass, C-glass, AR-glass, high-boron–low DK-glass, frit compositions, and mineral melts (including wollastonite, anorthite, albite, zircon, and kaolinite). Using cold batch to start up, rapid melt pool development and rapid startup of all glasses – even high electrically resistant glass compositions that are difficult to melt via conventional technologies – are routinely possible.

In summary, the benefits of using plasma melting are most directly applicable to those specialty fiberglass applications involving small tonnages, requiring intermittent production, rapid product changes with minimal scrap, high temperatures beyond conventional electrical melting systems, laboratory glass melting of wide-ranging compositions, or as a continuous pilot melter to produce tonnages of new experimental glass candidates before they reach production quantities.

1.3.1.4 Modeling of Glass Fiber Drawing

A computer model has recently been developed [55] for an industrial-scale, single-position fiber drawing tower and a dual package winder to anticipate break levels in the continuous commercial glass fiber drawing process.

In a typical continuous fiber-forming process, a vertical jet is generated [50] as the molten glass, which has a viscosity of log 2.5–3.0 poise, is extruded through a nozzle, called bushing tip. The jet is cooled as it is exposed to the atmosphere that surrounds it and it is simultaneously attenuated (Fig. 1.7) by the mechanical tension that is applied to it by the winder speed.

Any fiber-forming process would be perfectly continuous if (1) the mixed batch ingredients result in a perfectly uniform and melt at uniformly one end of the melt furnace; (2) a perfectly homogeneous melt results and reaches the other end of the furnace, i.e., the forehearth; (3) each jet at each bushing tip has the same diameter and cooling rate; and (4) each resulting fiber receives the same windup tension. Any deviation from this ideal behavior along can and does cause either breaks at the bushings or weak and more fragile fibers.

The recent computer modeling study [55] that has been developed (1) deals with process analysis and computer simulation of homogeneous melts from uniformly mixed ingredients for an experimental pilot plant process with a single position 200-tip bushing and (2) demonstrates how to achieve optimum jet cone shapes, fiber-forming stresses, fiber strength, and breaks at the bushing. The modeling study does not address the issue of how to achieve (1) uniformly mixed batch ingredients and (2) homogeneous melts.

1.3.2 General-Purpose Silicate Glass Fibers

Fiberglass is the world's most important continuous inorganic composite reinforcing fiber [52, 36, 20]. Commodity or general-purpose fibers are called E-glass. They contain 50–60% SiO_2, 10–15% Al_2O_3, and 0–7% B_2O_3 and are characterized by universal applicability, large sales volumes, and low unit cost. They represent ~99% of the commercial fiberglass market. The former A-glass in the United States and the current C-glass in China are alternate low-cost substrates containing 65–70% SiO_2, 1–7% Al_2O_3, and 0% B_2O_3.

1.3.2.1 Borosilicate E-Glass Fibers

Two variants of the commercial general-purpose E-glass fiber are on the market [36, 20]. The original variant is based on a calcium aluminum borosilicate glass composition [49] that generally contains 5–7% B_2O_3 and <1% fluorine. The more recent, and environmentally friendly, variant is based on a fluorine-free calcium magnesium aluminum silicate glass composition that is either boron-free [36] or essentially boron-free [20].

(a) Industry E-glass specifications. A fiberglass product that is sold as an E-glass must meet the compositional requirements of ASTM specification D-578-00 [64]. These requirements ensure that a product that is sold as an E-glass has about the same chemical composition, subject only to variations induced by the use and variations in local batch ingredients, and therefore the same in-use performance.

One specification governs a generic E-glass composition that is aimed at printed circuit board applications and the other is aimed at general reinforcement applications (Table 1.8). Since E-glass is an international commodity, other countries have similar specifications, e.g., DIN (Germany) and BS (the United Kingdom).

Table 1.8 ASTM E-glass specification D-578-00 [2, 64]

E-glass for printed circuit boards		E-glass for general applications	
Chemical	% by weight	Chemical	% by weight
B_2O_3	5–10	B_2O_3	0–10
CaO	16–25	CaO	16–25
Al_2O_3	12–16	Al_2O_3	12–16
SiO_2	52–56	SiO_2	52–62
MgO	0–5	MgO	0–5
Na_2O and K_2O	0–2	$Li_2O + Na_2O + K_2O$	0–2
TiO_2	0–0.8	TiO_2	0–1.5
Fe_2O_3	0.05–0.4	Fe_2O_3	0.05–0.8
Fluoride	0–1.0	Fluoride	0–1.0

There are notable differences between the two major E-glass specifications, but the primary difference pertains to the permissible percent boron content. An E-glass for printed circuit board applications must contain 5-10% B_2O_3, while an E-glass for general reinforcement applications may contain 0–10% B_2O_3. The use of Li_2O was approved by ASTM in 2000 [64] for use in general reinforcement applications but not for use in printed circuit boards.

(b) Commercial borosilicate E-glass fibers. The age of E-glass started in 1940 (Table 1.9) with a patent claiming new boron-free compositions near the eutectic in the quaternary SiO_2–Al_2O_3–CaO–MgO phase diagram [65] and with a product in 1943 claiming derivatives of the quaternary phase diagram modified with B_2O_3, fluorine, and Na_2O [66].

The batch cost was reduced in 1951 by simplifying the E-glass composition [67]. As a result, the B_2O_3 level was reduced from 10.0 to 5–7%, and the previously required addition of dolomite (4.5% MgO) was eliminated. But ~0.5% MgO continues to be present. It is due to an impurity (or tramp) in commercial batch ingredients. The reformulation of the E-glass composition [67] in 1951 represents a basic shift from a modified quaternary eutectic (60% SiO_2 – 9% Al_2O_3 – 27% CaO – 4% MgO) to a modified ternary eutectic (62.2 SiO_2 – 14.5% Al_2O_3 – 23.3% CaO), excluding tramp. This specific E-glass variant [67] has since become the generic borosilicate E-glass standard.

(c) Boron- and fluorine-free E-glass fibers. By the 1960s, concerns arose about the effect of boron and fluorine when emitted from a melt in a commercial furnace

Table 1.9 Evolution of commercial general-purpose E-glass fibers [36]

Year	1940	1943	1951	1996	2000
Composition, wt%					
SiO_2	60.0	54.0	54.5	60.01	56.50
B_2O_3	–	10.0	6.6	–	1.30
Al_2O_3	15.0	14.0	14.0	12.99	13.45
CaO	20.0	17.5	22.1	22.13	24.50
MgO	5.0	4.5	0.6	3.11	2.55
TiO_2	–	–	0.5	0.55	0.55
Na_2O	–	–	0.8	0.63	0.90
K_2O	–	–	0.2	0.14	–
Fe_2O_3	–	–	0.2	0.25	0.25
F_2	–	–	0.5	0.04	–
Log 3 forming temp., °C	1288	1200	1200	1259	1215
Liquidus temperature, °C	1233	1120	1064	1174	1157
Delta temperature, °C	55	80	136	85	55
Pristine strength, GPa	3.6	3.2	3.3	3.5	3.5
Added emission control	No	yes	yes	no	no
References	[65]	[66]	[67]	[59, 56]	[21, 27]

into the environment. Boron oxide is a costly batch ingredient and up to 15% of the added boron can volatilize. Fluorine [36] causes a similar problem and can emit fluorides into the atmosphere. The atmospheric temperature above the melt in most E-glass furnaces is between 1400 and 1500°C and, in the exhaust, boron and fluorine can react with potassium, sodium, and sulfur oxides to form particulates which are then emitted from the melt into the environment [36].

The emission of particulates was therefore regulated in North America and Europe. As a result, new and costly pollution control devices were required for the production of fluorine containing high-boron E-glass aimed at printed circuit board applications. And new fluorine- and boron-free, as well as new fluorine-free and essentially boron-free, E-glass compositions were therefore designed and commercialized for use in general reinforcement applications.

The first environmentally friendly boron- and fluorine-free E-glass variant that meets the ASTM specifications for general reinforcement applications was patented in 1985 [68] and the first environmentally friendly boron- and fluorine-free E-glass was commercialized in 1996 [59]. Two fluorine-free and essentially boron-free E-glass variants became known between 1997 and 2000 [2, 20, 150].

(d) New energy-friendly E-glass compositions. The log 3 forming, liquidus, and delta temperatures of a specific compositional variant that is based on the same set of oxides can change significantly with relatively minor percent changes of its oxides, specifically SiO_2, Al_2O_3, CaO, MgO, and B_2O_3. Several compositional design and/or reformulation studies were carried out between 1998 and 2008 to achieve the lowest log 3 forming temperature for a range of fiberglass compositions with a delta temperature >50°C [2, 20, 21–25, 26, 27].

The design of new eco-friendly fiberglass compositions is based on four premises: (1) the desired composition must have the lowest log 3 forming temperature (melt temperature at a viscosity of log 3 poise) and a crystallization-resistant delta between log 3 forming and liquidus temperatures; (2) the most energy- and environmentally friendly variant that meets these requirements must be fluorine-free and boron-free or essentially boron-free; (3) the target composition must be cost-competitive within the industry; and (4) E-glass compositions must meet the ASTM specifications.

Many new fluorine-free compositional variants were designed since 2000. Some were boron free [2, 20, 23], others contain <2% ZnO [2], ≤1.5% B_2O_3 [21], ≤1% Li_2O [22], as well as ≤1% Li_2O and ≤1.5% B_2O_3 [24]. The design of both energy- and environmentally friendly compositions and the effect of key oxides on melt viscosity, liquidus temperature, and energy demand [25, 26, 27] will be discussed in detail in Chapter 2.

1.3.2.2 E-Glass Properties and Fiber Structures

E-glass is mostly used to reinforce composite structures and, as such, it is the lowest cost candidate with the widest range of applications. E-glass has therefore become the benchmark for the product designer against which the value-in-use of other organic and inorganic fibers must be evaluated. The commercial composite applications of E-glass are discussed in Chapter 3.

(a) Mechanical properties. The mechanical properties of the general-purpose borosilicate and boron-free E-glass fibers are comparable (Table 1.9). Specifically, single filament strength (3.4–3.5 GPa) and elongation-at-break (4.5–4.9%) are about the same for both fibers, but the modulus of borosilicate E-glass is lower (72 GPa vs. 81 GPa) than that of the boron-free E-glass [59, 56]. Tensile strength and break elongations were determined by ASTM method D2101 at 23°C (2-in. gauge). The modulus was obtained by the sonic method [56].

Fibers are purchased on a cost-per-weight basis but they are generally tested on a function-per-weight basis. Two derived properties that are important to the product designer are specific fiber strength and specific fiber modulus, i.e., strength and modulus corrected for density or weight at equal volume. For composites aimed at weight-sensitive transportation uses, a similar correction is often applied to compare the weight of different reinforcing fibers at an equal fiber volume fraction.

Figure 1.9 compares the specific tensile properties of important reinforcing fibers [36, 56]. Borosilicate E-glass serves as the reference point since it offers a universally acceptable balance of properties at the lowest cost. The other inorganic fibers offer specific mechanical properties, which are not attainable with E-glass. But, S-glass, a generic high-strength fiber, costs ∼5× as much as E-glass. Carbon or aramid fibers cost ∼10× as much as E-glass and boron or SiC fibers cost >100× as much as E-glass. These inorganic reinforcing fibers offer increasing value-in-use with increasing cost. Still, E-glass continues to serve as the reinforcing fiber of choice composites having the highest sale volumes and lowest cost.

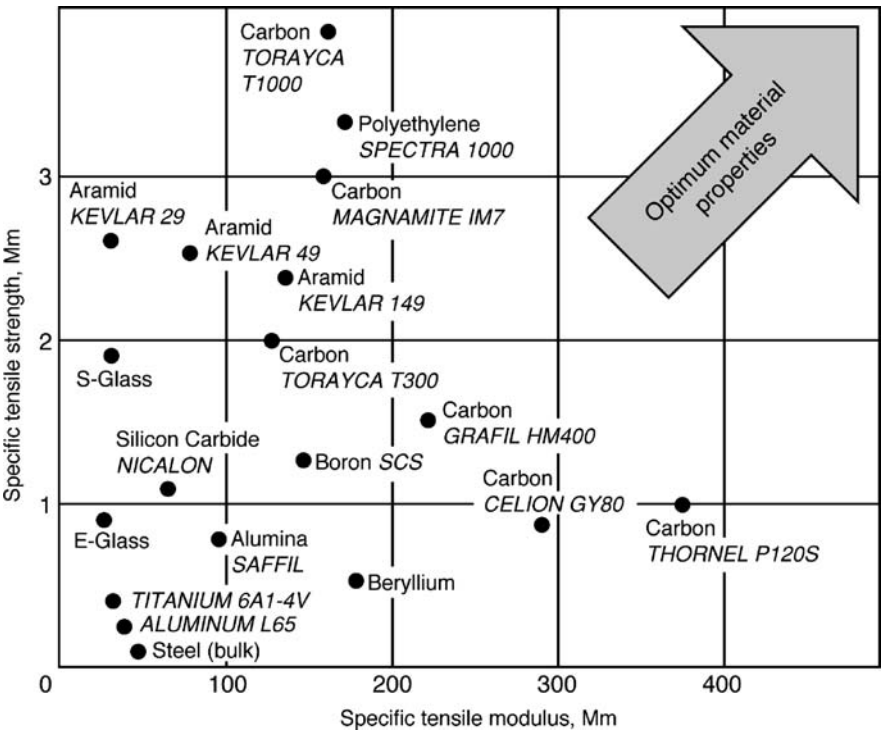

Fig. 1.9 Specific tensile properties of advanced reinforcing fibers. Redrawn from Starr [1, 71] (with kind permission of Springer Science and Business Media)

(b) Other glass fiber properties. Among the general-purpose fibers, the boron-free E-glass fibers exhibit higher acid resistance than borosilicate E-glass fibers (Table 1.10). In this test [56], single filament fibers were weighed, immersed in a 10% sulfuric acid solution for a period of 24 h, and re-weighed. The weight loss for borosilicate E-glass exceeded 40%; that for boron-free E-glass was less than 5%. After 499 days in a 5% sulfuric acid solution, a spray gun laminate made from boron-free E-glass lost half as much flexural strength as a comparable laminate made from a boron-containing E-glass fiber.

Table 1.10 Physical properties of commercial general-purpose E-glass fibers [36] (with kind permission of Springer Science and Business Media)

Fiber properties [59, 56]	Test method	Unit	w/6.6% B_2O_3	w/0.0% B_2O_3
Wt. loss, 10% H_2SO_4	Bare fibers	%/24 h	40	>5
Softening point	ASTM C 338	°C	830–860	916
Refractive index	Oil immersion	Bulk glass	1.547–1.562	1.560–1.562
Thermal expansion	ASTM D 696	ppm/°C	5.4	6.0

Borosilicate and boron-free E-glass exhibit equivalent corrosion resistance and modulus retention in water tests. The acid resistance of boron-free E-glass [68, 59] and of essentially boron-free E-glass with $\leq$1.5% B_2O_3 [2] is higher than that of major borosilicate E-glass variants with 5–7% B_2O_3 [1, 2] and of a minor variant with 4.26% B_2O_3 [69] that is not governed by ASTM E-glass specifications [64].

Boron-free E-glass fibers [56] have a higher softening point and estimated upper service temperature. The softening point of a fiber is the temperature at which a fiber will deform under its own weight. The estimated upper service temperature of a given fiber is the temperature at which it retains useful strength. The softening point of boron-free E-glass is 56–86°C higher than that of the borosilicate E-glass (Table 1.10) and affords a higher useful service temperature (<700°C vs. <600°C). This product advantage is the result of a process penalty, namely its fiber-forming temperature [59].

The electrical properties of both general-purpose glass fibers are comparable (Table 1.11). The refractive index is a property of considerable importance with regard to the appearance of a glass fiber in a laminate or composite. Electrical properties and the coefficient of linear expansion of borosilicate and boron-free E-glass were measured on bulk annealed samples. The differences in test results between both fibers are insignificant [56].

Table 1.11 Electrical bulk properties of general-purpose E-glass fibers [36] (with kind permission of Springer Science and Business Media)

Fiber properties [59, 56]	Test method	Unit	w/6.6% B_2O_3	w/0.0% B_2O_3
Dielectric constant	ASTM D150	23°C/1 MHz	6.9–7.1	7.0
Dissipation factor	ASTM D150	23°C/1 MHz	0.0001	0.0001
Dielectric breakdown	ASTM D149	V/mil	262	258
Volume resistivity	ASTM D257	Log 10/23°C	22.7–28.6	28.1

1.3.2.3 Commercial E-Glass Products and Applications

General-purpose E-glass fibers are the most important composite reinforcing fiber in today's market and they are used to serve a variety of markets: (1) rovings, yarns, chopped strands, and milled fibers; (2) woven rovings, weaver yarns, and braids; and (3) chopped strand, continuous and combination mats.

Rovings are essentially untwisted bundles of fiberglass strands wound up in parallel on cylindrically shaped packages. They are used in open lay-up moldings, woven fabrics, rods, and tubes. Woven rovings are used for open lay and press moldings. Yarns [52] consist of twisted fiber bundles. Weaver yarns are used for electrical and aircraft laminates, insulating tape, window shades, and filtration applications. The major use is in printed circuit boards.

Non-woven mats consist of specific arrays of glass fibers, held together by a binder. A continuous strand mat that consists of fine strands of glass fibers held together by a resin binder or by stitch bonding is used in sheet molding and

reinforced thermoplastic sheeting. A chopped strand mat is a non-woven fabric consisting of a random array of chopped glass fiber strands. It is used to reinforce composites for use in boat hulls and decks, car bodies, sheeting, and tanks. A roofing mat is used to manufacture roofing shingles.

A databook [70] that lists all commercial E-glass fibers and a directory and databook [71] that lists all commercial carbon, silica, high-strength glass fibers, and other high-performance fibers including Kevlar are available. Chapter 3 describes the generic fiberglass composite design, engineering and markets since glass fibers are almost exclusively used as composite reinforcing fibers and discusses wind mill blades and the respective market which rely on fiberglass composites. Finally, Chapter 11 is devoted to discussing plasma melting in greater detail.

1.3.3 Special-Purpose Silicate Glass Fibers

Specialty glass fibers are niche products, which may contain up to 65% SiO_2 and 25% Al_2O_3 and a range of other oxides which provide premium properties. Specialty glass fibers are characterized by small sales volumes and high unit cost and support ∼1% of the fiberglass market.

1.3.3.1 Designations of Special-Purpose Fibers

Specialty glass fibers have superior functional properties relative to those of general-purpose E-glass fibers. Many other fiberglass variants are known by letter designations [50]. “S” stands for high strength, “A” for high alkali content, “M” for high modulus, “AR” for high alkali resistance, “C” for chemical durability, “CC” for Chinese C-glass, “D” for low dielectric constant, and “ECR” for high acid resistance. “Z” has been used, but not consistently, for Zr-modified compositions. All variants, except the former A- and C-glass and the present E-glass and CC-glass, are premium products.

1.3.3.2 High-Strength–High-Temperature Glass Fibers

This section deals with specialty glass fibers having commercially a desirable balance of high-strength, intermediate modulus (or stiffness), and high-temperature resistance.

(a) Process and products. Higher service temperatures are often a more important design factor than higher strength or higher stiffness. High in-use temperatures require a fiber composition with higher thermal stability than that of E-glass, i.e., higher forming temperature, higher process energy, and higher overall cost. Higher strength or stiffness alone does not necessarily require a more costly fiber.

For a fiber to be usable at higher service temperatures than that of E-glass, it must have a higher glass transition temperature, softening point, forming temperature, and liquidus temperature. With one exception, these fibers can be made in a conventional melt spinning process; special refractory furnace linings and special precious metal

bushings are required. The production of Sudaglass basalt fibers requires a different process [72]. Higher materials, process and energy cost translate into a premium price.

HS- and HT-glass fibers possess $\leq 1.3\times$ the strength of E-glass fibers (4.5 GPa vs. 3.4 GPa), $\leq 2\times$ the service or in-use temperature (1250°C vs. 600°C), and $\leq 3.4\times$ the stiffness or modulus (35–37 GPa vs. 72 GPa). In contrast, high-modulus (HM) glass fibers have a modulus of up to 132 GPa and ultrahigh-modulus (UHM) glass fibers can have a modulus up to 248 GPa.

Four typical high-strength high-temperature glass fibers shown in Table 1.12 are commercial products [36, 71]. S-glass [50] and Te-glass [73] are derived from the ternary SiO_2–Al_2O_3–MgO eutectic. R-glass [74] is derived from the quaternary SiO_2–Al_2O_3–CaO–MgO eutectic. Sudaglass [72], a basalt fiber, is based on natural sources and contains high levels of Fe_2O_3. It is not shown in Table 1.12. High-strength glass fibers [71] are suitable for use in typical high-temperature applications. For applications see next section.

Table 1.12 High-strength and high-temperature silicate glass fibers [36]

Glass fiber	S-glass	Te-glass	R-glass	Experimental HS-glass fibers		
Eutectic	Ternary	Ternary	Quaternary	Quaternary	Ternary	Ternary
Wt%						
SiO_2	65.5	65.0	60.0	54.28	64.5	67.5
Al_2O_3	25.0	23.0	25.0	25.53	24.6	15.3
MgO	9.5	11.0	6.0		9.4	15.5
CaO	–	–	9.0	7.57	0.5	–
BaO	–	–	–	12.62	–	–
ZrO_2	–	1.0	–	–	–	–
B_2O_3	–	–	–	–	1.0	–
TiO_2	–	–	–	–	–	1.5
Fe_2O_3	Tr.	0.3	–	–	–	–
Na_2O	Tr.	0.1	–	–	–	–
Properties						
Strength, GPa	4.6	4.7	4.4	–	–	1.2
Elongation, %	5.2	5.5	5.2	–	–	–
Modulus, GPa	88.95	84.3	86.0	–	–	95.3
Density, g/cc	2.53	2.49	2.52	–	–	2.70
Sp. Strength	1.85	1.90	1.74	–	–	0.45
Sp. modulus	35.37	34.0	34.0	–	–	35.3
SP, °C	1056	975	975	–	–	–
Service T, °C	<1000	<900	<900	–	–	<1295
References	[50, 36]	[36, 73]	[36, 74]	[75]	[6, 36]	[36, 78]

Typical HS-glass fibers perform well at high temperatures (900–1000°C) but it may not be the optimum composition for prolonged uses. A novel quaternary glass fiber that is based on 54.28% SiO_2, 25.53% Al_2O_3, 7.57% CaO, and 12.62% BaO has recently been claimed to give superior long-term high-temperature performance as sound-absorbing material in engine muffler uses [75]. It contains 11% less SiO_2

than S-glass, and it contains BaO instead of MgO (Table 1.12). Therefore it has a log 3 forming temperature of only 1478°C and a delta temperature of 83°C [76], while S-glass has a log 3 forming temperature of 1560°C and a delta temperature of 65°C [50].

ZrO_2 and B_2O_3 are fluxes (Table 1.12). The addition of 1% ZrO_2 to the S-glass or ternary SiO_2–Al_2O_3–MgO eutectic composition causes a major drop in melt viscosity [36, 73], and the resulting Te-glass fibers have an 81°C lower softening and a 100°C lower practical use temperature than S-glass fibers. The addition of 1% B_2O_3 has a similar, if not more, pronounced effect. It also reduces both softening point and service temperature.

The addition of 1.5% TiO_2 to a ternary composition (Table 1.12) was found to raise its modulus, density, and service temperature [73, 75, 77, 78]. The resulting experimental fibers have a 295°C higher service temperature than commercial S-glass fibers but the development of a major nanocrystalline phase reduces its overall strength by over 50%.

Importantly, commercial HS-glass fibers, e.g., S-glass, also have higher elongations at break than E-glass [79] and therefore also higher mechanical (not to be confused with fracture) toughness, which translates into higher damage, including ballistic impact, resistance (Table 1.12). To wit, the energy required to break a relatively elastic fiber is proportionate to the area under the stress–strain curve (Fig. 1.10). As a result, the ballistic impact damage resistance of S-glass is also higher than that of E-glass and of nominally stronger, but more brittle, standard modulus (SM) carbon fibers having only 1/10th the elongation at break [70, 71].

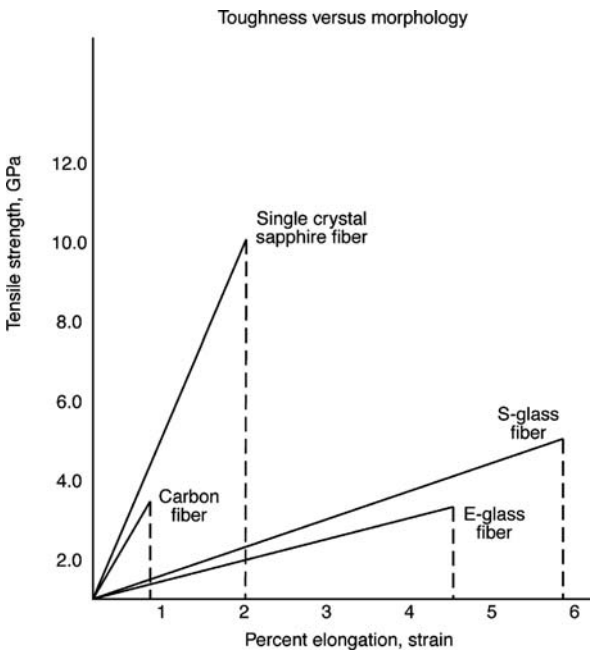

Fig. 1.10 Toughness and impact damage resistance of high-strength glass fibers [36] (with kind permission of Springer Science and Business Media)

Specific properties (properties divided by density) are a key design factor for transportation, especially aircraft, composites, where higher functionality at lower weight translates into higher value-in-use. At room temperature, HS-glass fibers (Table 1.12) have about equal specific strength (174–190 Mm) and specific moduli (34–37 Mm). General-purpose glass E-glass fibers have a specific modulus of 20 Mm at ∼1/5th the cost, and standard modulus carbon fibers have a specific modulus of 131 Mm at ∼2× the cost.

The utility of HS- and HT-glass fibers is ultimately determined by their softening point, the temperature above which a fiber will deform under its own weight. In practical terms, R- and Te-glass fibers retain usable functionality to about 900°C, B_2O_3–modified S-glass fibers to about 800°C, basalt fibers [72] to about 1000°C, and the TiO_2–modified glass ceramic fiber to 1295°C, while E-glass is limited to 620°C (Table 1.12). In contrast, the upper service temperature limit of unprotected carbon fibers is 350–500°C in an oxidative environment, that of coated carbon fibers is ∼1000°C in an oxidative environment, but that of uncoated carbon fibers is (1500°C in an inert environment such as helium.

HS-glass fibers retain useful properties at high temperatures. In the strand tensile test, a bundle of fibers is briefly exposed to a given temperature and broken. The strand tensile strength of R-glass, a typical HS-glass fiber shown in Fig. 1.11,

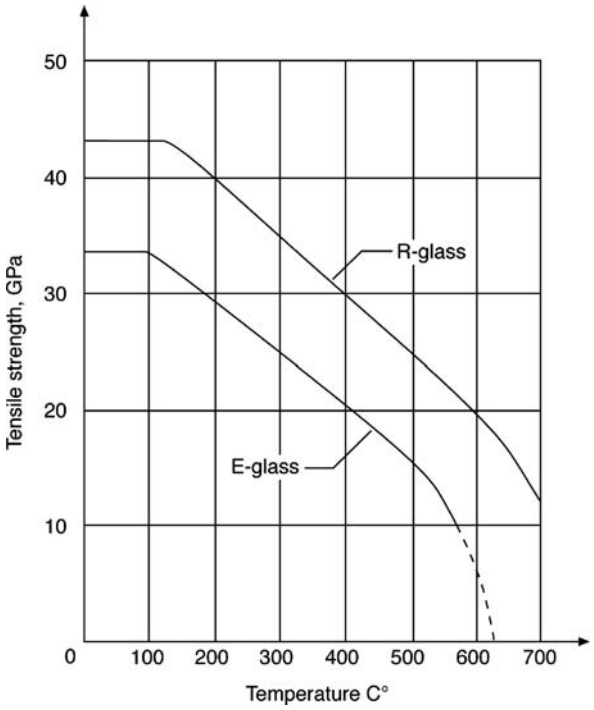

Fig. 1.11 Strength retention of R-glass and E-glass at elevated temperatures. Drawn from data contained in French patent 1,435,739, to Saint Gobain Company [74]

is higher than that of E-glass from room temperature to 750°C (and beyond). E-glass fails at ~600°C. In addition, it should be noted that the modulus of R-glass is also higher than that of E-glass over the entire temperature range tested, from room temperature to 750°C (and beyond).

In another tensile test, R-glass is exposed for prolonged periods of time to a specific elevated temperature before its strength is tested. At 750°C its tensile strength drops within the first 400 h to 1 GPa (or 1/4th its room temperature strength), but then remains nearly constant for at least the next 600 h of exposure. A temperature of 750°C is well beyond the reach of either of the two general-purpose E-glass fibers.

In summary, high-strength fibers have superior high-temperature resistance, superior impact damage resistance, high-strength retention at elevated temperatures, and a high, but lower modulus than high-modulus (HM) glass fibers. The formation of a nanocrystalline structure which facilitates the attainment of HS-glass fibers with the highest service temperatures tends to reduce strength, but in most cases this strength loss is minimal.

(b) Properties and applications. HS-glass fibers occupy an important niche in the composite reinforcement market between E-glass and the lowest cost carbon fibers. They are used in a variety of applications in the aerospace and aircraft industry, automotive industry, electrical and electronics industry, sporting goods industry, and military markets. The higher cost of other inorganic high-strength fibers can be reduced by hybridization, i.e., by designing composites reinforced with mixed HS-glass/carbon, HS-glass/aramid, or HS-glass/boron fibers.

In the aerospace and aircraft market HS-glass fibers are used because of their high specific properties and relatively low cost, e.g., in satellite components, motor cases, nose cones, aircraft flooring, cargo liners, and radome skin sheets. Their use in helicopter rotor blades benefits from the high damage resistance (toughness) of HS-glass fibers. In automotive composites, HS-glass fibers are used because of their high specific strength in pressure vessels and their superior toughness in leaf springs. Their use in compressed natural gas cylinders is one of the fastest growing applications.

In the electrical and electronics market, HS-glass fibers are used as strength members for optical fiber cables, printed circuit boards, and other cables, but mostly when high temperatures are involved. In sporting goods, they are used for product differentiation and because of their toughness in tennis racquets, squash racquets, fishing rods, surfboards, windsurfing masts, skis, archery bows, arrow shafts, and racing yachts.

In high-temperature applications, selected HS-glass fibers have been claimed to be a superior sound-absorbing material in engine exhaust mufflers [76]. In military markets, HS-glass fibers are used in aircraft fuel tanks because of their specific strength, and in rigid armor and helmets because of their superior ballistic impact resistance. They would be an ideal reinforcement for composite windmill blades but because of their high price they are less cost-effective in this application. For products and markets see Chapter 5.

1.3.3.3 High-Modulus–High-Temperature Glass Fibers

Conceptually, HM-glass fibers are achieved by adding BeO [50, 78], La_2O_3 [78], Y_2O_3 [6], or CuO [6, 78] to a typical HS-glass composition. HS-glass fibers have a modulus of 85–95 GPa while HM-glass fibers have a modulus of 100–132 GPa (Table 1.13). The addition of these oxides increases the fiber density, a fact that negatively affects their potential value-in-use [36, 80, 81]. In addition, these oxides are also known to be fluxes, and they should reduce the melt viscosity and therefore the log 3 forming temperature. Unfortunately, a systematic comparison of the properties (log 3 forming temperatures) of an unmodified base composition with compositions having the same levels of key modulus modifying oxides is not available.

Historically, the first HM-glass fiber contained 7.5% BeO. This fiber, YM-31A, had a higher density than a typical HS-glass fiber (2.60 g/cc vs. 2.53 g/cc), higher strength (5.1 GPa vs. 4.6 GPa), higher specific strength (1.96 vs. 1.85), a higher modulus (112 GPa vs. 95 GPa), and a higher specific modulus (43.0 Mm vs. 37.5 Mm). In summary, this composition affords the highest specific fiber modulus and the second highest fiber modulus among silicate glass fibers.

An HM-glass fiber with 5.0% BeO and 30.2% La_2O_3 also has a higher density (3.29 g/cc vs. 2.69 g/cc), higher strength than a typical HS-glass fiber (5.4 GPa vs. 4.6 GPa), lower specific strength (1.64 Mm vs. 1.85 Mm), the highest modulus (132 GPa) among silicate glass fibers, and second highest specific modulus

Table 1.13 High-modulus silicate glass fibers [36] (with kind permission of Springer Science and Business Media)

Modulus modifier	La_2O_3	ZnO	BeO	Y_2O_3	BeO/Y_2O_3
Composition, wt%					
SiO_2	50.0	45.8	50.0	52.6	36.2
Al_2O_3	32.5	–	35.0	35.8	20.5
CaO	–	11.0	–	–	–
MgO	12.5	7.7	7.5	5.4	8.1
La_2O_3	5.0	–	–	–	–
ZnO	–	22.4	–	–	–
BeO	–	–	7.5	–	5.0
Y_2O_3	–	–	–	6.2	30.2
ZrO_2	–	1.8	–	–	–
TiO_2	–	6.8	–	–	–
Li_2O	–	1.7	–	–	–
CeO_2	–	2.5	–	–	–
Fe_2O_3	–	0.3	–	–	–
Pristine properties					
Strength, GPa	4.8	–	5.1	4.5	5.4
Modulus, GPa	100	104	112	100	132
Density, g/cc	2.69	2.77	2.60	3.0	3.29
Sp. Strength, Mm	1.78	–	1.96	1.36	1.64
Sp. modulus, Mm	37.2	37.5	43.0	33.0	40.0
References	[78, 80]	[118]	[78]	[6]	[78, 80]

(40.0 Mm). Values for strength and therefore for specific strength must be accepted with caution for individual fibers for which no statistical support is available. Modulus data are more reliable for such compositions.

The addition of 22.4% ZnO and other oxides raised the density from 2.53 to 2.77 g/cc and the modulus from 95 to 104 GPa. Likewise the specific modulus remained unchanged (37 Mm). The effectiveness of BeO as a modulus builder is the result of the high field strength of the Be^{+2} ion and its ability to coordinate four oxygen ions tightly to it [1]. BeO has a wurtzite structure. The only other wurtzite structure with oxygen is ZnO, and $ZnSiO_4$ is isomorphous with Be_2SiO_4. On a molar basis, the ZnO-modified and the original BeO-modified YM-31A compositions are identical [36]. Because it has a higher density, ZnO is a less effective modulus builder than BeO.

The addition of 5.0% La_2O_3 (Table 1.13) raised the density of a typical HS-glass fiber from 2.53 to 2.69 g/cc and the modulus from 95 to 100 GPa. The specific modulus did not decrease but remained the same (∼37 Mm). The addition of 6.2% Y_2O_3 raised the density of a typical HS-glass fiber from 2.53 to 3.0 g/cc and the modulus from 95 to 100 GPa. The specific modulus dropped from 37 to 33 Mm. The addition of 26.8% Y_2O_3 and 4.3% La_2O_3 raised the density from 2.53 to 4.3 g/cc and the fiber modulus from 95 to 130 GPa. But the specific modulus dropped from 37 to 30 Mm.

These HM-glass fibers could be used only in applications which are not driven by the specific modulus, therefore not in aircraft, automotive, or windmill applications, which require a high specific modulus at the lowest possible cost. In both types of applications, carbon and aramid fiber reinforced composites afford much high stiffness at equal loading, i.e., a much higher modulus and specific modulus because of their low densities.

For example, the specific modulus of commercially available aramid fibers ranges from 40 to 122 Mm and that of commercially available carbon fibers ranges from 131 to 379 Mm [1, 71]. In contrast, the specific modulus of an unmodified HS-glass fiber is 37.5 Mm. When modified with 5.0% La_2O_3 or 7.5% BeO, the specific modulus of the resulting HM-glass fibers ranges from 37.2 to 43.0 Mm (Table 1.13).

BeO- and Y_2O_3/BeO-modified HM-glass fibers would not only be costly but also commercially unattractive because of known hazards involved in the process of handling BeO as an ingredient [36]. With regard to the others, the ingredient cost and availability rises from ZnO to La_2O_3 and Y_2O_3. Aside from availability and ingredient cost, CuO might be a useful modulus modifier but it affords melts with a deep blue color. So would be MnO, but it affords a dark brown color. Because of their dark color, both would increase the energy demand of the melt. For that reason they are not useful.

1.3.3.4 Ultrahigh-Modulus Glass Ceramic Fibers

By modifying the ternary SiO_2–Al_2O_3–MgO or the quaternary SiO_2–Al_2O_3–MgO–CaO eutectic compositions with appropriate oxide modifiers one can raise the fiber strength to 5.4 GPa (vs. 3.4 GPa for E-glass) and the fiber modulus to 132 GPa (vs.

72 GPa for E-glass). The increase in modulus is caused by an increase in internal order as evidenced by a change from an amorphous to a nanocrystalline structure.

An increase in fiber modulus up to 248 GPa can be achieved by inserting nitrogen into the oxide network [36], thus creating a nitride-modified silicate, Si–Al–O–N, or oxynitride glass fibers. This increase is caused by an increase in surface tension as evidenced by microhardness. Thus, one mechanism seems to depend on increasing structural order, the other on crosslinking.

(a) Process and products. Oxynitride fibers are formed by an adaptation of the conventional bushing process. Since nitrides would corrode precious metals in an oxidative environment, the bushings with up to 200 tips are therefore made from boron nitride-coated carbon or from molybdenum. The melts are formed under nitrogen at 1600–1750°C and refined at a lower temperature. Fibers with diameters ranging from 12 to 20 μm are continuously drawn from the melt, and mechanically wound at 1000–2000 m/min [82, 83].

Silicon formation:

$$SiO_2 + Si_3N_4 \longrightarrow 2Si + 2SiO + 2N_2 \tag{1.8}$$

$$SiO_2 \longrightarrow Si + O_2 \tag{1.9}$$

Oxygen formation:

$$Si_3N_4 \cdot SiO_2 + 12Mo \longrightarrow 4Mo_3Si + 2N_2 + O_2 \tag{1.10}$$

$$3Si_3N_4 \cdot SiO_2 + 20Mo \longrightarrow 4Mo_3Si_3 + 6N_2 + 3O_2 \tag{1.11}$$

Silicon oxidation:

$$Si + O_2 \longrightarrow SiO_2 \tag{1.12}$$

The melt process may cause the reduction of silica yielding particulate silicon. Increasing numbers of silicon defects, when formed, impart a blue-gray (hazy) to dark brown (opaque) appearance to the glass (Equations 1.8 and 1.9), and these defects may proportionately reduce the strength of the resulting fibers [83]. The formation of silicon defects can, however, be reversed by using molybdenum (but not boron nitride) as the bushing material (Equations 1.10, 1.11, and 1.12), and by inserting an 8 h refining cycle midway between the melt and fiber-forming temperatures (see second entry in Table 1.14).

A refined Si–Al–O–N glass is colorless and clear [83] and the resulting defect-free glass fibers [36] are stronger (>4.0 GPa) than those obtained from unrefined melts (2.0–3.0 GPa). Si–Al–O–N compositions with <15% nitrogen yield glass fibers with moduli ranging from 100 to 140 GPa, and a microhardness ranging from 660 to 700 kg/mm^2 [36] as shown in Fig. 1.12. Compositions with >15% nitrogen yield glass ceramic fibers with moduli ranging from 140 to 248 GPa and a microhardness ranging from 900 to 1200 kg/mm^2 [83]. The substitution of nitride for

Table 1.14 Ultrahigh-modulus Si–Al–O–N glass fibers [36] (with kind permission of Springer Science and Business Media)

Glass fiber	S-glass	Si–Al–O–N glass fiber		Si–Al–O–N glass ceramic	
Composition	Control	Mg^-	Ca^-	Y^-	Ca-Mg
Wt%					
SiO_2	65.50	56.75	32.38	50.3	11.1
Al_2O_3	25.00	25.33	–	7.6	2.2
CaO	–	–	50.78	–	62.6
MgO	9.50	10.42	–	–	0.7
Y_2O_3	–	–	–	25.1	–
Si_3N_4	0.00	7.51	16.84	–	23.4
Al_2N_2	–	–	–	17.0	–
N-content	0.00	2.54	10.00	4.37	13.5
Melting, °C	1650	1720	1750	1600	1790
Refining, °C	–	1600	–	–	–
Log 3 FTT, °C	1565	1500	1380	1560	1590
Bushing tips	200	200	–	1	1
Pristine fibers					
Strength, GPa	4.60	4.50	–	–	–
Modulus, GPa	88–95	115.00	137.0	213.00	248.0
Density, g/cc	2.53	2.80	2.8	3.94	(3.3)
Sp. Strength	1.85	1.61	–	–	–
Sp. Modulus	35–37	41.10	48.9	54.00	(75)
Structure	Amorphous	Amorphous	Amorphous	Nanocryst	Nanocryst
References	[50]	[83]	[83]	[82]	[83]

25% of a given oxide composition under the same conditions of synthesis no longer yields glasses. These melts will foam and crystallize [36].

Selected glass and/or glass ceramic Si–Al–O–N fibers are seen in Table 1.14. The first [83] is S-glass and the second is a Mg–Si–Al–O–N composition that is similar to the S-glass composition but modified to contain 7.5 wt.% Si_3N_4 [83]. Since the latter had been properly melt refined before it was fiberized, it yielded high-strength fibers. Its low nitrogen content produced a significant modulus increase beyond that of the S-glass control. The third example in Table 1.14, a Ca–Si–Al–O–N, has an even higher nitrogen content [36] and therefore a higher absolute and specific modulus. Its low strength suggests that the melt was not or could not be adequately refined.

The remaining examples in Table 1.14 are ultrahigh-modulus (UHM) glass ceramic fibers. The first example, a glass ceramic Y–Si–Al–O–N fiber, exhibits the very predictable effect of yttria that dramatically increases both the measured modulus and the density but offers only a small increase of the specific modulus in return. The second example, a glass ceramic Ca–Mg–Si–Al–O–N fiber, has the highest measured modulus (248.0 GPa) and the highest specific modulus (75 Mm) of any known oxide glass or glass ceramic fiber.

In summary, nitrides offer only a modest crystallization potential but instead seem to act as modulus builders by crosslinking the oxide structure they modify.

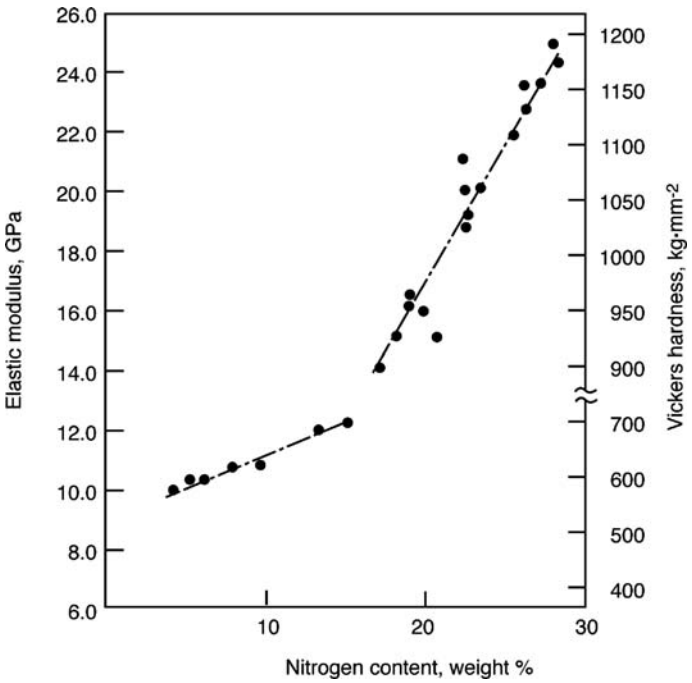

Fig. 1.12 Modulus and microhardness of oxynitride fibers. Redrawn from Kobayashi et al. [153]

And the presence of nitrogen in the network structure, once introduced, may restrict the dimensions of crystals which can be formed.

A selected oxynitride melt that has a high nitrogen content may yield nanocrystalline fibers with an ultrahigh modulus, while a nitrogen-free oxide melt with the same cation ratio may already yield microcrystalline fibers with lower moduli. Thus, the modulus of oxynitride fibers can be increased to much higher levels than that of fibers from oxide melts. Crystallinity of oxynitride glasses can be correlated with their nitrogen content by infrared methods. HM-oxynitride glass fibers are x-ray amorphous and UHM-glass ceramic fibers are nanocrystalline [36].

(b) Properties and applications. Glass and glass ceramic oxynitride fibers can be produced with high strength by properly refining melts while they are formed, and with ultrahigh moduli by inserting nitrogen into a suitable oxide network structure. The highest measured modulus (248 GPa) that has been reported lies between those of standard modulus (SM) and intermediate modulus (IM) carbon fibers (230 and 303 GPa, respectively) and the highest specific modulus (75 Mm) lies midway between those of SM carbon fibers (131 Mm) and E-glass fibers (27 Mm). Two types of applications are being pursued with oxynitride fibers.

Sialons are reinforcing fibers for metal matrix composites. An aluminum alloy 6601 matrix reinforced with a development fiber (Table 1.14) had a strength of 4.0

GPa and a modulus of 180 GPa. The bending strength of the MMC was 25% higher than that of an alumina fiber reinforced control, and almost the same as that of a silicon carbide fiber reinforced control. A high value-in-use may result if this fiber were to cost less than the incumbents did. Oxynitride fibers have high alkali durability and may be useful as a diaphragm material in the electrolytic production of chlorine from aqueous NaOH [36] and as a reinforcement for cementicious composites [36].

1.3.3.5 Glass Fibers with High Chemical Stability

The relationship between fiber composition and chemical stability in water, acids, and bases is complex. It depends on the interaction between (1) the chemical agent [48] to which the glass fiber surface is exposed, (2) the pH of the glass composition [84] in the fiber surface, and (3) the internal microstructure of the fiber [48].

The chemical stability of glass fibers, yarns, or fabrics is complex and depends on whether they have generic finish or not, or even an acid- or alkali-resistant coating. These issues will be discussed here. Due to the presence of the composite matrix, the corrosion resistance of fiberglass reinforced composites is even more complex in sensitive applications.

(a) Chemical resistance of glass fibers. The first step in the attack of water on the bare surface of an alkali-free or near-alkali-free glass fiber is its adsorption. The adsorbed water molecules hydrolyze the siloxane bond by protonation of the oxygen atom and yield a highly hydroxylated fiber surface:

$$\begin{aligned} &\equiv \mathrm{Si}-\mathrm{O}-\mathrm{Si} \equiv - \xrightarrow{\delta-} \equiv \mathrm{Si}-\mathrm{O}\cdots\mathrm{Si} \equiv - \xrightarrow{\delta+} \\ &\equiv \mathrm{S}-\mathrm{OH} + \mathrm{HO}-\mathrm{S} \equiv \mathrm{H}^+ + \mathrm{OH}^- \end{aligned} \tag{1.13}$$

With high alkali-glass fiber surfaces, the reaction of water represents an electrophilic attack by the addition of the proton (H^+) to the negatively charged oxygen atom of the =Si–O–M bond. It proceeds in the same fashion and results in the ion exchange between H^+ (or H_3O^+) and either alkali ions and/or network-modifying alkaline earth ions, and leads to the formation of SiOH groups [48]. The reaction products of water with a highly alkaline fiber surface are NaOH, $Ca(OH)_2$, and hydrated sodium silicate:

$$\equiv \mathrm{S}-\mathrm{OM} + \mathrm{H}^+ \longrightarrow \equiv \mathrm{S}-\mathrm{OH} + \mathrm{M}^+ \tag{1.14}$$

However, as soon as the supply of H^+ ions is exhausted, the corrosive attack of H_2O turns into a nucleophilic attack by alkali ions on the fiber surface. In other words, the reaction of a glass fiber with water turns into a reaction of a glass fiber with alkali. Siloxane bonds are broken and Si–O–Na groups are formed until the glass fiber is completely dissolved in the highly alkaline medium that initially consisted only of water.

The reaction of alkaline media starts with a nucleophilic attack by hydroxyl ions on silicon atoms in the bare surface of a glass fiber (–OH^- + ≡Si–O–S≡) where it forms new bonds (≡Si–OH and/or ≡Si–OM). Monovalent cations (e.g., sodium)

are removed from the glass fiber, leaving behind a hydroxylated surface. Bivalent cations (e.g., calcium) remain attached to the glass surface and form a crystalline sheath growing in thickness. Such a sheath develops when bare silicate glass fibers (>50% SiO_2) including E-glass [48], AR-glass [85, 86], basalt [87, 72] and oxynitride fibers [88], or when bare aluminate glass fibers (>50% Al_2O_3), e.g., calcium aluminate fibers [9] are exposed to alkaline media [89].

The crystalline sheath, mostly $Ca(OH)_2$ [36], increases the alkali resistance, but also limits the practical utility of the resulting fibers since it drastically reduces their strength. ZrO_2, SnO, La_2O_3, TiO_2, Fe_2O_3 [6], Y_2O_3, and Na_2O [36] enhance the alkali resistance perhaps by delaying sheath formation, but rather large amounts of Na_2O (>10%), ZrO (>15%), or Y_2O_3 (>30%) and combinations of Na_2O (11%) and ZrO_2 (16%) are often employed. These fibers are not really alkali resistant, only more alkali resistant than E-glass. In the end, all lose their physical integrity and are destroyed as evidenced from the accelerated leach test shown for E-glass in Table 1.15.

Table 1.15 Borosilicate E-glass solutes after acid leaching 8 h at 95°C [36] (with kind permission of Springer Science and Business Media)

Borosilicate E-glass	SiO_2	Al_2O_3	Fe_2O_3	CaO	MgO	B_2O_3
Oxide content (%)	53.8	14.9	0.3	17.1	4.7	8.7
Solute (%), in H_2O	0.2	0.2	–	0.2	0.1	0.7
In 2 N H_2SO_4	1.7	14.6	0.3	16.6	4.6	8.6
In 2 N NaOH	25.6	7.3	0.2	8.4	1.3	6.3

While alkaline media are known to create a crystalline deposit or sheath on the surface of glass fibers, mineral acids selectively dissolve specific components of the glass, first of all the ions of network modifiers [6]. Silanol bonds, as a rule, are not broken and SiO_2 is not dissolved. If, however, the amount of SiO_2 is not sufficient to create a continuous network structure, cations can selectively dissolve in acid media. The addition of Zr, Ti, and Fe oxides substantially increases the acid resistance [6], but in the end, the entire fiber, whether it is compositionally an E-glass or A-glass, is converted to a porous high silica fiber (see Table 1.15 and Section 1.2.2.2).

In summary, the effect on the pH of the bare fiber surface and the effect of the interaction between a chemical agent and a bare fiber surface are predictable. ZnO (as in ECR-glass) increases the acid resistance and ZrO_2 (as in CemFIL or AcroteX) increases both acid and base resistance. The effect of the internal microstructure [48] of a fiber is highly process dependent and not predictable without a thorough prior investigation of its microstructure. Importantly, however, all fibers, except experimental single fibers, have a primary finish; some have an additional secondary coating. These modifications further reduce the predictability of their chemical resistance from their compositional make-up alone.

(b) Alkali-resistant glass fibers. Commercial AR-glass fibers such as CemFil™ [1, 36, 90] and ArcoteX™ [85], an experimental and AR-glass fiber [86], and AR basalt fibers [87, 72], which are commercial only in Russia, are shown in Table 1.16.

Table 1.16 Glass fibers with high chemical stability [36] (with kind permission of Springer Science and Business Media)

Glass fiber	Alkali-resistant glass fibers			Acid-resistant glass fibers		
Type	CemFil	Exp. ARG	Basalt	A-glass	C-glass	CC-glass
Wt%						
SiO_2	71.0	68.11	49.06	71.8	65.0	65.15
Al_2O_3	1.0	0.78	15.70	1.0	4.0	6.70
B_2O_3	–	–	–	–	5.0	–
CaO	–	4.86	8.95	8.8	14.0	9.23
MgO	–	3.04	6.17	3.8	3.0	4.33
BaO	–	2.43	–	–	–	–
TiO_2	–	–	1.36	–	–	–
ZnO	–	–	–	–	–	0.20
ZrO_2	16.0	6.92	–	–	–	–
Li_2O	1.0	–	–	–	–	–
Na_2O	11.0	13.85	3.11	13.6	8.5	12.92
K_2O	–	–	1.52	0.6	–	–
FeO	–	–	6.37	–	–	–
Fe_2O_3	–	–	5.38	0.4	0.3	0.27
MnO	–	–	0.31	–	–	–
P_2O_5	–	–	0.45	–	–	–
H_2O	–	–	1.62	–	–	–
F_2	–	Trace	–	–	Trace	0.96
Log 3 FT, °C	1300	1212	1300	1280	1200	1192
LT, °C	1200	1074	1220	1010	1135	1068
ΔT, °C	100	138	100	270	65	124
Structure	Amorphous	Amorphous	Nanocryst	Amorphous	Amorphous	Amorphous
References	[50, 86]	[86]	[87]	[52]	[52]	[91]

CemFil and the experimental AR fiber are highly Na_2O- and ZrO_2–modified glass fibers. Basalt fibers are derived from volcanic rock with high Fe_2O_3 + FeO levels. The alkali resistance of basalt fibers lies between that of E- and AR-glass. All have higher fiber-forming temperatures than E-glass and require an energy-intensive, non-standard process.

In a test that simulates their suitability as a cement reinforcement [90], bare AR-glass and bare E-glass fibers were immersed at 25, 50, and 80°C in a solution (NaOH 0.88 g/l, KOH 3.45 g/l, $Ca(OH)_2$ 0.48 g/l, pH 12.5) that simulates the aqueous phase of Portland cement. Both fibers lost strength between 24 and 96 h, i.e., in the time frame during which the alkalinity of cement reaches its peak as it cures.

At 25°C, the strength of bare E-glass dropped to 2/3 of its original value in 24 h and that of AR-glass in 96 h. In the accelerated test at 80°C, the strength of E-glass dropped to 1/3 of its original value in 24 h and that of AR-glass in 96 h (Fig. 1.13). Thus, neither fiber is usable to structurally reinforce cement without having an effective secondary alkali-resistant coating.

The application of an alkali-resistant finish or secondary coating is known to render even E-glass suitable for continued use as a durable reinforcement of cement structures, whether they are composite wraps for bridge columns or net-like

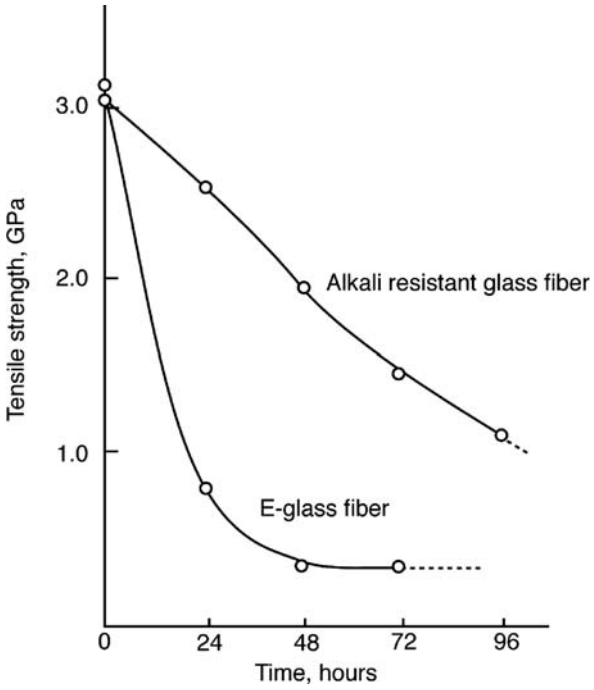

Fig. 1.13 Tensile strength of glass fibers in the aqueous phase of cement. Redrawn from Majumdar [36, 90] (reprinted with permission of Elsevier Science Publishers)

structures aimed at roadbed construction. But since even AR-glass loses strength in <96 h in a solution simulating an aqueous cement phase, it too would require a costly secondary alkali-resistant coating to be acceptable in continuous structural use.

In the Western world and Japan, AR-glass such as CemFIL costs 2× as much as E-glass. AR-coated E-glass rather than AR-coated CemFIL or ArcoteX is therefore the preferred reinforcement of structural, load-bearing cementicious composites. In CIS countries, e.g., Russia, AR-coated basalt fibers are apparently as economically viable as AR-coated E-glass as a replacement for asbestos in the fiber reinforcement of cement pipes.

In addition to specialty cementicious applications such as do-it-yourself driveway repair [85], the cost-considered use of AR-glass (such as ArcoteX or Cemfil) is the reinforcement of non-structural and decorative cement composites ranging from non-structural ready-mix cement and decorative architectural components to non-load bearing, building cladding systems such as balustrades, string courses and cornice elements, corbels and arch units, mullions and window surrounds, and consoles and copings [6].

In these uses [6, 85], AR-glass offers a simple solution to the problem of shrinkage cracking that often occurs during the initial curing phase (<96 h) of cement or concrete mixes, without requiring a costly secondary AR coating. They retain useful strength long enough to survive the alkaline curing cycle and therefore prevent

shrinkage cracking. E-glass without a costly AR coating loses its strength and totally disintegrates before the initial, alkaline cement curing cycle is complete.

(c) Acid-resistant glass fibers. Boron is readily removed by acid leaching from borosilicate E-glass fibers with ~6% B_2O_3. Therefore they have a lower acid resistance than boron-free E-glass fibers [36, 20] and essentially boron-free E-glass fibers [2, 24]. An intermediate level of acid resistance is obtained with soda-lime-silica fibers such as the boron-free former A-glass in the United States or the current boron-free CC-glass in China, and the former borosilicate C-glass in the United States.

The typical A- and CC-composition [2, 91] is boron-free but contains 65–72% SiO_2, 1–7% Al_2O_3, and >12% Na_2O. The former C-glass in the United States contained 65% SiO_2, 4% Al_2O_3, 8% Na_2O, and 2–5% B_2O_3 (Table 1.9).

Specifically, the oxides which are preferentially extracted from these fibers on acid leaching, e.g., with dilute H_2SO_4 or HCl [36, 69], are B_2O_3, Na_2O, Al_2O_3, CaO, MgO, Fe_2O_3, and only a very small amounts of SiO_2. Ultimately, a porous silica fiber structure remains after acid leaching of a borosilicate E-glass or a sodium silicate A- (CC-)glass fiber, yarn or fabric that can be consolidated into a near-solid silica fiber, yarn, or fabric structure.

Boron-free A- and CC-glasses have a much higher SiO_2 and Na_2O content and a much lower Al_2O_3 content (Table 1.9) than typical borosilicate E-glass variants. The high SiO_2 content translates into high acid resistance. The low Al_2O_3 content translates into reduced strength and stiffness. The high Na_2O content translates into a lower viscosity and therefore into a lower log 3 forming temperature. The absence of B_2O_3 translates into lower cost.

The cost of A-glass (and presumably also that of CC-glass) would be even lower if a fiberglass forehearth with multiple bushings were added, as has been suggested [52] to a float glass or container glass furnace and/or if the A- or CC-glass product were made from float or container glass waste [92].

The recent technical evaluation of a soda-lime-silica A-glass fiber highlights its value-in-use in automotive composites, especially when made from waste glass [92]. The product performed satisfactorily, but, as expected, the multifilament yarns and the resulting automotive composites had lower tensile strength and a lower modulus than comparable E-glass yarns and composites. To achieve the same strength and stiffness, more A- than E-glass would be required, thus offsetting the initial cost advantage.

Although the boron-free A-glass (or CC-glass) has a better acid resistance than high-boron E-glass, it is not equal to that of boron-free or essentially boron-free E-glass. If a higher acid resistance than that of boron-free E-glass were needed, one might want to consider ECR-, basalt, S-glass, pure silica sliver (Section 1.2.2.1), and ultrapure SiO_2 (quartz) fibers (Section 1.2.1).

Finally, while a commercial process in Russia uses acid leaching of A-glass fabrics to manufacture silica fabrics for low-cost, high-temperature insulation uses, a comparable commercial process in the United States uses acid leaching of high-boron E-glass fabrics (Section 1.2.2.2).

1.3.3.6 Other Special-Purpose Glass Fibers

This group of products includes commercial and experimental glass fibers with low dielectric constants and high dielectric constants, and with superconducting, semiconducting, and bone bioactive properties.

(a) Glass fibers with low dielectric constants. The ASTM specifications which govern E-glass compositions fall into two categories, E-glass for printed circuit board applications and E-glass for general reinforcement applications (Table 1.8). To qualify as an E-glass for printed circuit board applications, the composition may contain 5–10% B_2O_3, 16–25% CaO, 12–16% Al_2O_3, 52–56% SiO_2, 0–5% MgO, 0–2% Na_2O and K_2O, 0–0.8% TiO_2, 0.05–0.4% Fe_2O_3, and 0–1.0% F_2. To qualify as an E-glass for printed circuit board applications, the composition may not contain Li_2O, but an E-glass for general reinforcement uses may contain 0–2% Li_2O.

The electrical properties of glass fibers are characterized by volume resistivity, surface conductivity, dielectric loss, and dielectric constant. Glass fibers which have a lower, dielectric constant than borosilicate E-glass have been designated as D-glass or low Dk-glass. They were originally developed [50, 93] to allow the computer industry to achieve, at a premium cost, a faster response time in reinforced printed wire board composites.

D- and low Dk-glass compositions are not supported by the existing ASTM E-glass specifications and ASTM has not established generic specifications. The potential cost of these compositions to the manufacturer depends on ingredient cost and on melt viscosity, therefore implicitly on energy cost. The potential value-in-use to the computer industry depends on the price relative to specific dielectric properties [36, 94, 95, 149]. This section provides an overview. An in-depth discussion is offered in Chapter 4.

Table 1.17 compares the properties of the original D-glass fiber with those of silica, S-glass, hollow and solid E-glass fibers, and with low Dk-glass fibers. The fibers are arranged by increasing dielectric constants and by decreasing melt viscosities and energy demand. Hollow experimental E-glass fibers [96] have the lowest dielectric constant (2.98) and solid commercial E-glass fibers have the highest dielectric constant (6.86). All fibers in Table 1.17 have a delta temperature of $\geq$55°C. As the dielectric constant increases, the forming temperature decreases from >1800°C (for silica fibers) to $\leq$1200°C (for E-glass), the density increases from 1.80 g/cc (for hollow E-glass) to 6.68 g/cc (for solid E-glass).

Experimental hollow E-glass fibers have the lowest dielectric constant [96], melt viscosity, and log 3 forming temperature and therefore would require the least energy of all eight examples shown in Table 1.17. They can be made in a large conventional fiberglass furnace but would require special bushing technology. But they are not suitable for use in printed circuit boards. After drilling holes into a composite, water can enter into the hollow fiber cores, and the presence of water could uncontrollably raise the dielectric constant.

Twenty-eight energy-friendly compositions with 60–68% SiO_2, 7–13% B_2O_3, 9–15% Al_2O_3, 8–15% MgO, 0–4% CaO, 0.4–2% Li_2O, 0–2% TiO_2, and 0–1% F_2, log 3 forming temperatures ranging from 1372 to 1244°C, and dielectric

Table 1.17 Glass fibers with low dielectric constants [36]

	Hollow	Commercial		Exptl.	Comm.	Low-Dk glasses		Comm.
Glass fiber	E-glass	D-glass	Silica	D-glass	S-glass	(Chapter 4)		E-glass
Wt%								
SiO_2	54.3	74.5	99.99	55.7	65.5	52–60	61.03	54.3
Al_2O_3	14.0	0.3	–	13.7	25.0	10–18	12.04	14.0
B_2O_3	6.0	22.0	–	26.5	–	20–30	10.73	6.0
CaO	22.1	0.5	–	2.8	–	4–8	2.98	22.1
MgO	0.6	–	–	1.0	9.5	Trace	9.97	0.6
TiO_2	–	–	–	–	–	Trace	0.50	–
Li_2O	–	–	–	0.1	–		1.05	–
Na_2O	0.8	1.0	–	0.1	–		0.50	0.8
K_2O	0.2	1.3	–	0.1	–		0.40	0.2
Fe_2O_3	0.3	–	–	–	–		0.35	0.3
F_2	0.7	–	–	–	–	<2	0.45	0.7
Properties								
D_k, 1 MHz	2.98	3.56	3.78	4.10	4.35	<5	5.61	6.86
Log 3 FT, °C	1200	1410	>1800	1430	1560	<1340	1244	1200
Density, g/cc	1.80	2.16	2.15	–	2.48	–	2.42	2.54
Special process	Yes	Yes	Yes	Yes	Yes	Yes	No	No
Energy premium	–	+++	+++++	+++	++++	++	+	–
References	[36]	[50]	[36]	[93]	[50]	[95]	[94]	[36]

constants ranging from 5.30 to 5.95 were recently reported [94]. The composition with the lowest forming temperature (1244°C) and a liquidus temperature ≥55°C (Dk = 5.61) is shown in Table 1.17 since it would be the most energy efficient composition among the 28 examples.

The following issues will be discussed in detail in Chapter 4: (1) The scientific principles and technical concepts which support the printed wire board technology; (2) recently emerging compositional D- or low Dk-glass technology; (3) the value-in-use of various combinations of dielectric constant and cost; and (4) the predominant target applications of D-glass fibers such as large mainframe computers, workstations, and general-purpose minicomputers in terms of product requirements and product cost.

(b) Glass fibers with high densities and dielectric constants. Glass fibers with high dielectric constants tend to have high densities also, and their value depends on one or the other property, rarely on both. Three generic applications are known. The oldest application requires radiation resistance, e.g., absorption of gamma rays and relies on a high density [6, 97]. The newest application, which requires a concentration of electro-magnetic energy, e.g., in circuit boards for high-frequency uses, depends also on the electrical properties [98, 99]. Applications, e.g., in capacitors, which require electrical insulation, rely on their electrical properties [99].

Glass fibers with high densities (and high dielectric constants) are known as protective glass fibers [6, 36] since they can absorb gamma rays as well as fast and

Table 1.18 Glass fibers with high densities and/or high dielectric constants [36] (with kind permission of Springer Science and Business Media)

Glass fiber properties	E-glass (6.6% B_2O_3)	Cerium silicate (<30% CeO_2)	Lead silicate (<30% PbO)	Niobium silicate (<15% Ni_2O_5)
Strength, GPa	3.40	4.5	1.7	–
Modulus, GPa	72.00	95.0	51.0	–
Density, g/cc	2.54	3.0–3.8	3.0–4.0	–
Dielectric constant	6.80	7.0–8.0	8.0–10	10–15
References	[50, 52]	[97]	[6, 98]	[98, 99]

slow neutrons. For example, lead-, bismuth-, and/or barium-containing glass fibers have high densities (4.0–4.8 g/cc) and high dielectric constants (8–13) as shown in Table 1.18. They can be used to absorb gamma rays [6] in x-ray equipment and radiation-protective composites. The ability of lead glass fibers to absorb gamma rays increases with increasing density [6], but these fibers have low strengths (<2.0 GPa), low moduli (<55 GPa), and very low resistance to light, humidity, and/or elevated temperatures.

Glass fibers containing boron, cadmium, and/or cerium can be used for protection against neutrons [6, 36]. Their densities (3.0–3.5 g/cc) are not as high as those needed for gamma ray protection (4.0–4.8 g/cc). However, glass fibers in the SiO_2–Al_2O_3–CeO_2 system [36, 93] with 10–28% CeO_2 offer very high strengths (4.5 GPa) and very high moduli (95.0 GPa). They could be considered to be high-strength glass fibers (see Table 1.12), but their thermal stability, unlike that of true high-strength fibers (Section 1.3.3.2), is very low. For example, a major strength loss occurs after heat treatment at 100–200°C due to pre-crystallization and micro-separation of a second solid phase, which is revealed in x-ray diffraction patterns [6, 36].

(c) Glass fibers with very high dielectric constants. Glass fibers with high dielectric constants [98, 99] differ fundamentally in their applications from those requiring glass fibers with low dielectric constants [97]. They are aimed at circuit boards being designed for use in high-frequency applications. Again, using of E-glass as a control, Table 1.19 shows three different approaches to glass fibers with very high dielectric constants, i.e., potentially suitable for the presently emerging market needs [98, 99]. Lead (or L) glass fibers with extremely high levels of PbO (>70%) and silicate fibers with very high combined levels of BaO and TiO_2 offer significantly higher dielectric constants, i.e., 13.0 and 13.5, respectively.

Lead glass compositions possess a dielectric constant of 13.0, but glass fibers from lead glass compositions with such high PbO levels are difficult to form. They are very long melts which have a very high ΔT between log 2.5 forming and liquidus temperatures and are therefore quite crystallization resistant. However, PbO will evaporate violently during the melt process, thus affording highly non-uniform fiber compositions and frequent process discontinuities and fiber breaks [98, 99]. In addition, the use of PbO poses significant environmental concerns.

The silicate glasses based on high levels of BaO and TiO_2 have an equally high dielectric constant of 13.5, but fibers cannot be formed from their melts because

Table 1.19 Glass fibers with very high dielectric constants [36] (with kind permission of Springer Science and Business Media)

Glass fiber composition, wt.%	E-glass (6.6% B_2O_3)	Lead glass (>70% PbO)	$BaO–TiO_2$ silicate	$Nb_2O_5–BaO–TiO_2$ silicates	
SiO_2	54.3	26.0	40.0	55.0	47.16
Al_2O_3	14.0	–	–	2.5	–
B_2O_3	6.6	1.5	–	–	–
PbO	–	72.0	–	–	–
CaO	22.1	–	7.5	9.0	7.03
MgO	0.6	–	–	–	–
SrO	–	–	15.0	6.0	7.03
BaO	–	–	23.0	15.0	14.05
TiO_2	0.5	–	–	7.8	13.95
ZrO_2	–	–	7.0	1.7	3.27
Na_2O	0.8	–	–	–	–
K_2O	0.2	0.5	–	–	–
Nb_2O_5	–	–	–	3.0	7.51
Dk, ε_r, at 1 MHz	6.8	13.0	13.5	10.1	12.3
Log 2.5, °C	1299	850	1077	1199	1136
LT, °C	1063	650	1214	1085	1089
ΔT, °C	+236	+100	−137	+114	+51
Fiber-forming ability	Excellent	Very poor	Infeasible	Very good	Good
References	[1, 79]	[98, 99]	[98, 99]	[98, 99]	[98, 99]

the liquidus temperature is much higher than the preferred forming temperature. Crystallization would occur long before the melt reaches the preferred fiber-forming viscosity of log 2.5 poise. In summary, glass fibers with very high levels of PbO are sublimation prone and glass fibers with high combined levels BaO and TiO_2 are crystallization prone.

In contrast, addition of 0.5–15.0 mol% of Nb_2O_5 to glass compositions having high levels of BaO and TiO_2 slightly reduces the dielectric constant, and dramatically reduces the liquidus temperature, thereby reversing the delta between the log 2.5 forming temperature and liquidus temperature from –137 to +117°C [98, 99]. Customarily the delta temperature (ΔT) quoted in the technical literature refers to the difference between the log 3 forming and liquidus temperatures. The difference does not affect the conclusions.

High-speed and high-frequency information transmission is becoming increasingly important with the recent development of advanced information systems including mobile communication by car telephones and personal radios, as well as satellite broadcasting and cable television. As a result, there is an increasing demand for miniaturizing electronic devices and also microwave circuit elements such as dielectric resonators in conjunction with the electronic devices.

Nb_2O_5-containing glass fibers are embedded for these applications in a resin such as polyethylene oxide that has a low dielectric tangent (tan δ) loss to obtain the desired high-frequency performance of the resulting circuit boards for microwave applications [98, 99]. In summary, microwave circuit elements can be made more

compact by using a circuit board having a high dielectric constant. It acts to concentrate the electromagnetic energy within the board and thereby minimizes the leakage of electromagnetic waves.

(d) Glass fibers with super- and semiconducting properties. Superconducting glass fibers are obtained by incorporating a suitable ceramic material in the fiber core, yielding superconducting bicomponent sheath/core glass fibers [36]. Superconducting single-component fibers can be made drawing single superconducting ceramic preform rods by the laser-heated float zone or pedestal growth process [36]

Semiconducting glass fibers have been known for over 30 years [6, 36] but have never attracted commercial interest because significant technical problems have never been solved. Such fibers (e.g., CuO–CaO–Al_2O_3–SiO_2) can be made by adding oxides of monovalent metals such as copper or silver to a suitable base glass and by subsequently reducing the glass fibers in various gaseous media, e.g., hydrogen. However these fibers are moisture sensitive, and prolonged storage leads to increased glass conductance [6].

The electrical properties of glass fibers are best modified by (1) applying a permanent chemical coating to the fiber surface, (2) adding a suitable material to the binder or finish formulations, or (3) modifying the composite matrix that is being reinforced with a glass fiber. A semiconducting or conductive coating is applied by vacuum deposition, metallization from metal salts, decomposition of organometallic compounds, or chemical metallization. Also, carbon black can be added to the composite matrix [36].

(e) Glass fibers with bone bioactive oxide compositions. Bioactive glasses have been developed since 1969 [100] and continuous bioactive glass fibers since 1983 [101, 102]. And very recently [103], bone bioactive glass fibers were found to bond to bone tissue and help bone tissue growth when they are preferentially placed on the surface of a thermoplastic composite while carbon fibers are used to stiffen the core of the structure.

A glass composition which was found particularly suitable for these applications [100] contained 52% SiO_2, 30% Na_2O, 15% CaO, and <3% P_2O_5 (in mole %). Fiber bundles or tow of up to 5000 filaments were drawn from a melt of this composition and were interwoven with carbon fiber tow into a cylindrically braided sheath/core textile preform. The carbon fibers formed the core of the braided structure and provided the required stiffness and load support, and the bone bioactive fibers formed the sheath and functionality.

To create a practical reinforcing structure of this nature, two braids are in effect braided simultaneously, one forming the carbon fiber core, the other the bioactive fiber surface layer or sheath, and both are suitably interwoven, overlaid, or otherwise intermingled. The carbon fibers in the core are first co-mingled with a suitable polymer such as a polysulfone and coarse fibers of the same polymer are intermingled with the bone bioactive glass fibers.

The hybrid preform is then processed in a closed die in a hot press. The combined amount of polymer is calculated to give the final total volume fraction; no additional polymer or injection molding step is required. In summary, superior composite

materials can now be designed and manufactured for use in practical prosthetic devices, facilitating bone tissue growth that has a structural stiffness matching that of human bone.

1.3.4 Non-round, Bicomponent and Hollow Silicate Fibers

Fibers having a special shape, a non-round fiber cross section or multiple compositions across the fiber composition can offer special properties.

1.3.4.1 Glass Fibers with Non-round Cross Sections

A circular cross section has the smallest circumference for a given area. Any increase in circumference of a fiber while retaining the cross-sectional area will increase the fiber surface. Any increase in the fiber surface offers significant product advantages including higher adhesion and strength in composites, but also creates increased process complexity.

(a) Processes and structures. The effect of the surface tension of a molten jet is the driving force toward the formation of fibers with round cross sections. Thus, a fiber with a round cross section is obtained from a bushing tip with a round cross section. With a bushing tip having a non-round cross section, the effect of surface tension tends to force the melt into a round cross section. This tendency is opposed by the effect of the quench rate which would otherwise stabilize a non-round fiber cross section. Since glass melts have higher surface tensions than polymer organic melts, it is more difficult from glass fibers with non-round cross sections than polymer fibers with non-round cross sections [104].

The basic fiber cross section technology was developed in the early 1950s for nylon yarns. Not surprisingly, the development of glass fibers with non-round cross sections was more demanding and the required technology is still not being practiced on a commercial scale. Two processes were developed for forming continuous single glass ribbons [36], tapered, trilobal fibers [104], and for continuous oval shaped as well as trilobal multifilament glass fibers [105] as shown in Fig. 1.14. But these early processes were slow.

A recent redesign of nozzle tips [106] has been claimed to afford non-round multifilament E-glass at fast, i.e., potentially commercial production rates (Fig. 1.15). For example, ribbon, oval, trilobal triangular, or rectangular cross sections can be produced with 400 tip bushings and windup speeds of 1800–3000 m/min under otherwise conventional E-glass process conditions. This critical technological advance uses an entirely new bushing tip design. An edge, shield, or baffle protrudes from the surface of each tip at critical points to induce preferential cooling of the fibers and thereby to assist the formation of well-defined non-round cross sections.

Non-round fiber cross sections are characterized by their modification or mod ratio. For ribbons, the mod ratio is their width-to-thickness ratio. For trilobal fibers (Fig. 1.14) it is the ratio of the diameter B of the outer circle around the lobes of the fiber cross section to the diameter A of the inner circle within the core of the

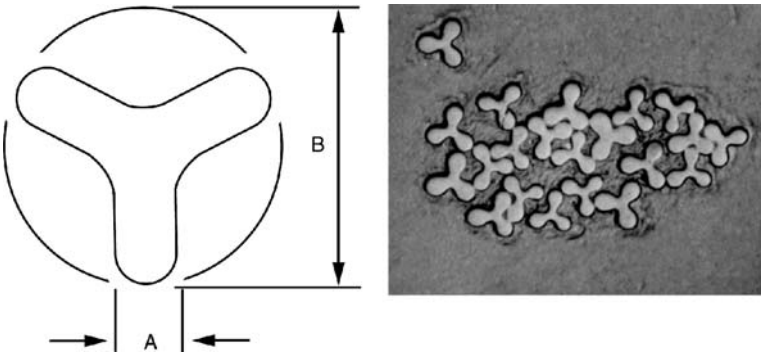

Fig. 1.14 Trilobal glass fibers with high modification ratio. Redrawn from Huey [104]

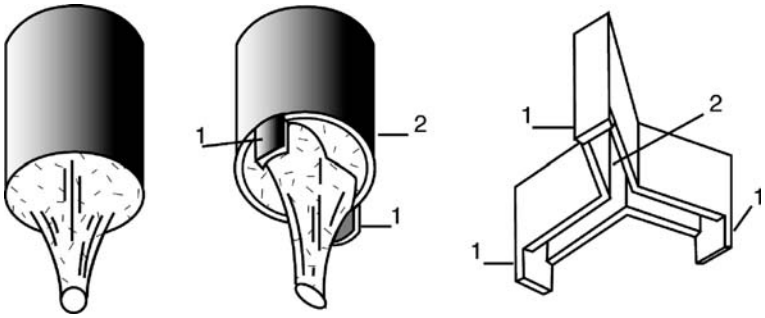

Fig. 1.15 Tip design for the fabrication of non-round glass fibers at high process speeds. Redrawn from Taguchi et al. [106]

fiber cross section. The term mod ratio has been used since the early development of trilobal nylon fibers. The newer term, "deformation ratio" [106], is less intuitive and therefore less desirable.

(b) Products and applications. Several potentially desirable properties increase with increasing mod ratio. Nylon fibers with a high mod ratio offer a high degree of external light reflection and, therefore, the appearance of a silk-like sheen or luster in a yarn or fabric. Nylon ribbons with a high mod ratio offer the appearance of a metallic sparkle in a fabric or garment. They offer large reflective surfaces which constantly shift with the motion of the garment. The visual effect of a trilobal or ribbon-shaped glass fiber does not seem to possess practical value, but the structural effect appears to be useful in limited applications.

The older technology for forming non-round glass fibers afforded a premium application for lead glass ribbons in ribbon wound capacitors [36]. The process, however, is slow and not sufficiently cost-effective to facilitate the growth of large volume applications in the composites market. The newer technology [106] offers higher process speeds and therefore a more cost-effective route to ribbon-shaped and trilobal glass fibers. The potential value of fibers with non-round cross sections has

long been understood [36]. When used as composite reinforcing fibers, they have a higher surface area, therefore offer higher matrix adhesion and higher composite strength.

1.3.4.2 Bicomponent Silicate Glass Fibers

Commercially significant inorganic bicomponent fibers have either a concentric sheath/core or a side-by-side fiber structure. Polymer organic fibers with an additional eccentric sheath/core structure are known, but inorganic fibers with this structure are not known.

(a) Sheath/core and side-by-side bicomponent fibers. Structural bicomponent ceramic fibers [36] and optical bicomponent glass fibers [36] have a concentric sheath/core structure (Fig. 1.16). A sheath of one composition surrounds a core of another composition. Either the core or the sheath is responsible for the functionality. For example, the boron sheath of boron/tungsten fibers is responsible for the functionality while the core is sacrificial. The core (or wave guide) of optical fibers is responsible for the functionality while the silica sheath provides strength and load support. Side-by-side bicomponent structures afford non-straight, crimped, or bulky fibers since the components show differential shrinkage during processing.

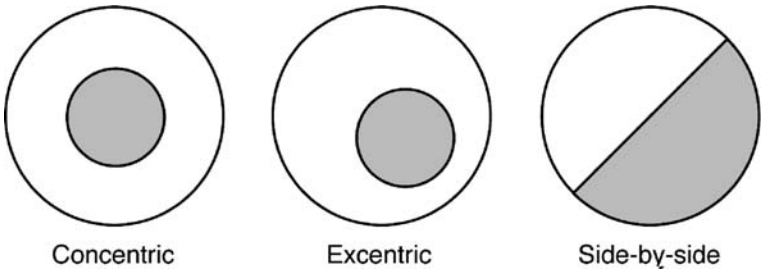

Fig. 1.16 Schematic drawing of concentric, eccentric, and side-by-side bicomponent fiber cross sections [36] (with kind permission of Springer Science and Business Media)

Solid bicomponent glass fibers have different sheath-core (s-c) or side-by-side (s-b-s) compositions. Hollow glass fibers are sheath-core bicomponent fibers having a continuous glass sheath that surrounds a continuous void or hollow core. Hollow porous glass fibers have a microporous, instead of a solid, glass sheath. Hollow superconducting glass fibers have three different compositions, an outer silicate sheath that surrounds a functional ceramic sheath that, in turn surrounds, a hollow core.

(b) Hollow sheath/core silicate glass fibers. Hollow fibers have a concentric bicomponent structure with a solid sheath and a void- or air-filled core. Flame drawing from glass tubes yielded the earliest examples of hollow fibers. Commercial technology relies on introducing air into the core of a molten glass jet, the fiber precursor, and dates to 1966 [36]. In one process, air is injected through feeder tubes

into the core of the melt in each tip [107]. In another process, the bushing tips aspirate air from the forming zone into the core of the forming cone [108]. In the third process, a double-crucible design is used to manufacture three-component superconducting glass fibers, whereby air is aspirated into the core of the forming cone from the inner crucible [109].

Hollow glass fibers have a lower weight at equal volume than solid glass fibers, greater thermal insulation, a lower dielectric constant, better long-term fatigue characteristics, but also lower strength and modulus. Hollow E-glass fibers and hollow S-glass fibers are known. Hollow S-glass fibers have short melts and a much greater crystallization behavior. Hollow E-glass fibers have long melts and a more forgiving crystallization behavior. Because of the additional manufacturing cost, both are specialty fibers, but since hollow E-glass fibers are much easier to fabricate, they have found a wider range of potential applications than hollow S-glass fibers [6].

Hollow borosilicate E-glass fibers with an outside diameter (OD) of 13 μm and an inside diameter (ID) of 8 μm have a coefficient of capillarity (K = ID/OD) of 0.62 and therefore a nearly 40% lower specific gravity than solid E-glass fibers. These fibers are potentially available in the form of yarns, rovings, fabrics, mat, chopped strand, and tape. By definition, hollow E-glass fibers have lower tensile strength (2.5–2.8 GPa) than solid E-glass fibers (3.3 GPa). Their modulus is also lower than that of solid E-glass fibers, and it increases with decreasing capillarity [6]. However, the specific modulus of hollow E-glass fibers is higher than that of solid fibers [6].

Hollow E-glass fibers with a capillarity of K = 0.5–0.6 are more sensitive to moisture and/or heat treatment than solid E-glass fibers. Upon exposure to high humidity (>90%), the residual strength drops to about 80–85% of the low original strength. Upon exposure to temperatures between 300 and 500°C, surface crystallization occurs and residual tensile strength drops to about 35–50% of the original strength. Because of their thin walls, hollow fibers are more fragile than solid fibers and need to be handled more carefully. They will not, however, crush under pressure in a laminating press.

Hollow E-glass fibers can produce composite parts with equal thickness and up to 25% lower part weight than E-glass, or composite parts with equal weight and up to 25% higher thickness. In equal weight cylinders, the hydrostatic collapse pressure is increased by 30% and the dielectric constant is reduced from 6.8 to 4.0. In equal thickness laminates, acoustic transmission is increased due to lower mass, dynamic fatigue is significantly increased, and thermal conductivity is reduced by up to 40%. In a hybrid laminate, partial substitution for graphite does not reduce the high specific modulus while removing up to one-half of the more expensive graphite fiber.

Weight reduction is a powerful incentive in aircraft design and construction. Every kilogram of structure that can be eliminated facilitates a major reduction in fuel consumption and cost or a commensurate increase in payload at equal fuel cost. Hollow glass fibers qualify for use in non-load-bearing interior aircraft applications such as sidewall and ceiling panels. The use of hollow glass fibers is more prevalent in Russia and CIS countries [110] than in the United States and the Western world.

(c) Hollow porous sheath/core silicate glass fibers. Hollow porous glass fibers with >95% SiO_2 were produced by acid leaching of hollow glass fibers including borosilicate E-glass [111]. Acid leaching of hollow glass fiber-based compositions having 35–62% SiO_2, 1–11% Al_2O_3, 0–54% B_2O_3, 3–9% ZrO_2, and l–29% Na_2O (but no CaO) gave silica-rich, porous hollow glass fibers with good alkali resistance. Acid leaching of hollow glass fibers containing 54.0% SiO_2, 22.4% CaO, 14.3% Al_2O_3, 7.2% B_2O_3, and 1.0% Na_2O (but no ZrO_2) gave porous, hollow glass fibers with low alkali resistance [111].

One of the most challenging tasks is to produce porous, hollow glass fibers with controlled pore size and uniform mechanical properties including strength and stiffness, thermal and chemical stability, photochemical and biochemical durability, and superior resistance to compaction under high membrane pressures. The required control over the desired pore size in fibers has been demonstrated [110] with a glass primarily consisting of 57.2 mol%, 22.8% B_2O_3, 9.2% CaO. This study serves as a model for the evaluation of hollow porous glass fibers in reverse osmosis, phase separations, salt extraction, and biochemical research.

(d) Solid side-by-side bicomponent glass fibers. Dual or bicomponent glass fibers [112] can be made as continuous fibers in a standard melt process or as staple or discontinuous fibers in a centrifuge process. Either way, two separate glass melts, each having a different composition and therefore viscosity, are supplied to round cross section tips in a typical multifilament bushing. The melt streams meet under the tips, fuse, and, as they cool, yield side-by-side bicomponent glass fibers with essentially round cross sections. The fibers develop an irregular crimp since a differential stress develops at the interface of the components.

Backscattered electron images (BEI) show that the individual bicomponent fibers have cross sections ranging from round to oval and low, but widely variable, fiber diameters (3–10 μm). Individual fibers can split at their dual glass interface either during manufacture or in subsequent processing and handling, thus producing fine, low diameter chaff considered to be undesirable in use. An individual cross section is shown in Fig. 1.17. Component (A) has a different composition than component (B), and the interface between both components is clearly discernable.

Successive secondary electron image (SEI) profiles can be used to determine the composition in components (A) and (B). This is accomplished by traversing a polished cross section of the fiber at a right angle to the interface between the two components (Fig. 1.18). Accordingly, the Mg (or MgO) level in this sample is higher in component (A) than in component (B), and the Ca (or CaO) level is higher in component (B) than in component (A).

In addition, the SiO_2 and Na_2O levels (not shown in Fig. 1.20) were also higher in component (A) than in component (B) and the Al_2O_3 levels were lower in component (A) than in component (B). Only component (A) contained potassium and only component (B) contained boron.

In summary, the individual components of the dual component fiber differ with regard to their SiO_2, MgO, CaO, Al_2O_3, B_2O_3, K_2O, and Na_2O content. The differential stress between the two components during fiber formation produces a three-dimensional, crimped, non-straight fiber geometry. In thermal insulation batts,

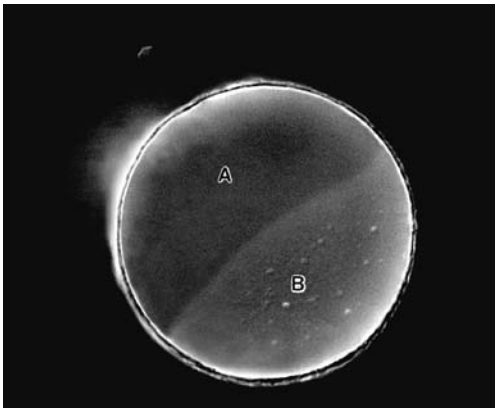

Fig. 1.17 Backscattered electron image (BEI) of a polished cross section of a commercial bicomponent glass fiber [36] (with kind permission of Springer Science and Business Media)

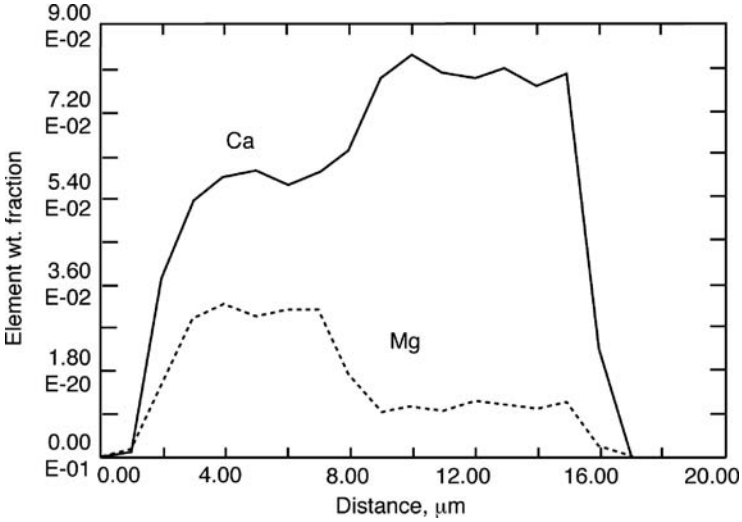

Fig. 1.18 Secondary electron image (SEI) profiles of calcium and magnesium [36] (with kind permission of Springer Science and Business Media)

a main application, arrays of crimped bicomponent glass fibers offer higher bulk and loft than possible with a comparable array of straight fibers. Arrays of crimped fibers can trap more air in their dead spaces and therefore offer higher thermal insulation than comparable arrays of straight fibers having the same basis weight.

Arrays of crimped staple fibers can be processed on conventional textile staple process equipment by carding, needle punching, or air laying [113]. In these conventional textile processes, crimped bicomponent glass staple fibers aim to compete with commodity fibers, e.g., cotton and polyester staple [114].

1.3.5 Summary and Conclusions

Melt spinning glass fibers from strong viscous silicate melts represents the most significant glass fiber-forming process among the multitude processes which have been described in Section 1.3. The most important commercial fibers which are being made by this process include borosilicate E-glass, boron-free, and essentially boron-free E-glass, S-glass, D-glass, ECR-glass, AR-glass, bicomponent insulation glass fibers, and Chinese C-glass (i.e., the former A-glass in the United States and Europe).

1.4 Aluminate Glass Fibers (≤81% Al_2O_3, ≤50% SiO_2)

Strong viscous E- and S-glass melts (50–100% SiO_2, 0–25% Al_2O_3) have high viscosities above and below their liquidus temperature. Fragile viscous melts (25–50% Al_2O_3, 4–10% SiO_2) have high viscosities below their liquidus temperature, but low viscosities at and above their liquidus temperature. Inviscid, literally non-viscous, melts (50–81% Al_2O_3, 4–0% SiO_2) have a sharp melting and crystallization point. Thus, a decrease in %SiO_2 and increase in %Al_2O_3 leads from strong to fragile and inviscid melts [4].

1.4.1 Glass Fibers from Fragile Melts (25–50% Al_2O_3, 10–4% SiO_2)

Strong silicate melts are preferred for developing commercial glass fibers. Fragile silicate [7], aluminate [8, 5], tellurite [115], fluoride [116, 117], chalcogenide [128], and fluorophosphate [119] melts have been used to explore theoretical relationships in optical and other specialty fields.

1.4.1.1 Downdrawing from Supercooled Melts

Melt spinning from supercooled fluoride melts affords optical single and bicomponent glass fibers [116]. The latter have a concentric fluoride core and a fluoride sheath or clad with a slightly different composition.

(a) Single- and double-crucible process. The double-crucible apparatus (Fig. 1.19) yields concentric bicomponent fluoride fibers. Two melts are separately maintained under controlled conditions in a supercooled state that is well below the liquidus temperature of the fluoride glasses [116, 117]. The inner and outer crucibles form the concentric tip system through which the glass melts flow.

In this process [116], the inner and outer crucibles are heated to about 750–800°C and held at that temperature for approximately 30 min to allow the melts

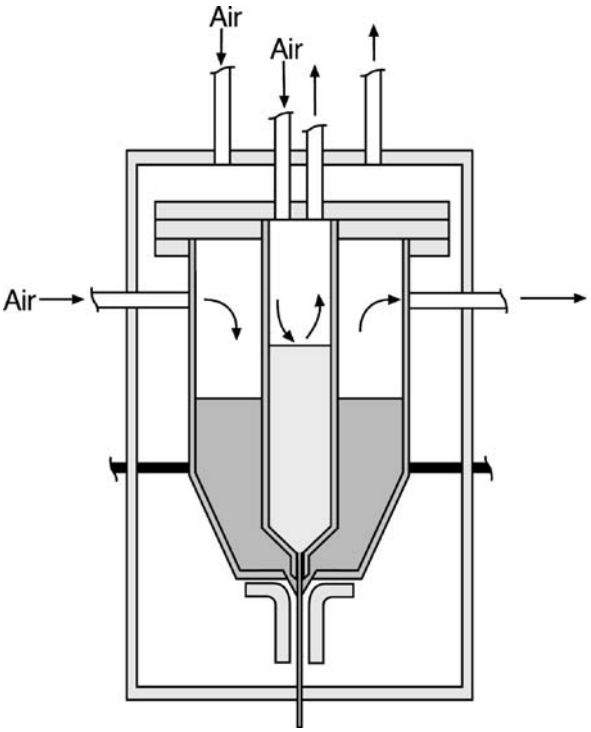

Fig. 1.19 Double-crucible melts spinning process depicting the outer and inner crucible. Redrawn from Nice [116]

to cure. The melts are then rapidly quenched until the core melt reaches about 350°C. The outer crucible is then rapidly raised to a fiberizing temperature of about 315°C, and fibers are drawn, depending on the pressure in the crucibles, at speeds of 900–3300 m/s. Low pressures are adequate to facilitate high drawing speeds.

This transient operating cycle [116] minimizes devitrification as the melt passes from refining to fiberizing conditions. The low pressures which are independently applied to each crucible facilitate the formation of solid concentric sheath/core fibers and prevent the formation of hollow fibers. The core diameters can range from 8.4 to 75.1 μm and the overall fiber diameter, including sheath or clad, can range from 140 to 149 μm.

(b) Single and bicomponent fluoride fibers. Core/clad bicomponent fibers were obtained with core diameters ranging from 8.4 to 75.1 μm, and single-component fluoride fibers having these diameters were obtained by a single-crucible version of the double-crucible process [116]. Single-component calcia–alumina and alumina–telluria glass fibers could also be made by this process, and the process could be used to fabricate concentric sheath/core fibers from fragile dual calcia–alumina or fragile dual alumina–telluria melts, if there were demand for such fibers.

1.4.1.2 Updrawing from Supercooled Melts

A narrow region exists near the eutectic of alumina–telluria with 5–11% Al_2O_3 and calcia–alumina melts with 25–50% Al_2O_3. They have fiber-forming viscosities (log 2.5–log 3.0 poise) below, but not above the liquidus. These compositions are discussed in this section. Calcia–alumina compositions with higher alumina levels (e.g., 50 and 81%) form inviscid melts, have very low melt viscosities (<5 poise), and they instantly crystallize at a sharp melting point. They will be discussed in Section 1.4.2.

(a) Tellurite glass fibers. The alumina–telluria phase diagram offers a glass-forming region between 5.0 and 11.0 weight (or 7.8–16.8 mol) percent of alumina, where high viscosity compositions can be found surrounded by low viscosity compositions. Within this region, alumina–telluria glass fibers could be manually updrawn from supercooled melts [115] at 800–850°C, yielding the first self-supporting tellurite glass fibers on record. These fibers had tensile strengths ranging from 0.4 to 1.1 GPa, moduli ranging from 69 to 83 GPa, and diameters ranging from 40 to 150 μm. They were x-ray amorphous, clear but pale yellow, and are of interest primarily because of their potentially valuable spectral transmission properties [115].

(b) Aluminate glass fibers. Over 500 quaternary aluminate glass fibers were manually updrawn from fragile melts, which were supercooled to about 50°C below their liquidus while carefully controlling the temperature of the melt [8, 120, 121]. The glass compositions in this narrow region of the phase diagram contained 30–55% calcia, 45–55% alumina, and 0–10% silica. The ratio of oxygen ions to network-forming ions (Al^{+3} and Si^{+4}, and an occasional minor component) was between 2.35 and 2.6 [35], a ratio that is a necessary but not sufficient condition for the formation of fragile fiber-forming aluminate glass melts.

A continuous updrawing process (Fig. 1.20) was designed [35, 122] using a quaternary low silica composition (44.3% CaO–48.7% Al_2O_3–3.5% MgO–3.5% SiO_2). The melt properties of this composition (Table 1.20) confirm the steep drop in melt viscosity from 182 poise at a temperature 50°C above the liquidus temperature to 278 poise at the liquidus temperature and to 720 poise at a log 3 fiber-forming temperature that is 50°C below the liquidus.

This calcium aluminate fiber was evaluated in structural applications but it was not suitable for infrared optical applications because it contained bound water as evidenced by a strong hydroxyl band at 2.9 μm in the IR transmission spectra. Hydroxyl-free compositions were made in carbon crucibles by the Davy process [123], i.e., by a process that is commercially used to fabricate optical calcium aluminate bulk glasses for applications in disposable optical windows [124].

One quaternary calcium aluminate glass fiber was also downdrawn from a solid preforms with a development unit [125]. Downdrawing from preforms is a rare, and costly, method for fiberizing fragile melts. And only one of >500 compositions could be fiberized on a conventional melt fiberizing unit [35]. This process is therefore not generally suitable for fragile melts either.

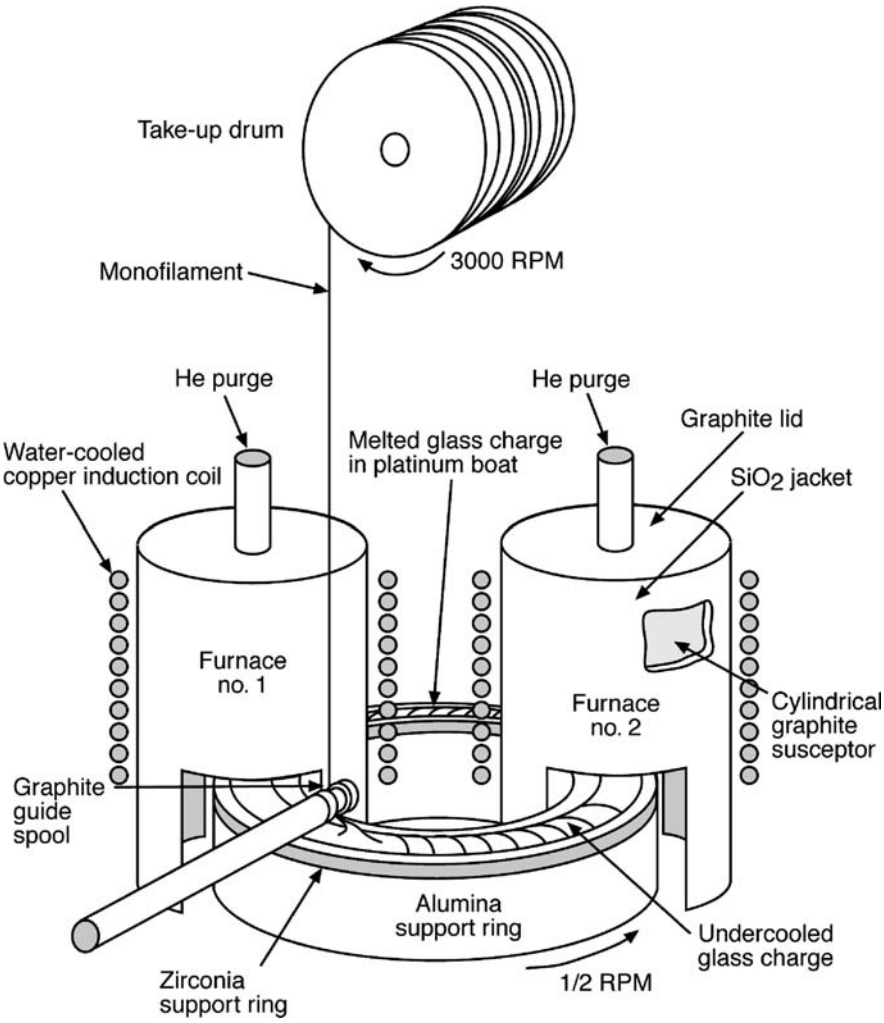

Fig. 1.20 Continuous updrawing process. Redrawn from Schroeder et al. [122]

Table 1.20 Fragile aluminate melt (3.5% SiO_2, 44.3% Al_2O_3, and 48.7% CaO) [1] (with kind permission of Springer Science and Business Media)

Melt temperature (°C)	Melt viscosity, poise
LT + 100	58.0
LT + 50	182.0
LT	278.0
LT – 50	720.0
LT – 200	10000.0
Literature references [8, 5]	

1.4.1.3 Quaternary Calcium Aluminate Fibers

Quaternary calcium aluminate glass fibers made by updrawing from a supercooled fragile melt offer superior mechanical properties and sapphire-like infrared transmission spectra.

(a) Structural and optical fiber properties. The highest reported pristine strength (8.3 GPa) was obtained (Table 1.21) with low silica (e.g., 44.3% Al_2O_3–48.7% CaO–3.5% MgO–3.5% SiO_2) glass fibers when they were updrawn from supercooled melts in an induction furnace [121]. When updrawn in an oxyacetylene furnace, they had a somewhat lower strength (4.2 GPa), but it was still higher than that of E-glass (3.5 GPa). The modulus (110.3 GPa) of these fibers was 1.5× that of E-glass. The lowest modulus of any calcium aluminate fiber shown in Table 1.21 was 10% higher than that of E-glass. The stiffest fibers in this table were zinc oxide-modified calcium aluminate glass fibers with moduli of up to 122.7 GPa or 1.7× the stiffness of E-glass.

Table 1.21 Modulus of calcium aluminate fibers updrawn from fragile melts [1] (with kind permission of Springer Science and Business Media)

	Composition, wt%						
Examples [80]	SiO_2	Al_2O_3	CaO	MgO	Other oxides	Modulus (GPa)	References
Example (1)	3.5	44.5	46.6	5.3	–	108.9	[35]
Example (2)	–	46.2	36.0	4.0	13.8% BaO	109.6	[35]
Example (3)	10.0	30.0	30.0	–	30.0% ZnO	109.6	[35]
Example (4)	3.5	44.3	48.7	3.5	–	110.3	[35]
Example (5)	4.1	42.6	47.7	5.6	–	110.3	[35]
Example (6)	2.8	35.2	36.2	–	25.7% PbO	110.3	[35]
Example (7)	10.0	30.0	35.0	–	25.0% ZnO	111.7	[35]
Example (8)	4.0	32.0	44.0	–	20.0% ZnO	115.8	[35]
Example (9)	4.0	32.0	44.0	–	ZnO and Li_2O	122.7	[35]
Controls							
E-glass	54.5	14.0	22.1	0.6	6.6% B_2O3	72.0	[50]
S-glass	65.5	25.0	–	9.5	–	86.9	[50]
Si–Al–O–N	11.1	2.2	62.6	0.7	23.4% Si_3N_4	248.0	[83]

With two exceptions, all fibers shown in Table 1.21 had strong hydroxyl bands in their infrared transmission spectra. The exceptions are two recent hydroxyl-free compositions made by the Davy process [123]. One is a low silica composition and the other is a non-silica composition (46.2% Al_2O_3 – 36.0% CaO – 4.0% MgO – 13.8% BaO). An in-depth analysis of the physical properties of fibers is shown in Table 1.21 [120, 121].

Their resistance to alkaline media exceeds that of commercially available AR silicate glass fibers (Section 1.3.3) having a zirconia content of up to 15% [52]. Hydroxyl-free quaternary calcium aluminate glass fibers (Fig. 1.21), e.g., non-silica fibers containing 46.2% Al_2O_3–36.0% CaO–4.0% MgO–13.8% BaO, afford sapphire-like infrared transmission properties.

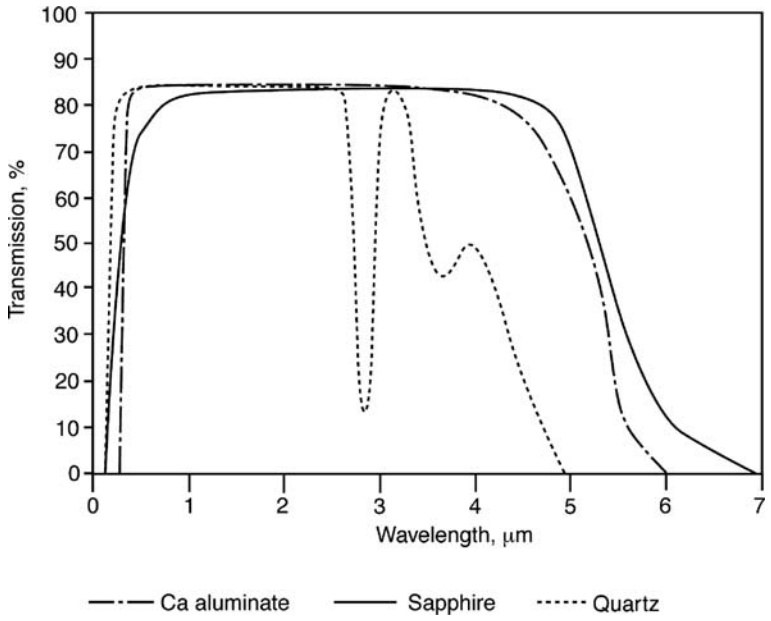

Fig. 1.21 Spectral transmission of calcialumina glass fibers. Redrawn from Wallenberger et al. [126] (Reprinted with permission of Elsevier Science Publishers)

(b) Potential applications. The commercial potential of updrawn quaternary calcium aluminate glass fibers was tested in two stages. In the early 1960s, they were evaluated because they yielded higher moduli than those which could then be achieved with silicate glass fibers [120, 121]. Timing for this development coincided with the onset of the commercial development of carbon fibers and no new aluminate or silicate glass fiber was commercialized until 1995.

In the early 1990s, a renewed evaluation of quaternary calcium aluminate glass fibers was triggered by their sapphire-like optical properties [35, 126, 127]. Coated aluminate fibers might afford sapphire-like sensors at a more affordable cost than single-crystal sapphire fibers, but unlike the latter, they would be limited to ambient and moderately high temperatures [127]. Calcium aluminate fibers are not commercially available, but so far they offer valuable models for important structure–property relationships [80] with regard to strength, modulus, and optical properties.

1.4.1.4 Hybrid Fiber-Forming Processes

The most important glass-forming systems contain elements from the sixth, or chalcogenide, column of the periodic table which includes oxygen, sulfur, selenium, and tellurium. Oxygen-containing (or oxide) glasses are insulators; the others tend to be semiconductors. Some melts are fragile such as the tellurite melts described in the previous section. Others are viscous, and whether they represent strong or fragile melts, they are difficult to fiberize.

A hybrid process for forming chalcogenide glass fibers [128] has been described that uses elements of downdrawing from preforms and fiberizing through bushings. Specifically, a cylindrical chalcogenide preform is vertically inserted into a cylindrical crucible furnished with a nozzle in its bottom plate. The crucible is heated only in the vicinity of the nozzle, and a fiber is continuously drawn from the nozzle at a forming temperature that corresponds to a melt viscosity of log 3 poise.

Heavy metal fluoride fibers require a fiber-forming process that relies on a supercooled melt, while certain fluorophosphate melts can be fiberized by pulling fibers from the melt in a conventional bushing process [129]. Fluorophosphate glass fibers are difficult to pull from the melt. Strong, 27 μm diameter fibers were made with a tensile strength of 334 MPa for making reinforced visible-IR transparent poly (chloro-trifluoroethylene) composites.

1.4.2 Glass Fibers from Inviscid Melts (55–81% Al_2O_3, 4–0% SiO_2)

Melts of metals as well as crystalline ceramic oxides have low viscosities. When cooled, they crystallize at a sharp melting point. Above their melting point their viscosity is comparable to that of motor oil at room temperature. Yet, continuous glass and metal fibers can be formed from inviscid melts.

1.4.2.1 Principles of Fiber Formation from Inviscid Melts

In a typical melt spinning process the quench rate is $\sim 10^4$ K/s. When it is extruded through a bushing tip, a viscous melt with a viscosity of log 2.5–log 3.0 poise readily solidifies and forms a continuous fiber at this quench rate. When extruded, an inviscid melt with a viscosity of <0.2 poise will form a liquid jet at this quench rate that readily breaks up into droplets and subsequently forms shot.

(a) Jet formation from inviscid melts. The key principle governing the formation and breakup of a liquid jet is well known [10]. A liquid jet is unstable with respect to viscosity, diameter, and surface tension. A jet has a tendency to break up due to axisymmetric surface pressures, and produces Rayleigh waves or periodic variations of increasing amplitude in the jet diameter (Fig. 1.22). Ultimately, these diameter variations cause the jet to break up into separate droplets, and they, in turn, crystallize and form shot. For any process to yield a continuous fiber from a low viscosity liquid, the transient viscosity of the melt exiting the bushing tip or spinneret orifice must quickly reach the fiber-forming level of log 2.5–log 3.0 poise before jet instability (formation of Rayleigh waves) and potentially disruptive crystal growth can occur.

The straight, cylindrical fiber in Fig. 1.22 represents an inviscid melt spun calcium aluminate glass fiber that had been surface stabilized with particulate carbon. The frozen Rayleigh wave structure represents a calcium aluminate fiber that was not surface stabilized and solidified while it was in the process of breaking up into droplets and shot.

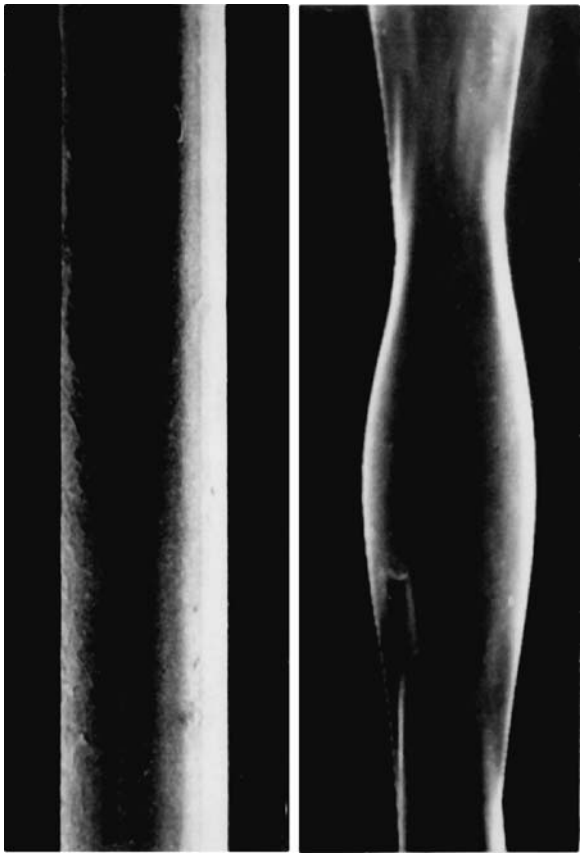

Fig. 1.22 Straight fiber and frozen Rayleigh waves. The *straight*, *cylindrical* fiber represents an inviscid melt spun calcium aluminate glass fiber that had been surface stabilized with particulate carbon. The frozen Rayleigh wave structure represents a calcium aluminate fiber that was not surface stabilized and solidified while it was in the process of breaking up into droplets and shot [1] (with kind permission of Springer Science and Business Media)

For fiber formation (Equation 1.15), a jet must have a lifetime (t) sufficient for the viscosity to reach log 2.5–log 3.0 poise before the onset of turbulence or breakup [10]. The viscosity (η) of the jet is the key factor since it depends exponentially on the temperature. The diameter (D) of the jet is the next most important factor. Thus, a reduction of the viscosity (η) shortens the jet lifetime (t) and limits the attainment low diameter fibers. The surface tension (γ) and density (ρ) are less important, less sensitive to temperature:

$$t = 14[(\rho D^3/\gamma)^{1/2} + (3\eta D/\gamma)] \tag{1.15}$$

$$\mathrm{d}\eta/\mathrm{d}\tau \,\Sigma \mathrm{d}V_\mathrm{c}/\mathrm{d}\tau \tag{1.16}$$

$$T_\mathrm{L} < T_\mathrm{F} \tag{1.17}$$

The conditions (Equation 1.16) under which oxide or metal fibers can be formed from inviscid melts is also defined by the dynamics of the relationship in the forming

zone between the rate of solidification or the change of the viscosity (η) and the rate of crystal growth (V_c) with time (t). Any change in melt viscosity, even if only of the surface viscosity, of a molten jet will disproportionately affect its lifetime. If the lifetime is short, the jet will, on cooling, break up into Rayleigh waves, liquid droplets, and shot, and if it is long, the jet will instead solidify into a continuous fiber on cooling.

(b) Fiber formation from inviscid jets. Three processes are known which facilitate the formation of glass and/or metal fibers from inviscid melts. In the containerless laser-heated (CLH) fiber-forming process, a solid aluminate sample is acoustically levitated, laser melted, and instantly supercooled to increase both the viscosity of the inviscid melt and the jet lifetime at a normal quench rate of 10^4 K/s, i.e., to achieve a transient viscous melt from which fibers can be downdrawn.

In the inviscid melt spinning (IMS) process an inviscid aluminate or metal jet is extruded into a chemically reactive environment that raises their surface viscosity and thereby facilitates the formation of continuous fibers. In the rapid jet solidification (RJS) process, an inviscid jet is extruded through an orifice, and the quench rate is increased by casting it onto the surface of a quench wheel where it solidifies.

1.4.2.2 Containerless, Laser Heating (CLH) Process

In this melt process, a solid aluminate sample is acoustically levitated in a containerless environment, laser melted, and instantly supercooled. Both the viscosity of the inviscid melt increases from <2 to >log 2 poise, and the jet lifetime increases at a normal quench rate of 10^4 K/s. As a result, a viscous melt is obtained from which glass fibers can be downdrawn, including yttrium aluminum garnet (YAG or $Y_3Al_3O_{12}$), glass fibers [12], erbium-, neodynium-, and lanthanum-oxide-doped YAG glass fibers [13], mullite ($Al_6Si_2O_{13}$) glass fibers and holmium-, erbium-, and other rare earth-doped mullite glass fibers [14]. Small additions of SiO_2 improve the glass formability but slightly reduce the long wavelength limit for IR transmission.

(a) Process concept. Containerless liquid phase processing has been successfully used to achieve deep undercooling of molten oxides to a temperature where the viscosity is sufficiently high for fiber pulling. And in principle, containerless conditions eliminate heterogeneous nucleation by containers (crucibles, spinning cells or bushings, and precious metal tips) and help deep undercooling [12].

One may assume that the fiber-forming viscosity, although not reported was between log 2.5 and log 3.0 poise. The liquidus temperature and the delta temperature at the fiber-forming viscosity were not reported either. For the following reasons, they might be responsible for spontaneous crystallization that reportedly occurred toward the end of the fiberizing process [13, 14].

In a batch process that lasts only a very short period of time, it would be inconsequential whether the liquidus temperature were higher or lower than the actual fiber-forming viscosity of log 2.5–3.0 poise. By definition [2], the liquidus temperature is the temperature of a melt at which crystals can form over a short period of time and remain in equilibrium with the melt. In a batch process that lasts longer than a very short time, the melt will spontaneously crystallize, if its viscosity at the

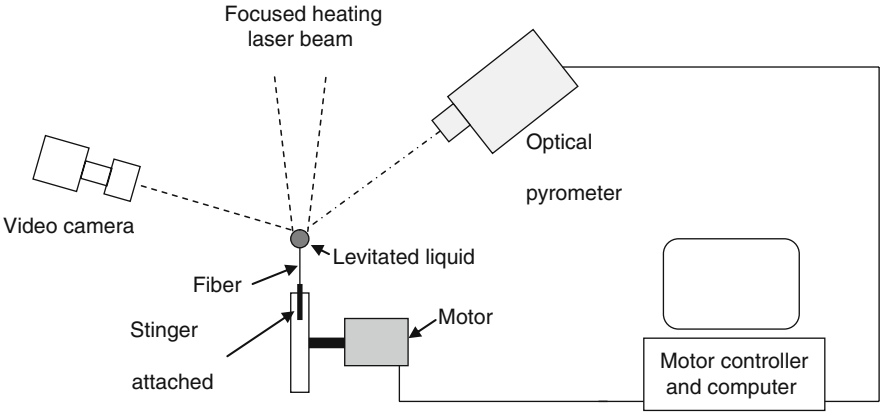

Fig. 1.23 Containerless laser-heated melt process. Redrawn from Weber et al. [12] (supplied by and printed with permission from Richard Weber, April 6, 2009)

fiber-forming temperature were equal to, or lower than, the liquidus temperature (see Section 1.1.3).

(b) YAG glasses and glass fibers. In this process (Fig. 1.23), solid YAG samples, 3 mm in diameter, were levitated in a flow of argon gas. The levitated material was completely melted in a continuous wave CO_2 laser heating beam. The viscosity of the inviscid melt above the melting point was 0.05 Pa s (0.5 poise). The laser beam was then blocked, resulting in a cooling rate of ∼250 K/s.

At a pre-selected temperature between 1600 and 1660°C, i.e., well below the liquidus temperature, fibers were pulled from the levitated droplet by rapidly introducing and withdrawing a 100 μm diameter tungsten wire "stinger." At higher temperatures the stinger pulled out of the melt without forming a fiber, while crystallization was likely to occur at lower temperatures [12].

Glass fibers, up to 0.5 m in length and 5–30 μm in diameter, were pulled from the apparatus at rates of 1.0–1.5 m/s before crystallization terminated the process. The fibers were homogeneous and had smooth surfaces. They were transparent, highly flexible, and x-ray amorphous.

Rare earth oxide–aluminum oxide glasses and glass fibers have properties similar to sapphire and sapphire fibers, respectively. They exhibit infrared transmission up to a wavelength of about 5000 nm. They are hard, strong, stiff, and thermally stable up to about 1000°C. Their homogeneity depends on selected concentrations of optically active dopants. Increasing add-on levels of SiO_2 also increase the homogeneity but reduce the long wavelength limit for infrared transmissions. The average tensile fracture strength of the YAG composition fibers was 5.0±0.3 GPa.

Rare earth oxide–aluminum oxide glasses (REAl^{TM}) are being explored by the Food and Drug Administration as a host glass for mid-IR optical devices in surgical and diagnostic applications, and erbium holmium- and oxide-doped devices in the ∼2100 and 2900 nm wave bands [13]. The economics and scalability of YAG-based

glass fibers are promising but remain unexplored. The materials cost is the same for an amorphous YAG sensor fiber made by the containerless laser-heated melt process as for a single-crystal YAG sensor fiber made by laser-heated pedestal growth (Section 1.5.1). But the process for making glass fibers is faster than that for making single-crystal fibers, and it may require less process energy.

(c) Mullite composition glass fibers. Strong and chemically homogeneous mullite-based glass fibers were made with a diameter of 5–40 μm by pulling fibers from supercooled laser-levitated oxide melts. Under transient cooling conditions, the fiber pulling rates ranged from 0.2 to 1.6 m/s. The average tensile fracture strengths of the glass fibers were 5.6±0.7 GPa. Glass fibers with lower strength levels often showed the presence of equiaxial crystallites with diameters ranging from 20 to 50 μm. Transmission electron microscopy confirmed that the crystalline material was mullite [14].

The information that has been presented [14] shows that the crystallization of mullite glass melts begins to occur at approximately 1200 K at a very low heating rate of 2.5 K/min and that bulk crystallization increases when the heating rate is increased. The synthesis of uniform polycrystalline oxide fibers was achieved in a two-step process, i.e., by downdrawing glass fibers from supercooled melts and then crystallizing the resulting glass fibers by an appropriate heat treatment. The mullite-based glass fibers crystallized and produced dense crystalline fibers with grain sizes ranging from 0.5 to 1 μm. A crystalline mullite fiber with a 10 μm radius that had been made by this process had a tensile strength of 1.8 GPa and an elastic modulus of 360 GPa.

(d) Summary and conclusions. In summary, the process of forming glass fibers from laser-heated, acoustically levitated, supercooled, and otherwise inviscid (essentially non-viscous) oxide melts greatly expands the range of materials which have high strength and superior functionality. The process is inherently fast and potentially inexpensive. Glass fibers made by this process may replace costly single-crystal fibers and polycrystalline fibers made by an extension of this process may replace polycrystalline fibers made by other processes.

1.4.2.3 Inviscid Melt Spinning (IMS) Process

In the inviscid melt spinning (IMS) process an inviscid aluminate or metal jet is extruded into a chemically reactive environment that raises their surface viscosity and thereby facilitates the formation of continuous fibers. The theory governing inviscid melt spinning by chemically modifying the jet as well as fiber surface is well established.

(a) Forming metal fibers in a reactive environment. Commercial wire drawing processes produce metal wires with round cross sections but they are highly energy and labor intensive. These processes fall outside the scope of this book. Commercial rapid solidification processes yield amorphous metallic ribbons. Inviscid melt spinning yields metal fibers by a chemically assisted jet stabilization process.

In the inviscid melt spinning process [11, 130], steel fibers are formed by the same mechanism as glass fibers. In this case, the process shown in Fig. 1.24 requires

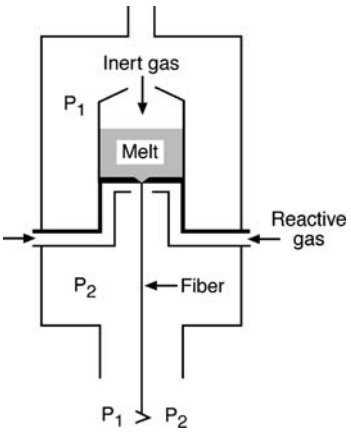

Fig. 1.24 Inviscid melt spinning process (schematic drawing). Redrawn from Wallenberger et al. [9] (reprinted with permission of Elsevier Science Publishers)

the presence of silicon in the steel formulation and the presence of carbon dioxide in the process environment.

A commercial pilot production unit based on the schematic process diagram shown in Fig. 1.24 consisted of a 0.9 m long furnace, a 1.5 m long cooling column, and a windup [9, 11]. In this process, 50 kg of steel was heated and melted with a 4 kHz power unit supplying 70 KW in a ceramic crucible having an orifice in its bottom plate. An essential ingredient in the cooling medium was carbon dioxide. Wires with diameters of 100–200 μm can be made at 1500°C with speeds of 10–20 m/s, respectively. At a rate of 15 m/s, the spinning of a 165 μm diameter wire lasted 4 h. In this pilot process, unbroken wire was obtained for periods in excess of 1 h which represents a continuous length of about 80 km.

As shown in Equations 1.18, 1.19 and 1.20, carbon dioxide diffuses into the surface of the inviscid molten jet. Its concentration decreases with increasing distance from the surface, but wherever it finds silicon that is evenly distributed throughout the melt (and therefore the surface of the liquid jet), it forms silicon dioxide and carbon which cause a steep increase in the surface viscosity. Carbon may further react to form carbides. The surface skin is neither a sheath nor a film:

$$\mathrm{Si} + 2\mathrm{O} \longleftrightarrow \mathrm{SiO_2} \tag{1.18}$$

$$2\mathrm{Si} + 2\mathrm{CO} \longleftrightarrow \mathrm{SiO_2} + 2C \tag{1.19}$$

$$\mathrm{Si} + \mathrm{C} \longleftrightarrow \mathrm{SiC} \tag{1.20}$$

ESCA analysis confirms the presence of oxidized silicon and oxidized iron in the fiber surface or skin [11, 130]. The silica peak gradually disappears at a depth of 100 nm, giving way to the peaks of iron and silicon. Analysis with a CAMECA ion analyzer shows that the intensity of Si^+ peaks decreases to naught between 17 and

55 nm from the surface of a 165 μm diameter steel wire. The results parallel those noted for carbon with aluminate fibers.

Silica is the most viscous inorganic material known, especially at 1500°C. It is the ideal surface viscosity builder to increase the lifetime of a hot inviscid steel jet long enough to prevent formation of Rayleigh waves and shot. Other viscosity builders can be formed in situ at the spinning temperature to stabilize a given molten metal jet [11, 130]. They must have a higher melting point than the metal, and be insoluble in the molten jet [11, 130].

Inviscid melt spinning is considered to be a potentially viable alternative to wire drawing [130] for making steel wires for radial automobile tires, but a prior product development did not reach beyond the pilot plant level. Using silica steels, the complex chemistry (Equations 1.18, 1.19 and 1.20) produces also minute amounts of iron oxides which were detected by ESCA [130] and are a potentially undesirable trace byproduct. The challenge [1, 80] remains to fine-tune the chemistry of this process in a commercial development effort.

(b) Forming oxide glass fibers in a reactive environment. Calcium aluminate glass fibers can also be formed by inviscid melt spinning. In this case, carbon particles which are formed by the decomposition of propane enter into the surface of the molten jet and raise its surface viscosity, a process step that lengthens the lifetime of the jet and prevents its breakup.

In this process variant (Fig. 1.4, Example E, and Fig. 1.24), alumina and calcia are placed in a tungsten crucible having an orifice in its bottom plate [11, 121]. The crucible is placed in a furnace and the surrounding air is replaced with argon. The oxide powder is melted. The melt is maintained 100°C above its melting point. Propane is introduced below the crucible and the argon pressure is increased above the crucible.

A liquid jet of the oxide melt is extruded through the orifice in the bottom of the crucible. Propane decomposes on the hot surface of the molten jet, forms carbon particles which enter into the surface of the jet, and sometimes also deposits an additional secondary carbon sheath on the fiber surface but only after the jet solidifies.

The fibers in the examples contained 51.5–80.2% alumina, 43.5–19.8% calcia, and occasionally also 3.8–4.0% silica and/or 0.1–7.5% magnesia (Table 1.22). Their pristine strength ranged from 0.16 to 1.05 GPa (vs. 3.5 GPa for E-glass) and their moduli ranged from 41.1 to 61.2 GPa (vs. 72.5 GPa for E-glass). Their moduli [9] were much lower than those of updrawn high viscosity calcium aluminate fibers, suggesting much lower internal order. By SEM, the fracture patterns were typical of glass fibers, and fibers with $\leq$80% alumina were amorphous.

Some fibers had a secondary carbon sheath which was up to 600 nm thick [35]. Not surprisingly, these fibers were black. The secondary overgrowth is not an integral part of the fiber [9, 10]. It does not affect the fiber properties and can be peeled or burned off. A few fibers had no carbon sheath. These fibers were translucent. Carbon that is present in the fiber surface or skin does not affect its transparency,

Table 1.22 Properties of inviscid melt spun calcium aluminate glass fibers [1] (with kind permission of Springer Science and Business Media)

	Composition wt%							
Examples [9]	Al_2O_3	CaO	MgO	SiO_2	FT (°C)	Dia. (μm)	Strength (GPa)	Modulus (GPa)
Example (1)	54.0	39.0	3.0	4.0	1700	170	0.5	50.8
Example (2)	54.6	39.0	2.5	3.9	1500	190	0.7	
Example (3)	54.8	38.9	2.5	3.8	1500	216	0.6	46.6
Example (4)	59.0	40.8	0.2	–	1500	190	0.7	45.9
Example (5)	60.8	39.1	0.1	–	1700	225	0.5	41.0
Example (6)	66.8	33.2	–	–	1800	102	0.9	
Example (7)	67.3	32.7	–	–	1700	167	0.8	
Example (8)	80.2	19.8	–	–	1800	117	1.1	
Controls								
E-glass	14.0	22.1	0.6	54.5	1200	10	3.5	72.0
Silica fiber	–	–	–	100.0	1750	100	3.5	69.0

whether the fiber had originally no carbon sheath as-spun or whether the sheath had been removed from the as-spun fiber [10].

Sputtered neutral mass spectrometry (SNMS) depth profiles document that carbon is present in the skin of all fibers to a depth of about 50 nm (Fig. 1.25), whether a given fiber has a secondary carbon sheath overgrowth or not [9]. X-ray photoelectron spectroscopy (XPS) showed that carbon in the surface or skin [10] consists of carbide (51%), carbon (41%), and carbonate (8%). Infrared depth profiling by diffuse reflectance infrared spectroscopy (DRIFT) provided further important insights [131]. It showed that carbon alters the oxygen environment of the aluminum atoms near the fiber surface from octahedral to tetrahedral coordination and promotes the generation of carbonaceous species such as ethers and esters in addition to carbonates and carbides [80] which have also been found with XPS [10].

In summary, a typical aluminate fiber is spun between 1500 and 1700°C (Table 1.22). Carbon enters into the skin of the still liquid jet and stabilizes it. Some fibers have a carbon sheath. The carbon sheath is obtained after the jet is solidified (<500°C), i.e., when more carbon is present in the reactive propane environment than needed to stabilize the liquid jet and form a fiber.

Inviscid melt spun calcium aluminate glass fibers have low strength (0.5–1.1 GPa) and low moduli (46–58 GPa). Low strength and low stiffness can be attributed to the random structure frozen into the fibers during rapid solidification. As a result, these fibers are not likely to become composite reinforcing fibers, despite their excellent alkali resistance which they share with quaternary calcium aluminate fibers [121].

(c) Mechanism of jet solidification. Continuous aluminate glass fibers are formed in the presence of propane, but not in its absence. A viable mechanism of jet stabilization must therefore explain (1) the function of carbon which enters into the surface or skin of the molten jet, (2) the function of carbides and carbonates which

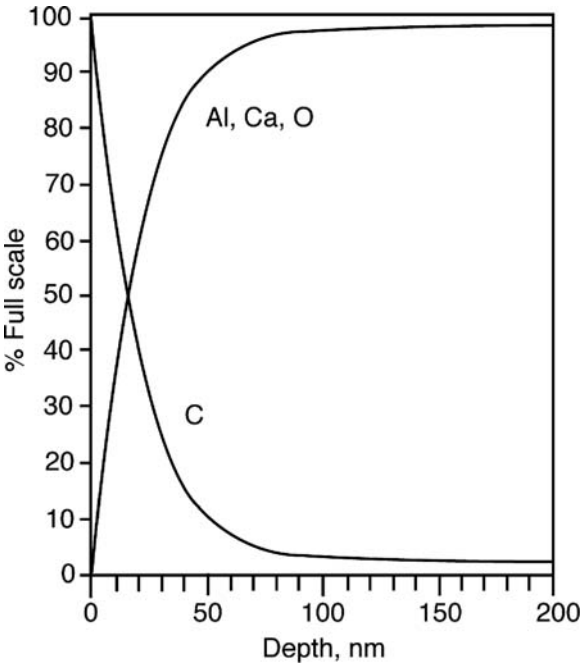

Fig. 1.25 SNMS depth profile of a translucent calcium aluminate fiber. Redrawn from Wallenberger and Brown [1, 35] (reprinted with permission of Elsevier Science Publishers)

are instantly formed in the molten jet surface, and (3) the increase in tetrahedral from octahedral coordination of aluminum atoms in the surface [131] before the fiber solidifies and secondary overgrowth with carbon can occur.

The principle governing jet formation and jet breakup has been discussed in Section 1.4.2.3 [10]. A liquid jet is unstable, degrades into Rayleigh waves (Fig. 1.22, right), and then droplets. The jet stability (Equation 1.15) depends on liquid density, jet diameter, melt viscosity, and surface tension. The lifetime of a jet is the time required for the melt to traverse the continuous length of the jet before the onset of Rayleigh waves [10]. A jet of a silicate glass or an organic polymer melt has a high viscosity ($>10^2$ Pa s) and a lifetime of $>10^0$ s; it can be spun or drawn from the melt by conventional methods, and it solidifies well before it can form Rayleigh waves.

A jet of an aluminate melt with >50% alumina has a low viscosity (<1 Pa s) and a calculated lifetime less than 10^{-2} s (Table 1.23). If ejected into an ambient or neutral environment, it will form Rayleigh waves and droplets (or shot when they freeze) rather than uniform continuous fibers.

Equation 1.15 shows that viscosity is the major factor in determining jet lifetime; surface tension is a secondary factor [10]. Any increase in the surface viscosity of the molten oxide will disproportionately increase the jet lifetime from that calculated for an unassisted jet (2.0×10^{-3} s) to that calculated for an assisted jet (2.0×10^{-1} s) which must have been obtained since continuous fibers were obtained.

Table 1.23 Properties of inviscid calcium aluminate jets [1] (with kind permission of Springer Science and Business Media)

Reference [9] Al_2O_3(%)	Melt Temp. (°C)	Spin Temp. (°C)	Jet/fiber Diam. (μm)	Melt Density (g/cm^3)	Surface Tension (mN/m)	Melt Viscosity (Pa s)	Unassisted jet Life (s)
51.5	1415	1500	375	2.70	680	0.34	1.4×10^{-2}
54.6	1390	1500	190	2.70	680	0.55	8.7×10^{-2}
66.8	1650	1700	105	2.68	625	0.14	2.0×10^{-3}
80.2	1830	1900	118	2.68	575	0.06	1.7×10^{-3}

Particles, especially shaped particles, are known to increase the viscosity of a suspension, following Mooney–Einstein [132]. Thus, carbon particles [10] may enter into the surface or skin of a liquid inviscid jet and increase its viscosity sufficiently and long enough to facilitate its solidification and fiber formation.

For this mechanism to be viable, three conditions must be fulfilled: (1) the increase in the jet surface viscosity must afford a stabilized (assisted) jet lifetime that at least matches the jet cooling time; (2) the assisted lifetime resulting from the viscosity increase must be comparable to the actual (unassisted) lifetime of a typical silicate fiber such as E-glass; and (3) the surface viscosity increase needed to achieve this lifetime must be realistically achievable by carbon insertion in the jet surface.

The pyrolytic production of carbon has been said to create a "snowstorm of large, flat molecules containing the hexagonal ring structure of graphite" [133], i.e., flakes or flat aggregates of smaller particles. They enter into the surface of the molten jet and act as viscosity builders, where they and their instant reaction products such as carbides can be detected by ESCA. Since jet geometry and surface forces tend to constrain particle formation into planar structures parallel to the jet surface, the rheological treatment for flakes is appropriate. The viscosity (η) of a Newtonian fluid containing solid, suspended particles, relative to that (η_o) of the suspending fluid, is governed by the following equation [132]:

$$\ln(\eta/\eta_o) = k_E f_2/[1 - f_2/f_m] \tag{1.21}$$

The Einstein coefficient (k_E) for incorporated particles depends on particle shape, f_2 is the volume fraction of filler, and f_m is the maximum packing fraction for the flakes. The viscosity of the suspending fluid (bulk molten) oxide is 0.14 Pa s, and the required 36.6 Pa s viscosity for the surface layer of the jet can be attained with flake shapes having *L*/*D* between 4 and 9, and volume fractions of solids between 0.32 and 0.45. The combined volume fraction of the solids in the oxide skin detected by SNMS was calculated [11] to be 0.508, a value well above that needed for rheological jet stabilization.

E-glass jets with a diameter comparable to that of the 66.8% alumina jet can be melt spun at temperatures ranging from 1100 to 1480°C [9] where they have a viscosity between 6.1 and 816 Pa s and a calculated lifetime between 8.8×10^{-2}

Table 1.24 Chemical stabilization of inviscid calcium aluminate jets [1] (with kind permission of Springer Science and Business Media)

Jet/fiber comp. [10] (105 μm diameter)	Melt behavior	Temp. (°C)	Viscosity (Pa s)		Jet lifetime (s)	
			Bulk	Surface	Unassisted	Assisted
$CaO\text{-}Al_2O_3$ (66.8%)	Inviscid	1700	0.14	36.6	2.0×10^{-3}	2.6×10^{-1}
E-glass	Strong	1360	31.7	31.7	2.6×10^{-1}	–

and 1.2×10^1 s (Table 1.24). The assisted lifetime of the 66.8% alumina jet (2.6×10^{-1} s) is therefore well within the range of the unassisted E-glass jet lifetimes [10].

In summary, the stabilization of inviscid aluminate jets can be attributed to the increase in surface viscosity due to suspension of solid carbon and carbide particles in the molten oxide surface [10]. The viscosity (rheology)-controlled jet stabilization process is accompanied by a change [131] from an octahedral to a tetrahedral coordination of aluminum atoms near the surface.

1.4.2.4 Rapid Jet Solidification (RJS) Processes

In the rapid jet solidification (RJS) process, the quench rate increases almost instantly from $\sim 10^4$ to $>10^6$ K/s, and the liquid jet quickly reaches a high viscosity range and solidifies before it can crystallize. Unlike the inviscid melt spinning process, a chemically reactive environment that contains, for example, carbon dioxide, is not required to stabilize the metal ribbon [135].

A commercial process has been developed for the production of amorphous metal ribbons [15–17]. The attainment of self-supporting glass ribbons has so net yet been achieved by true rapid solidification.

(a) Amorphous metal ribbons. Glass-forming metal alloys [134] include late transition metal–metalloids (e.g., $Fe_{100\text{-}x}B_x$), early transition metal–metalloids (e.g., $Ti_{100\text{-}x}Si_x$), early transition–late transitions metal alloys (e.g., $Nb_{100\text{-}x}Ni_x$), aluminum-based alloys (e.g., $Al_{83}Cu_{16}V_7$), lanthanum-based alloys (e.g., $La_{100\text{-}x}Au_x$), alkaline earth-based alloys (e.g., $Mg_{100\text{-}x}Zn_x$), and actinide-based alloys (e.g., $U_{100\text{-}x}Co_x$). The techniques for producing amorphous metal alloys [19] include rapid liquid cooling, supercooling of liquids, physical vapor deposition, chemical methods, irradiation, and mechanical methods [134].

The planar flow casting process facilitates the formation of continuous ribbons of metallic glasses or metal alloys from their inviscid melts without requiring a chemically reactive environment as the inviscid melt spinning process or laser levitation. The molten metal is extruded through a ribbon-shaped orifice onto a cold rotating quench wheel. The ribbon is formed without losing its precision shape and is collected on a continuous windup roll; see [58, 15, 134, 135, 16] for details.

The industrial fabrication of amorphous metal ribbons dates back to the late 1970s and to a process known as planar flow casting [17]. The continuous ribbon that is formed has a width ranging from 1 to 100 mm, a thickness of >10 μm, and a uniform rectangular cross section.

(b) Products and applications. Amorphous magnetic glass ribbons based on alloys of iron, nickel, or cobalt are among the softest magnetic materials known. Their tensile strengths range from 1.0 to 1.7 GPa, their moduli from 100 to 110 GPa, and their service temperatures from 90 to 150°C. Their high degree of softness combined with excellent mechanical properties has benefited applications ranging from microscopic recording heads to large architectural EMI shielding, electronic and power cores, and anti-theft sensors [16].

Tin–lead alloy Metglas ribbons, having moduli as low as 18 GPa, are used as solders for diebonding applications. Their liquidus ranges from 190 to 314°C and their solidus ranges from 182 to 310°C. Metglas brazing foils are made from nickel-, cobalt-, palladium-, and copper-based alloys as melting point depressors, and come in ribbons 10 cm wide and >25 μm in thickness. Solder and brazing ribbons have solidus temperatures from 770 to 1130°C and liquidus temperatures ranging from 925 to 1150°C. Applications include aerospace components, electric motors, and brake pads [16].

(c) Amorphous fiberglass ribbons. No ribbons were so far made from inviscid oxide glass melts. Production of glass ribbons and glass fibers from inviscid melts by a rapid solidification process that does not require a chemically reactive environment or acoustic levitation in a containerless process remains a challenge for the future.

1.5 Appendix: Single-Crystal Alumina Fibers

The following review of single-crystal aluminate and alumina fibers is meant to serve as a reference to the chapters on aluminate and alumina glass fibers – and as a challenge. For example, YAG glass fibers, which are aimed at sensor applications (Section 1.4.2.2), can be made with higher process speeds and are more energy-friendly than single-crystal YAG sensor fibers. As a result, this section provides potential targets for developing the technology to make glass fibers which correspond to a range of other commercial single-crystal fibers, including sapphire fibers.

1.5.1 Single-Crystal Fibers from Inviscid Melts

Continuous single-crystal fibers can be grown from inviscid melts by the very slow edge-defined film-fed growth (EFG) process [18] and by the slow equally slow laser-heated float zone (LHFZ) or laser-heated pedestal growth (LHPG)

process with growth rates ranging from 0.3 to 0.7 mm/s [19]. As previously discussed, aluminate glass fibers can be formed at much higher rates from inviscid melts and commercial polycrystalline alumina fibers require different fabrication processes [32].

1.5.1.1 Edge-Defined Film-Fed Growth

Edge-defined film-fed growth (EFG) is a commercial process [18] that facilitates the fabrication of continuous void-free single-crystal oxide fibers from tungsten or other growth orifices.

(a) Growth of sapphire fibers. This process yields commercial single-crystal sapphire fibers. A liquid pool from which the continually growing filamentary crystal is withdrawn is formed on top of a planar surface of the orifice and fed by capillaries which extend down through the orifice into a liquid reservoir. The crystal shaping or edge definition is maintained by the geometry of the top surface of the orifice and the fulfillment of a contact angle of <90° between the liquid and material from which the orifice is fabricated.

Single-crystal alumina (sapphire) fibers grow in this process in the <0001> growth direction. These fibers are void free and have a density of 3.97 g/cm^3, a tensile strength of 2.1–3.4 GPa at room temperature, Young′s modulus of 453 GPa, superior electrical and optical properties, and superior chemical stability. Although individual fibers can be obtained with diameters ranging from 64 to 350 μm, their commercial diameters range from 150 to 250 μm.

Sapphire is produced commercially throughout the world and is used in virtually every industry. The optical, electrical, chemical, mechanical, and nuclear properties of sapphire fibers, as described in the literature [18], make them an ideal material for many applications other than their use as sensor or reinforcing fibers for metal and ceramic matrix composites. Frequently, the combination of two or more of its properties renders sapphire as the only material available to solve complex engineering design problems.

(b) Process versatility. The edge-defined film-fed growth method (EFG) is a "near-net-shape" process for growing continuous sapphire fibers and for prototyping a wide variety of other shaped parts. Unlike other crystal growth methods used to make sapphire structures, only the edge-defined film-fed growth method can be used to also produce grown-to-shape tubes, rods, ribbons, and three-dimensional shapes. All other processes form ingots of various sizes, which must be cut to shape by highly skilled workers using costly diamond impregnated tools.

1.5.1.2 Laser-Heated Float Zone Growth

In the laser-heated float zone (LHFZ) or pedestal (LHPG) growth process, a circumferential laser is placed around a preform rod (e.g., polycrystalline alumina) to zone refine a segment of the material while at the same time updrawing a single-crystal fiber (e.g., sapphire).

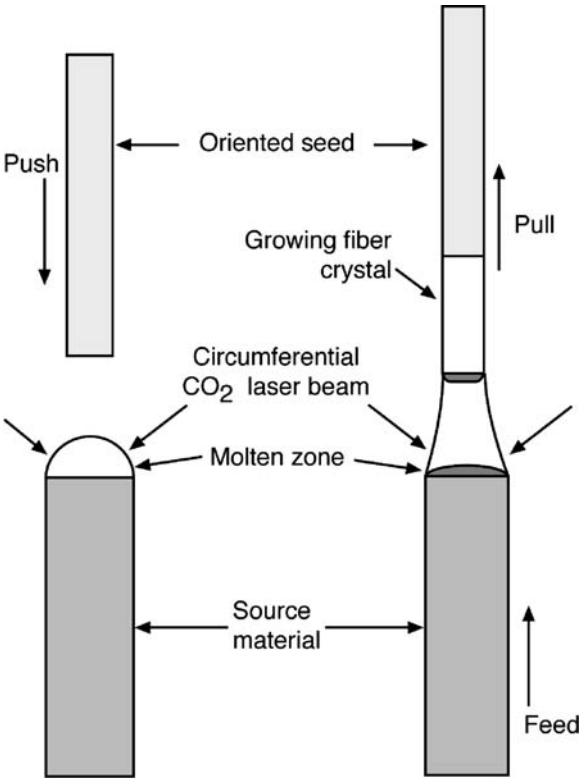

Fig. 1.26 Laser-heated float zone or pedestal growth process (schematic). Redrawn from Feigelson [18, 36] (reprinted with permission of Elsevier Science Publishers)

(a) Growth of single-crystal fibers. Materials may melt congruently or incongruently in the float zone [19, 136, 137]. The singular function of the laser in this process (Fig. 1.26) is to provide uniform circumferential heating. The tip of the preform rod is melted, and a seed rod is introduced into the melt and slowly withdrawn to initiate the growth of a potentially endless filamentary single crystal. Sapphire fibers [19, 33] updrawn from sintered polycrystalline alumina preform rods are the best researched material made by this process. They offer a superior value in end uses requiring prolonged exposure to ultrahigh temperatures.

The properties of these sapphire fibers are comparable to those made by edge-defined film-fed growth, except that potentially lower diameters are possible at about equal growth rates [19]. Growth rates of 0.7 mm/s are possible, but growth rates below 0.3 mm/s are typically used with pure materials [19]. For comparison, sapphire fibers grown by edge-defined film-fed growth were reported to have growth rates up to 0.5 mm/s.

The laser-heated float zone process is not limited to sapphire fibers or even to oxides. Table 1.25 lists fibers other than sapphire which have been grown by

Table 1.25 Single-crystal fibersgrown float zone or pedestal growth [1] (with kind permission of Springer Science and Business Media)

Oxides	MP (°C)	Orientation	Dia. (μm)	Application
Nd:YAG	1940	[124, 126]	6–1000	Laser
YAG	1940	[124, 126]	100–1000	Laser
Al_2O_3	2045	a, c	55–600	Remote sensor
Ti:Al_2O_3	2045	c	200–800	Laser
Cr:Al_2O_3	2045	c	3–170	Laser
$LiNbO_3$	1260	a, c	20–800	Acoustics
Nd:$LiNbO_3$	1260	c	800	Laser
$LiTaO_3$	1650	[124]	600	SAW device
Li_2GeO_3	1170	a, c	100–600	Raman device
$Gd_2(MoO_4)_3$	1157	[124]	200–600	Ferroelastic
$CaSc_2O_4$	2200	a, b, c	100–600	Model
Nd:$CaSc_2O_4$	2200	c	600	Laser
$SrSc_2O_4$	2200	–	600	Model
YIG	1555	[124]	100–600	Insulator
Eu:Al_2O_3	2410	c	500–800	Laser
Ti:$MgAl_2O_4$	2105	–	1000	Laser
Ti:$YAlO_3$	1875	–	1000	Laser
BaB_2O_4	1095	–	500	Nonlinear optics
Nd_2SiO_5	1980	–	750	Laser
$SrTiO_3$	1860	–	600	Model
Nb_2O_5	1495	–	700–1700	Model
$BaTiO_3$	1618	c	300–800	Ferroelectric
$SrBaTi_2O_6$	1700	a, c	200–600	Ferroelectric
$ScTaO_4$	2300	a	200–600	Ferroelectric
$ScNbO_4$	2100	–	200–600	Ferroelectric
$SrBaNb_2O_6$	1500	a, c	600–1700	IR guide
Cr:Y_2O_3	2400	c [124],	600	Laser
Cr:Sc_2O_3	2400	c [124],	600	Laser
Cr:Lu_2O_3	2400	c [124],	600	Laser
Li_2O–GeO_2	1106	–	–	Eutectics
($Bi_{1.8}Sr_{1.8}Ca_{1.2}Cu_{2.2}O_8$)		–	250–1000	High T_c s/c wires

this process. This includes filamentary single salts, eutectics, oxides, ceramics, and semiconductors, as well as superconductor and metallic fibers.

Sapphire, $LiNbO_3$, Li_2O–NaF, Nd:YAG, and Cr:Al_2O_3 fibers have been grown with diameters as low as 55, 40, 20, 6, and 3 μm, respectively. Some of the more important fibers grown by this method are Al_2O_3–$Y_3Al_5O_{12}$ (YAG) eutectic fibers [138] and Y_2O_3–stabilized, cubic ZrO_2 single-crystal fibers [129]. A major motivation for current research is the potential of single-crystal fibers in optoelectronic applications [139].

Single-crystal fibers of potassium lithium niobate are known to be useful materials for electro-optic applications. They can be grown with a growth rate of 11 mm/h with diameters of 0.9 mm by the halogen lamp-assisted laser-heated pedestal growth method, alternatively known as the laser float zone method. The single-crystal fibers,

like the ceramic feed rods from which they were grown, consisted of 30% K_2O, %17 Li_2O, and 53% Nb_2O_3 [140].

As core clad waveguide structures of the *c*-axis, 200 μm diameter single-crystal lithium niobate fibers have potential applications as second harmonic generators, optical modulators, lasers, and optical oscillators. They are obtained by a magnesium ion diffusion process [137].

Filamentary eutectic ZrO/CaO crystals can also be grown by the laser-heated float zone process. They have a high degree of ion conduction and are aimed at advanced applications such as solid electrolytes, where their conductivity at high temperatures may be exploited in heating elements and in situ gas sensors [141]. The starting materials are ZrO_2/CaO powders with a eutectic composition. Single-crystal fibers are prepared by a polymer matrix route or a ceramic route. The phase formation in both routes is similar.

The laser float zone process has also been used successfully to synthesize phosphorescent single crystals of $SrAl_2O_4$:Eu^{2+}, Dy^{3+} and $CaAl_2O_4$:Eu^{2+}, Nd^{3+} [142]. These single-crystal fibers may have important applications in optoelectronic technology. The crystals show bright green and purple phosphorescence, respectively, with persistence times exceeding 16 h. Their brightness is 10 times stronger than that of traditional sulfide phosphors. Sulfide phosphors vaporize near their melting points and single crystals are therefore difficult to grow. Alkaline earth aluminates have low vapor pressures near their melting points and single crystals can be grown directly from their inviscid melts [142].

Typically, fibers having diameters up to 100 μm are readily possible; fibers with diameters above 200 μm are technically speaking no longer fibers but rods. This includes the niobate fibers [140] and the superconducting fibers [19, 143–145] discussed below. In principle, the float zone method is a containerless process. There is a nominal diameter reduction in the float zone from that of the preform rod to that of the final fiber. Zone (or overall process) stability for the growth of oxide and fluoride fibers is usually achieved with diameter reductions in the range of 1/2 to 1/3 [19].

(b) High T_c superconducting fibers. These materials may also melt congruently or incongruently in the float zone [19]. Congruently melting materials do not undergo a phase transformation above room temperature, have a low vapor pressure at their melting, and are easy to grow in single-crystal form by this method. Incongruently melting preform materials first yield a phase that is different from that of the source rod and the melt [136]. As growth proceeds, the melt composition changes, and the liquidus drops until it reaches the peritectic decomposition temperature. At this point, the desired phase crystallizes and steady-state growth will be achieved [19].

The laser float zone process is an effective method for growing oriented $Bi_2Sr_2CaCu_2O_8$ fibers [143]. Single-crystal $Y_3Fe_5O_{15}$ (YIG) and polycrystalline high T_c superconducting $Bi_{1.8}Sr_{1.8}Ca_{1.2}Cu_{2.2}O_8$ fibers [143] (Fig. 1.26) were first grown by the float zone process with diameters of 0.7 and 1 mm, respectively, from incongruently melting compounds. The critical current measurements on the high T_c fiber were 5×10^{-4} A/cm^2 at 68 K with zero resistance near 85 K [144].

More recently, careful processing afforded Pb-substituted Bi–Sr–Cu–Ca–O fibers with critical temperatures (T_c) of 106 K and critical current densities (J_c) of 1015 A/cm^2 (77 K, O T) after annealing [145]. Magnetic susceptibility and critical current density of superconducting fibers of the Bi–Sr–Ca–Cu–O system grown by the laser float zone method are strongly dependent on the pull rates. A favorable grain orientation for current transport and highest critical currents was obtained at high pulling rates, e.g., >4 μm/s [136].

In summary, the laser-heated float zone (LHFZ) method [136], in particular the traveling solvent zone melting (TSZM) configuration [137], is a highly effective technique to grow centimeter long crystals of high T_c and other low-dimensional cuprates. High-temperature superconducting fibers, wires, tapes, and ribbons have also been made by the powder-in-tube method. These are sheath/core bicomponent fibers or ribbons having a protective metal sheath and a functional core consisting of an appropriate multiple oxide. In this fabrication process [146] the superconducting powder is continuously introduced into a metal tube and the filled tube is drawn by conventional wire drawing methods.

Although the powder-in-tube method did yield the highest current density [147] reported so far (> 1,000,000 A/cm^2, 77 K, O T), it is not reviewed here in detail because it is a metal drawing, not a melt-forming process. High-temperature superconducting sheath/core bicomponent fibers have also been made by introducing the superconducting material into the core of hollow glass fibers as they are formed under the bushing (Section 1.3.4.2).

1.5.2 The Future of Alumina and Aluminate Fibers

Continuous single-crystal sapphire fibers offer an impressive performance as reinforcing fibers in ceramic and metal matrix composites. It is therefore appropriate to note some important commonalties and differences between single-crystal and inviscid alumina fibers.

1.5.2.1 Amorphous Alumina vs. Single-Crystal Sapphire Fibers

Sapphire fibers are hard, strong, and scratch resistant to most materials and provide excellent wear surfaces. They can withstand higher pressures than polycrystalline alumina since they lack the grain boundary interface breakdown of the latter. Sapphire fibers transmit ultraviolet, visible, infrared, and microwaves and serve as excellent wave guides between 10.6 and 17 μm, and offer durable and reliable IR transmission. By virtue of their high thermal conductivity they can be rapidly heated and cooled.

EFG sapphire fibers melt sharply at 2050°C and maintain measurable strength at extreme temperatures [18]. Table 1.26 shows tensile strength as a function of test temperature from 25 to 1500°C. The room temperature strength, 3.57 GPa, is low for a single-crystal fiber but typical for sapphire fibers, irrespective of process. The strength of crystal oxide fibers at room temperature should be approaching the

Table 1.26 Strength retention of sapphire fibers at elevated temperature [1] (with kind permission of Springer Science and Business Media)

Fiber testing temperature (°C)	Average tensile strength (GPa)	Standard deviation (GP)
25	3.57	0.66
400	2.08	0.49
800	1.85	0.34
1094	1.03	0.14
1500	0.55	0.09

theoretical value, which is >10 GPa. In fact, room temperature strength of EFG sapphire fibers is only 2.5–3.0 times higher than that of about an equal diameter polycrystalline alumina (1.2–2.6 GPa) such as Fiber FP or PRD-166, respectively [32]. This deficiency of single-crystal EFG sapphire fibers still needs to be corrected.

The tensile strength of EFG sapphire fibers at 1500°C in Table 1.26 is 0.55 GPa. In addition, isolated literature values report strength levels of 0.40 GPa up to 1900°C. These are impressive results since they refer to an oxidative environment. In an oxidative environment, unprotected (uncoated) carbon fibers are stable up to 500°C, especially for longer term exposures.

1.5.2.2 Amorphous YAG vs. Single-Crystal YAG Fibers

Continuous single-crystal oxide fibers, including sapphire, have significant property advantages over the corresponding polycrystalline oxide fibers [32]. They include microstructural stability at high temperatures, retention of high elastic moduli at high temperatures, and high-temperature creep for which even further improvements are being sought [18, 19, 138, 148]. But because of their high fiber diameters, they cannot be woven. They must be filament wound or used as inserts.

1.5.2.3 Summary, Conclusions, and Outlook

Commercial single-crystal sapphire fibers [33, 139], single-crystal yttrium aluminum garnet (YAG) fibers [138], and polycrystalline oxide fibers [32] are commercially available, but they are costly, and commercial opportunities exist for new non-structural continuous single-crystal and polycrystalline oxide fibers for high T_c superconductors, optoelectronics, nonlinear optics and acoustic IR guides, lasers, and remote sensors [1, 33,136–146,148].

The advent of glass fibers, which are made from inviscid oxide melts, serves as a challenge. YAG glass fibers, which are aimed at sensor applications, rely on a more energy-friendly process than the single-crystal YAG sensor fibers and they can be made with higher process speeds. Other single-crystal fibers, including sapphire fibers, offer further potential targets for exploring the development of the corresponding glass fibers and their value-in-use.

References

1. F. T. Wallenberger, Continuous melt spinning processes, in *Advanced inorganic fibers: processes, structures, properties, applications*, Chapter 4, Kluwer Academic Publishers, Dordrecht/Boston/London, pp. 81–122 (1999).
2. F. T. Wallenberger, R. J. Hicks, P. N. Simcic and A. T. Bierhals, New environmentally and energy friendly fiberglass compositions (E-glass, ECR-glass, C-glass and A-glass), Glass Technol. Eur. J. Glass Sci. Technol. A, 48 (6), 305–315 (2007).
3. C. A. Angell, Glass formers and viscous liquid slowdown since David Turnbull: enduring puzzles and new twists, MRS Bull., 33 (5), 544–555 (2008).
4. F. T. Wallenberger, The structure of glasses, Science, 267, 1549 (1995).
5. F. T. Wallenberger, N. E. Weston and S. D. Brown, Calcia-alumina glass fibers: drawing from super-cooled melts versus inviscid melt spinning, Mater. Lett., 11 (89), 229–235 (1991).
6. V. E. Khazanov, Yu. I. Kolesov and N. N. Trofimov, Glass fibers, in *Fibre science and technology*, V. I. Kostikov, ed., Chapman and Hall, London, pp. 15–230 (1995).
7. F. T. Wallenberger, Continuous solvent spinning processes, in *Advanced inorganic fibers: processes, structures, properties, applications*, Chapter 5, Kluwer Academic Publishers, Dordrecht/Boston/London, pp. 123–128 (1999).
8. G. Y. Onoda, Jr. and S. D. Brown, Low silica glasses based on calcia-aluminas, J. Am. Ceram. Soc., 53 (6), 311–316 (1970).
9. F. T. Wallenberger, N. E. Weston and S. A. Dunn, Inviscid melt spinning: as-spun amorphous alumina fibers, Mater. Lett., 2 (4), 121–127 (1990).
10. F. T. Wallenberger, N. E. Weston, K. Motzfeldt, and D. G. Swartzfager, Inviscid melt spinning of alumina fibers: Chemical jet stabilization, J. Am. Ceram. Soc., 75 (3), 629–639 (1992).
11. R. E. Cunningham, L. F. Rakestraw and S. A. Dunn, Inviscid melt spinning of filaments, in *Spinning wire from molten metal*, J. Mottern and W. J. Privott, ed., AIChE Symposium Series, AIChE, New York, 74 (180), 20–32 (1978).
12. J. K. R. Weber, J. J. Felton, B. Cho and P. C. Nordine, Glass fibres of pure and erbium- or neodymium-doped yttria-alumina compositions, Nature, 393, 769–771 (1998).
13. J. K. R. Weber, R. W. Waynant, I. Ilev, T. S. Key and P. C. Nordine, "Rare earth oxide-aluminum oxide glasses for mid-range IR devices," Proc. SPIE, Optical Fibers and Sensors for Medical Applications III, I. Gannot, ed., 4957, 16–22 (2003).
14. J. K. R. Weber, B. Cho, A. D. Hixon, J. G. Abadie, P. C. Nordine, W. M. Kriven, B. R. Johnson and D. Zhu, Growth and crystallization of YAG- and mullite-composition glass fibers, J. Eur. Ceram. Soc., 19, 2543–2550 (1999).
15. H. H. Liebermann, *Rapidly solidified alloys*, Marcel Decker, New York. (1993).
16. H. H. Liebermann, Metglas®, Allied Signal, Parsippany, NJ (1993).
17. D. M. C. Narashima, Planar flow casting of alloys, US Patent 4,142,571 (1979).
18. R. S. Feigelson, Growth of fiber crystals, in *Crystal growth of electronic materials*, E. Kaddis, ed., Elsevier Publishers, London, pp. 127–145 (1985).
19. J. Monbleau, *Single crystal technology, product bulletin*, Saphikon Inc., Milford (1994).
20. F. T. Wallenberger and R. J. Hicks, The effect of boron on the properties of fiberglass melts, Glass Technol. Eur. J. Glass Sci. Technol. A, 47 (5), 148–152 (2006).
21. F. T. Wallenberger, R. J. Hicks and A. T. Bierhals, Design of energy and environmentally friendly fiberglass compositions derived from the quaternary SiO_2–Al_2O_3–CaO–MgO phase diagram – Part I: structures, properties and crystallization potential of selected multi-oxide E-glass compositions, Ceramic Transactions, Volume 170, H. Li et al., eds., 181–199 (2004).
22. F. T. Wallenberger, R. J. Hicks and A. T. Bierhals, Effect of key oxides, including Li_2O, on the melt viscosity and energy demand of E-glass compositions, 66th Conference on Glass Problems, University of Illinois at Urbana-Champaign, Collection of Papers, W. M. Kriven, American Ceramic Society, John Wiley & Sons, 155–165 (2006).

23. F. T. Wallenberger, R. J. Hicks and A. T. Bierhals, Design of environmentally friendly fiberglass compositions: ternary eutectic SiO_2–Al_2O_3–CaO and related compositions, structures and properties, J. Non-Cryst. Solids, 349, 377–387 (2004).
24. F T. Wallenberger, R. J. Hicks and A. T. Bierhals, Design of energy and environmentally friendly fiberglass compositions derived from the quaternary SiO_2–Al_2O_3–CaO–MgO phase diagram – Part II: Fluorine-free E-Glass compositions containing low levels of B_2O3 and Li_2O, in Proceedings of the Norbert Kreidl Memorial Conference, Glastechnische Berichte – Glass Science and Technology, Vol. 77C, 170–183 (2004).
25. F. T. Wallenberger, R. J. Hicks and A. T. Bierhals, Effect of oxides on decreasing melt viscosity and energy demand of E-glass, The Glass Researcher, Vol. 15, No. 1, Am. Ceram. Soc. Bull., 85 (2), 38–41 (2006).
26. F. T. Wallenberger, Glass fiber forming compositions, US Patent 7,153,799 B2, December 26, 2006.
27. F. T. Wallenberger, Glass fiber forming compositions, US Patent 6,962,886 B2, November 8, 2005.
28. T. P. Seward and T. Vascott, eds., *High temperature glass melt property database for process modeling*, The American Ceramic Society, Publisher, Westerville, p. 258 (2005).
29. K. H. Karlson and R. Backman, Thermodynamic properties, in *Properties of glass-forming melts*, L. D. Pye, A. Montenero and I. Joseph, eds., Taylor and Francis, CRC Press, Boca Raton, pp. 11–23 (2005).
30. P. Hrma, D. E. Smith, J. Matyas, J. D. Yeager, J. V. Jones and E. N. Boulos, Effect of float glass composition on liquidus temperature and devitrification behavior, Glass Technol. Eur. J. Glass Sci. Technol. A, 47 (3), 78–90 (2006).
31. P. A. Bingham and M. Marshall, Reformulation of container glasses for environmental benefit through lower melt temperatures, Glass Technol., 46 (1), 11–29 (2005).
32. R. Naslain, Ceramic oxide fibers from sol-gels and slurries, in *Advanced inorganic fibers: processes, structures, properties, applications*, F. T. Wallenberger, ed., Chapter 8, Kluwer Academic Publishers, Dordrecht/Boston/London, pp. 216–225 (1999).
33. J. T. A. Pollock, Filamentary sapphire – the growth of void-free sapphire filament at rates up to 3.0 cm/min, J. Mater. Sci., 7, 786–792 (1972).
34. J. E. Ritter and J. D. Helfinstine, A tougher fiber for the FOG-M, Photonics Spectra, 8, 90–93 (1967).
35. F. T. Wallenberger and S. D. Brown, High modulus glass fibers for new transportation and infrastructure composites and for new infrared uses, Compos. Sci. Technol., 51, 243–263 (1994).
36. F. T. Wallenberger, Continuous melt spinning processes, in *Advanced inorganic fibers: processes, structures, properties, applications*, Chapter 6, Kluwer Academic Publishers, Dordrecht/Boston/London, pp. 129–168 (1999).
37. E. M. Rabinovitch, Sol-gel processing: general principles, in *Sol-gel optics, processing and applications*, L. C. Klein, ed., Kluwer Academic Publishers, Boston, pp. 1–37 (1994).
38. R. Brückner, Silicon Dioxide, in Encyclopedia of Applied Physics, VCH Publishers, Inc., 18, 102–131 (1997).
39. Asahi, Product Bulletin (1986).
40. K. Matsuzaki, D. Arai, N. Taneda, T. Mukaiyama and M. Ikemura, Continuous silica glass fiber produced by sol-gel process, J. Non-Cryst. Solids, 112, 437–441 (1989).
41. K. Kamiya and T. Yoko, Synthesis of SiO_2 glass fibres from Si $(OC_2H_5)_4$ – H_2O–C_2H_5OH–HCl solutions through sol-gel method, J. Mater. Sci., 21, 842–848 (1986).
42. K. Kamiya, R. Uemura, J. Matsuoka and H. Nasu, Effect of preheat treatment on the tensile strength of sol-gel derived SiO_2 glass fibers, J. Ceram. Soc. Jpn, 103 (3), 245 (1995).
43. W. Zhou, Y. Xu, L. Zhang, X. Sun, J. Ma and S. She, Crystallization of silica fibers made from metal alkoxide, Mater. Lett., 11 (10–12), 352–354 (1991).
44. A. Wegerhoff and H. D. Achtsnit, High temperature resistant fibrous silicon dioxide material, US Patent, 4,786,017, November 22, 1988.
45. G. H. Vitzhum, H. U. Herwig, A. Wegerhoff and H. D. Achtsnit, Silica fiber for high temperature applications, Chemiefasern/Textilindustrie, 36/88, E-126-127 (1986).

46. H. D. Achtsnit, Textile silica sliver, its manufacture and use, US Patent 5,567,516, October 23, 1996.
47. Product Bulletin, Silfa silica yarns, Ametek/Haveg, Wilmington, DE (1996).
48. G. Wiedermann and N. Frenzel, Untersuchungen zur chemischen Beständigkeit der Glasseide, Faserforschung und Textiltechnik, 24 (9), 335–340 (1973).
49. P. F. Aubourg and W. W. Wolf, Glass fibers, in *Advances in ceramics, Vol. 18, commercial glasses*, D. C. Boyd and J. F. MacDowell, eds., American Ceramic Society, Westerville, pp. 51–63 (1986).
50. P. K. Gupta, Glass fibers for composite materials, in *Fibre reinforcements for composites materials*, Chapter 2, A. R. Bunsell, ed., Composite materials series 2, Elsevier, Amsterdam, pp. 19–71 (1988).
51. B. A. Proctor, Continuous filament glass fibers, in *Concise encyclopedia of composite materials*, A. Kelly, ed., Pergamon Press, Oxford/New York/Beijing/Frankfurt, pp. 62–69 (1989).
52. K. L. Loewenstein, *The manufacturing technology of continuous glass fibres*, Edition 3, Elsevier, Amsterdam (1993).
53. F. T. Wallenberger, H. Li and J. Watson, Glass fibers, in *ASM Handbook, Vol. 21, composites*, ASM International, Metals Park, pp. 27–35 (2001).
54. J. R.Gonterman and M. A. Weinstein, High Intensity Plasma Glass Melter Project, Final DOE Report, October 27, 2006. The report is available at www1.eere.energy.gov/industry/glass/pdfs/894643_plasmelt.pdf
55. S. Rehkson, J. Leonard and P. Sanger, Continuous glass fiber drawing, Am. Ceram. Soc. Bull., 6, 9401–9407 (2004).
56. F. Rossi and G. Williams, A new era in glass fiber composites, 28th AVK Conference, Baden-Baden, Germany, 1–10, October 1–2, 1997.
57. T. D. Erickson and W. W. Wolf, Glass composition, fibers, and methods for making same, US Patent 4,026,715, May 31, 1977.
58. F. T. Wallenberger, Design factors affecting the fabrication of fiber reinforced infrastructure composites, Annual Wilson Forum, Santa Ana, CA, March 20–21, 1995; in Applications of Composite Materials in the Infrastructure, 1–10 (1995).
59. W. L. Eastes, D. A. Hofmann and J. W. Wingert, Boron-free glass fibers, US Patent 5,789,325, August 4, 1998.
60. M. J. Cusick, M. A. Weinstein and L. Olds, Method for the melting, combustion or incineration of materials and apparatus thereof, US Patent No. 5,548,611, August 29, 1996.
61. J. K Williams, C. P. Heanley and L. E. Olds, Method of melting materials and apparatus thereof, US Patent 5,028,248, July 2, 1991.
62. D. A. Dalton, Plasma and electrical systems in glass manufacturing, IEE Colloquium [Digest], 229, p3/1-2 (1994).
63. C. Ross, P. Tincher and G. Tincher, *Glass melting technology: A technical and economic assessment*, GMIC Publication, October, 2004.
64. ASTM Specification D 578-00, Standard for E-glass fiber strands and stating the composition limits for E-glass, Annual Book of Standards, American Society for Testing and Materials, Conshohocken, PA, March 10, 2000.
65. Naamlooze Vennootschap Maatschapij tot Beheer en Exploitatie van Octoorien, New and improved glass compositions for the production of glass fibers, Brit. Patent, GB 520,247, April 18, 1939.
66. R. A. Schoenlaub, Glass compositions, US Patent 2,334,961, November 23, 1943.
67. R. L. Tiede and F. V. Tooley, Glass composition, US Patent 2,334,961, November 2, 1951.
68. J. F. Sproull, Fiber glass composition, US Patent 4,542,106, September 17, 1985.
69. R. L. Jones, The role of boron in the corrosion of E-glass fibres, Glass Technol. Eur. J. Glass Sci. Technol. A, 47 (6), 167–171 (2006).
70. T. F. Starr, *Glass-fibre databook*, Edition 1, Chapman & Hall, London/Glasgow/New York/Tokyo/Melbourne/Madras (1993).

71. T. F. Starr, *Carbon and high performance fibers, directory and databook*, Edition 6, Chapman & Hall, London/Glasgow/New York/Tokyo/Melbourne/Madras (1995).
72. Product Bulletin, Comperative technical characteristics of filament made from E-glass, basalt and silica, Sudaglass Fiber Technology, Inc., 14714 Perthshire, Suite A, Houston, TX, 77079 USA (2003).
73. S. Tamura, M. Mori and S. Saito, Compositions for the production of high-strength glass fiber, Japanese Patent, 8[1996]-231-240, September 10, 1996.
74. French Patent 1,435,739 to St. Gobain Company, Chambrey, France (1963).
75. P. B. McGinnes, High temperature glass fibers, International Patent Application WO 02/42233 A2, May 30, 2002.
76. P. B. McGinnis, High temperature glass fibers, International Publication WO 02/42233 A2 under the Patent Cooperation Treaty (PCT) on May 30, 2003.
77. Product Bulletin, High strength glass fibers, Advanced Glass Fiber Yarns, LLC, 2558 Wagener Road, Aiken, SC 29801 (2003).
78. J. F. Bacon, High modulus, high temperature glass fibers, Appl. Polym. Symp., 21, 179–200 (1973).
79. P. K. Gupta, Strength of glass fibers, in *Fiber fracture*, M. Elices and J. Llorca, eds., Elsevier, Amsterdam, pp. 127–153 (2002).
80. F. T. Wallenberger, Melt viscosity and modulus of bulk glasses and fibers – challenges for the next decade, in Present State and Future Prospects of Glass Science and Technology, Kreidl Symposium, Triesenberg, Liechtenstein, July 3–8, 1994, Glasstech. Ber. Glass Sci. Technol. 70 C, 63–78 (1997).
81. F. T. Wallenberger, Introduction to reinforcing fibers, in *ASM handbook, Vol. 21, Composites*, ASM International, Metals Park, pp. 23–26 (2001).
82. H. Kaplan-Diedrich and G. H. Frischat, Properties of some oxynitride fibers, J. Non-Cryst. Solids, 184, 133–136 (1995).
83. M. Oota, T. Kanamori, S. Kitamura, H. Fujii, T. Kawasaki, K. Sekine and C. Manabe, Decrease of silicon defects in oxynitride glass, J. Non-Cryst. Solids, 209, 69–75 (1997).
84. A. Carre, F. Roger and C. Variot, Study of acid/base properties of oxide, oxide glass, and glass-ceramic surfaces, J. Colloid Interface Sci., 154 (1), 31–40 (1992).
85. P. C. Almenera and P. Thornburrow, A new glass fiber reinforcement for anti-corrosion composites, Advanced Polymer Composites for Structural Applications in Construction, Proceedings 69IFS8 (2004).
86. P. Simurka, M. Liska, A. Plsko and K. Forkel, Development of a composition suitable for the production of alkali-resistant glass fibres with a low fiberising temperature, Glass Technol., 33 (4), 130–135 (1992).
87. V. I. Kostikov, M. F. Makhova, V. P. Sergeev and V. I. Trefilov, Ceramic fibres, in *Fibre science and technology*, V. I. Kostikov, ed., Chapman and Hall, London, pp. 581–606 (1995).
88. K. Suganuma, H. Minakuchi, K. Kada, H. Osafune and H. Fujii, Properties and microstructure of continuous oxynitride glass fiber and its application to aluminum matrix composite, J. Mater. Res., 8 (1), 178–186 (1993).
89. S. Loud, Composites News, Solana Beach, CA, Infrastructure Newsletter Number 11, page 3, September 1994, and Number 28, page 5, June 30, 1995.
90. A. J. Majumdar, Alkali-resistant glass fibres, in *Strong fibers*, W. Watt and B. V. Perov, eds., Elsevier Publishers, North-Holland, pp. 61–85 (1985).
91. Chinese C-glass, Government Specification (1997).
92. D. A. Steenhammer and J. L. Sullivan, Recycled content of polymer matrix composites through the use of A-glass fibers, Polym. Comp., 18 (3), 300–312 (1997).
93. Nitto Boseki, Glass fibers having low dielectric loss tangent – composed of silica, alumina, boria, calcia, opt. magnesia etc., Japanese Patent 9002839, January 7, 1997.
94. H. Li, Low dielectric glass and fiber glass for electronic applications, US Patent Application 2008/0146430 A1, June 19, 2008.

95. D. S. Boessneck et al., Low Dielectric Glass Fiber, US Patent Application 2008/0103036 A1, May 1 2008.
96. G. Demidov, Hollow fibres make light and strong reinforcements, Reinf. Plas., 9, 19 (1995).
97. J. F. Bacon, Composition of glasses with high modulus of elasticity, US Patent 3,573,078, March 30, 1971.
98. K. Komori, S. Yamakawa, S. Yamamoto, J. Naka and T. Kokubo, Substrate for circuit board including the glass fibers as reinforcing material, US Patent 5,334,645, August 2, 1994.
99. K. Komori, S. Yamakawa, S. Yamamoto, J. Naka and T. Kokubo, Glass fiber forming composition, glass fibers obtained from the composition and substrate for circuit board including the glass fibers as reinforcing material, US Patent 5,407,872, April 18, 1995.
100. L. L. Hench, Bioactive glasses and glass ceramics, in *Handbook of bioactive ceramics, Vol. I,* T. Yamamuro, L. L. Hench and J. Wilson, eds., CRC Press, Boca Raton, pp. 7–23 (1990).
101. H. Tagai et al., Preparation of apatite glass fiber for applications as biomaterials, in *Ceramics in surgery*, P. Vincenzini, ed., Elsevier Sci. Pub. Co., Amsterdam, p. 387 (1983).
102. U. Pazzaglia et al., Study of the osteoconductive properties of bioactive glass fibers, J. Biomed. Mater. Res., 23, 1289–1297 (1989).
103. M. S. Marcolongo, P. Ducheyne, F. Ko and W. La Course, Composite materials using bone bioactive glass and ceramic fibers, US Patent 5,721,049, February 24, 1998.
104. L. J. Huey, Method and apparatus for making tapered mineral and organic fibers, US Patent 4,666,485, May 19, 1987.
105. K. Shioura, S. Yamazaki and H. Shono, Method for producing glass fibers having non-circular cross sections, US Patent 4,698,083, October 6, 1987.
106. H. Taguchi, K. Shioura and M. Sugeno, Nozzle tip for spinning glass fiber having deformed cross section and a plurality of projections, US Patent 5,462,571, October 31, 1995.
107. T. H. Jensen, Hollow glass fiber bushing, method of making hollow fibers and the hollow glass fibers made by that method, US Patent 4,758,259, July 19, 1988.
108. L. J. Huey, Method and apparatus for producing hollow glass filaments, US Patent 4,846,864, July 11, 1989.
109. J. Huang, Hollow high temperature ceramic superconducting fibers, International Patent Application WO 97/22128, June 19, 1997.
110. T. Yazawa, H. Tanaka and K. Eguchi, Preparation of porous hollow fibre from glass based on SiO_2–B_2O_3–RO–ZrO_2 (R = Ca, Zn) system, J. Mater. Sci. Lett., 13, 494–495 (1994).
111. R. P. Beaver, Method for producing porous hollow silica rich fibers, US Patent 4,778,499, October 18, 1988.
112. J. E. Loftus, C. R. Strauss and R. L. Houston, Method for making dual-glass fibers by causing one glass to flow around another as they are spun from a rotating spinner, US Patent 5,529,596, June 25, 1996.
113. N. T. Huff, Innovative technology can create products, Glass Res., 5 (1), 1–9 (1995).
114. M. C. Kenny, S. K. Barlow and S. L. Eikleberry, New glass-fiber geometry – a study of non-woven processability, TAPPI J., 30, 169–177 (1997).
115. F. T. Wallenberger, N. E. Weston and S. D. Brown, Infrared optical tellurite glass fibers, J. Non-Cryst. Solids, 144 (1), 107–110 (1992).
116. M. L. Nice, Apparatus and process for fiberizing fluoride glasses using a double crucible and the compositions produced thereby, US Patent 4,897,100, January 20, 1990.
117. H. Tokiwa, Y. Mimura, T. Nakai and O. Shinbori, Fabrication of long single-mode and multi-mode fluoride glass fibers by the double crucible technique, Electron. Lett., 21 (24), 1130–1131 (1985).
118. F. T. Wallenberger, S. D. Brown and G. Y. Onoda, ZnO-modified high modulus glass fibers, J. Non-Cryst. Solids, 152, 279–283 (1993).
119. H. Lin, W. L. Dechent, D. E. Day and J. O. Stoffer, Preparation and properties of mid-infrared glass fibers and poly(chlorotrifluoroethylene) composites, J. Mater. Sci., 32, 6573–6578 (1997).

120. S. D. Brown and G. Y. Onoda, Jr., High modulus glasses based on ceramic oxides, Report R-6692, Contract NOw-65-0426-d, US Department of the Navy, October 1966.
121. G. Y. Onoda, Jr. and S. D. Brown, High modulus glasses based on ceramic oxides, Report R-7363, Contract N00019-67-C-301, US Department of the Navy, February 1968.
122. T. F. Schroeder, H. W. Carpenter and S. C. Carniglia, High modulus glasses based on ceramic oxides, Technical Report R-8079, Contract N00019-69-C-0150, US Navy Dept., Naval Air Systems Command, Washington, DC, December 1969.
123. J. R. Davy, Development of calcia-alumina glasses for use in the infrared spectrum, US Patent No. 3,338,694 (1967), Glass Technol., 19 (2), 32–36 (1978).
124. R. Maddison, Calcia-aluminas, Product Bulletins WB37A and WB39B, Sassoon Advanced Materials LTD, Dumbarton, UK (1994).
125. P. R. Foy, T. Stockert, J. Bonja, G. H. Sigel, Jr., R. McCauley, E. Snitzer and G. Merberg, Meeting Abstracts, American Ceramic Society, 94th Annual Meeting, Presentation 7-JXV-92, Minneapolis, MN, April 12–16, 1992.
126. F. T. Wallenberger, N. E. Weston and S. A. Dunn, Melt spun calcia-alumina fibers: infrared transmission, J. Non-Cryst. Solids, 12 (1), 116–119 (1990).
127. F. T. Wallenberger, N. E. Weston and S. D. Brown, Melt processed calcia-alumina fibers: optical and structural properties, in *Growth of materials for infrared detectors*, R. E. Longshore and J. Baars, eds., Proceedings of the SPIE, Society of Photo-Optical Instrumentation Engineers, Bellington, Vol. 1484, 116–124 (1991).
128. J. Nishii, I. Inagawa, T. Yamagishi, S. Morimoto and R. Iizuka, Process for producing chalcogenide glass fiber, US Patent, 4,908,053, March 13, 1990.
129. F. T. Wallenberger, New melt spun glass and glass-ceramic fibers for polymer and metal matrix composites, in *High performance composites: Commonalty of phenomena*, K. K. Chawla, P. K. Law and S. G. Fishman, eds., The Minerals, Metals and Materials Soc., Warrendale, PA, pp. 85–92 (1994).
130. J. M. Massoubre and B. F. Pflieger, Small diameter wire making through solidification of silicon steel jet, in *Spinning wire from molten metal*, J. Mottern and W. J. Privott, eds.; AIChE Symp. Ser., (180), Vol. 74, pp. 48–57 (1978).
131. F. Fodeur and B. S. Mitchell, Infrared studies of calcia-alumina fibers, J. Am. Ceram. Soc., 79 (9), 2469–2473 (1996).
132. M. Mooney, The viscosity of a concentrated suspension of spherical particles, J. Colloid Sci., 6 (2), 162–170 (1951).
133. R. J. Diefendorf and E. R. Stover, Pyrolytic graphites: how structure affects properties, Metal Prog., 81 (5), 103–108 (1962).
134. A. L. Greer, Metallic glasses, Science, 267, 1947 (1995).
135. D. E. Polk and B. C. Giessen, Amorphous or glassy materials, in *Rapid solidification technology source book*, R. L. Ashbrook, ed., American Society for Metals, Metals Park, pp. 213–247 (1983).
136. A. Revcoleschi and J. Jegoudez, Growth of large high-T_c single crystals by the floating-zone method: a review, Prog. Mater. Sci., 42, 321–339 (1997).
137. P. H. Keck and M. J. E. Golay, Traveling solvent zone melting, Phys. Rev., 39, 1297 (1953).
138. T. Mah, T. A. Parthasarathy, M. D. Petry and L. E. Matson, Processing, micro-structure, and properties of Al_2O_3–$Y_3Al_5O_{12}$ (YAG) eutectic fibers, Ceramic Engineering and Science Proceedings, 622638, 17th Ann. Conference on Composites and Advanced Ceramic Materials, Am. Ceram. Soc., Westerville OH (1993).
139. W. M. Yen, Preparation of single-crystal fibers, in *Insulating materials for opto-electronics*, F. Agulló-Lopez, ed., World Sci., Singapore (1995).
140. M. Matsukura, Z. Chen, M. Adachi and A. Kawabata, Growth of potassium lithium niobate single-crystal fibers by the laser-heated pedestal growth method, Jpn. J. Appl. Phys. 1, 36 (9B), 5947–5949 (1997).
141. J. I. Peña, H. Miao, R. I. Merino, G. F. de la Fuente and V. M. Orera, Polymer matrix synthesis of zirconia eutectics for directional solidification into single-crystal fibers, Solid State Ionics, 101–103, 143–147 (1997).

142. W. Jia, H. Yuan, L. Lu, H. Liu and W. M. Yen, Phosphorescent dynamics in $SrAl_2O_4:Eu^{2+},Dy^{3+}$ single-crystal fibers, J. Lumin., 76–77, 424 (1998).
143. R. S. Feigelson, D. Gazit, D. K. Fork and T. H. Geballe, Superconducting Si–Ca–Sr–Cu–O fibers grown by the laser-heated pedestal growth method, Science, 240, 1642–1645 (1988).
144. F. M. Costa, R. F. Silva and J. M. Vieira, Influence on epitaxial growth of superconducting properties of LFZ Bi–Sr–Ca–Cu–O fibres, Part I. Physica C, 289, 161–170 (1997) and Part II., Physica C, 289, 171–176 (1997).
145. H. Miao, J. C. Dietz, L. A. Angurel, J. I. Peña and G. F. de la Fuente, Phase formation and micro-structure of laser floating-zone grown BSCCO fibers: reactivity aspects, Solid State Ionics, 101–103, 1025–1032 (1997).
146. U. Balchandran, A. N. Iyer, P. Haldar and L. R. Motowidlo, The powder-in-tube processing and properties of Bi-223, J. Metals, 45 (9), 54–67 (1993).
147. G. Geiger, New record for super-conducting wire, Am. Ceram. Soc. Bull., 74 (12), 19 (1995).
148. K. J. McClellan, H. Sayir, A. H. Heuer, A. Sayir, J, S. Haggerty and J. Sigalovsky, High strength, creep resistant Y_2O_3– stabilized cubic ZrO_2 single-crystal fibers, Ceramic Engineering and Science Proceedings, 651–659, 17th Ann. Conf. on Composites and Advanced Ceramic Materials, Am. Ceram. Soc., Westerville, OH (1993).
149. E. L. Lawton, F. T. Wallenberger and H. Li, Recent advances in oxide glass fiber science – low dielectric constant fibers, in *Advanced fibers, plastics and composites*, F. T. Wallenberger and N. E. Weston et al., eds., Materials Research Society, Symposium Proceedings, Vol. 702, MRS, Warrendale, 165–172 (2002).
150. M. H. Gallo, J. van Genechten, J. P. Bazin, S. Creux and P. Fournier, Glass fibers for reinforcing organic and/or inorganic materials, French Patent Application, 2,768,144 A1, September 10, 1997.
151. F. T. Wallenberger, N. E. Weston and S. A. Dunn, Melt spun calcium IR aluminate fibers: Product value, conference proceedings, Second International Conference on Electronic Materials, R. P. H. Chang, T. Sugano and V. T. Nguyen, eds., Material Research Society, pages 295–300, 1990.
152. H. D. Achtsnit, Textile silica sliver, its manufacture and use, US Patent 5,567,516, October 23, 1996.
153. J. Kobayashi, M. Oota, K. Kada and H. Minakuchi, US Patent 4,957,883, September 18, 1990.